Characterization of the (pro)renin receptor *in vitro* and *in vivo*

Dissertation
zur Erlangung des akademischen Grades

doctor rerum naturalium
(Dr. rer. nat.)

im Fach Biologie

eingereicht an der
Mathematisch-Naturwissenschaftlichen Fakultät I
der Humboldt-Universität zu Berlin

von

Diplom-Biologin Ulrike Maschke

Präsident der Humboldt-Universität zu Berlin
Prof. Dr. Jan-Hendrik Olbertz

Dekan der Mathematisch-Naturwissenschaftlichen Fakultät I
Prof. Dr. Andreas Herrmann

Gutachter:
1. Prof. Andreas Herrmann
2. Prof. Dominik N. Müller
3. Prof. Oliver Daumke

Tag der mündlichen Prüfung: 17.04.2012

Content

1. Abstract

The (pro)renin receptor (PRR) is an evolutionary conserved transmembrane receptor that was first discovered to bind renin and prorenin. Upon binding, PRR was shown to influence the activity of the renin-angiotensin-system (RAS) and to induce MAP kinase signalling. It was previously shown that a truncated, transmembrane part of PRR was associated to vacuolar H^+-ATPase (vATPase), a proton pump which is important for acidification. Recently, a new function of PRR in the WNT/β-catenin signalling pathway was described. Here, the PRR was shown to be an adaptor between WNT receptors and the vATPase. The precise mechanisms by which PRR functions, are still elucidative but the PRR is supposed to regulate various cellular processes.

Currently, no biochemical characterization or structural analysis is available for PRR. In order to gain understanding of the function of the PRR, structural studies were performed with several truncated proteins of the extracellular part of the PRR. All PRR proteins (hsPRR170-303, hsPRR 101-257 or hsPRR 166-257) showed an overall alpha helical folding and did not bind renin or prorenin. The oligomeric assembly of the proteins was investigated. The hsPRR (101-257) was shown to be in a concentration and pH dependent monomer/oligomer equilibrium, whereas hsPRR (166-257) is only present in a monomer/dimer equililibrium. These data are the basics for further structural and functional studies.

Additionally, conditional KO animals are an excellent tool to investigate the physiological role of the PRR *in vivo*. As the major mediator of the Wnt/β-catenin signaling pathway, β-catenin, is crucial for T cell maturation, a conditionel deletion of PRR in T cells was analyzed. PRR deletion resulted in a loss of mature T cells. Moreover, a defect in T cell maturation in the thymus was determined. Our data showed that PRR is critical for proper T cell development and support the hypothesis that PRR contributes to Wnt/β-catenin signaling in T cells.

2. Introduction

The (pro)renin receptor (PRR) was first described in 2002 by Nguyen *et al* as a receptor that binds renin or prorenin [1]. On the basis of this it was supposed that PRR was a new member of the renin angiotensin system (RAS); an important cascade involved in maintaining blood pressure homeostasis [2]. However, during the last few years it has become clear that the PRR is not only involved in blood pressure regulation but also plays a role in WNT signalling, vacuolar H^+-ATPase mediated acidification and consequently influences early cellular development and neuronal function. The precise function of this receptor and how it is involved in cellular processes is still unclear.

2.1. The (pro)renin receptor

PRR is ubiquitously expressed in all cell types. It consists of 350 amino acids with a molecular weight of 39 kDa. The amino terminus contains a short 16 residue signal peptide, and a long extracellular domain (amino acids 17 to 303). The intracellular C-terminus covers amino acids 327 to 350 with the amino and C-terminus flanking the single transmembrane region from amino acids 306-326 (Figure 1).

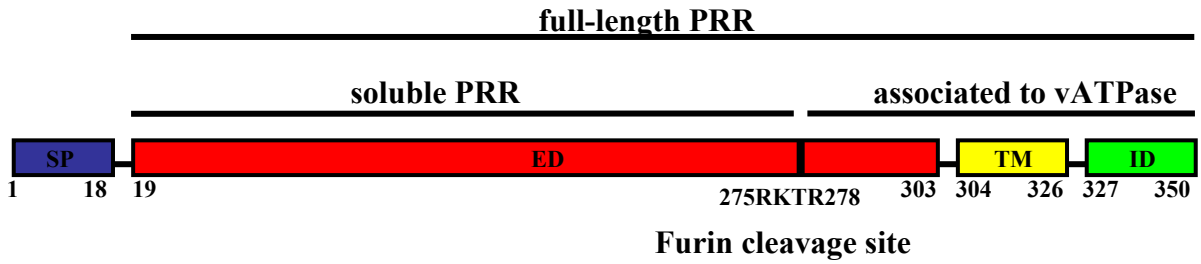

Figure 1. Schematic representation of the domains of PRR.
The PRR consists of a short intracellular (ID), transmembrane (TM), extracellular domain (ED) and signalpeptide (SP). A furin cleavage site (275RKTR278) is located in the extracellular domain.

The PRR shows no homology to any known proteins [1]. The extracellular domain possesses a furin cleavage site (275RKTR278). Furin is a cellular endoprotease that proteolytically activates large numbers of proprotein substrates in secretory pathway compartments [3]. Upon cleavage with furin, a 28 kDa soluble form of the PRR is detectable in the conditioned media of cultured cells [4, 5]. This soluble PRR fraction is generated intracellularly and is hypothesized to be secreted into the blood. Yoshikawa *et al* have recently described the presence of a soluble form of PRR which is secreted into the extracellular space. In contrast, they show that

ADAM19 is the protease responsible for cleaving the extracellular region of PRR, instead of furin [6]. These studies both illustrate the existence of a soluble PRR, but its function remains unknown.

It was subsequently realised that PRR was not described for the first time by Nguyen *et al* [1]. In 1998, Ludwig *et al* co-purified a shorter fragment of PRR (8.9 kDa) with the V_0 subunit of the vacuolar H^+-ATPase (vATPase) from chromaffin granule membranes [7]. This fragment of PRR was later renamed ATP6AP2 (vATPase associated protein 2). Approximately 70 amino acids were characterized, consisting of the C-terminal intracellular region, the transmembrane region and some additional amino acids from the extracellular domain. A link between PRR and vATPase was assumed, and therefore PRR is also known as ATP6AP2 [7]. Interestingly, only a minor amount of the PRR is localized at the plasma membrane, whereas the majority is located in intracellular vesicles [8].

The intracellular domain of PRR contains only 24 amino acids and a crystal structure of part of this domain was published [9]. Fusion of 18 amino acids of this domain to maltose binding protein forms a flexible loop. The authors state that these short fragments form a dimer, but the dimerization interface remains unknown. Currently, no other structural information is available about the PRR.

The PRR is found in a wide variety of species from invertebrates, such as *Drosophila,* to vertebrates, such as *Xenopus* and up to mammals including human, mouse and rat. Interestingly, not all of these species have a functional RAS, which, so far, is found almost exclusively in mammals. A gene for renin [10] as well as all other components of the RAS (http://www.uniprot.org/) is found in zebrafish, but whether these animals have a functional RAS is unclear. In *Xenopus,* no RAS components except for the angiotensin II type I receptor are present, and in *Drosophila* no RAS components exist. Despite this, PRR demonstrates a high evolutionary conservation. Bader and Burckle described that the N-terminal extracellular region of PRR is exclusively conserved in vertebrates, whereas the intracellular and transmembrane domain display a high amino acid sequence identity among all species investigated [11]. These authors raise the hypothesis that the PRR might have diverse functions due to the different regions of the protein having different evolutionary backgrounds. They propose that the renin binding capacity of the extracellular domain is evolutionary younger,

whilst the highly conserved C-terminus has a different function. Additionally, they suggest that the PRR might be involved in processes that are independent of renin and prorenin [11].

The only known human disease associated mutation of PRR is described in patients suffering from mental retardation and epilepsy. An X-linked mutation in an exonic splice enhancer results in the production of a shorter PRR fragment with a deletion of exon 4 and thereby reducing full-length PRR levels by around 50% [12]. The blood pressure of these patients was unchanged. Mutagenesis of the PRR in zebrafish also displays early developmental abnormalities. These mutants demonstrate eye and body hypopigmentation, neuronal cell death and have early lethality [13]. Conventional complete knock-out approaches in mice were not successful as no chimeras could be obtained [11, 14]. These results all suggest an important function for the PRR in early cellular development and also neurogenesis, perhaps in a renin and prorenin independent manner.

Details are already known about the function of the PRR *in vivo*; in particular its role in the cardiovascular system [15], its implication on WNT/β-catenin signalling [16] and its link to vATPase [7, 17]. These described roles of the PRR cover a wide area, including RAS-related and RAS-independent functions, and will be explored in the following sections.

2.2. RAS-related functions of PRR

2.2.1. The renin-angiotensin system (RAS)

The renin-angiotensin system (RAS) is a hormone cascade controlling and regulating cardiovascular, renal and adrenal functions. Blood pressure is increased by the secretion of specific hormones, which regulate water and sodium resorption thereby influencing blood volume and also inducing the constriction of blood vessels. The proteolytic enzyme renin is produced in juxtaglomerular cells of the kidney. The only known substrate of this protease is angiotensinogen. Angiotensinogen is synthesized predominatly in the liver, with minor amounts also detectable in the heart, kidney and adipose tissue. Cleavage of angiotensinogen by renin is the first step in the RAS cascade. The decapeptide angiotensin I is then cleaved at its N-terminus by the angiotensin converting enzyme (ACE), producing the octapeptide angiotensin II. Angiotensin II is the intrinsic effector of the RAS and binds to the angiotensin II type 1 receptor (AT1R). Angiotensin II induces both directly (*via* binding to the AT1R) and indirectly (*via* a stimulation of the aldosterone production) increased sodium and water reabsorption [18]. The angiotensin II/AT1R interaction furthermore mediates the constriction of

blood vessels, an increased thirst and salt appetite. All of these actions results in an increase in blood pressure (Figure 2). Angiotensin II directly acts on juxtaglomerular cells and is thereby able to regulate the secretion of renin by a negative feedback loop [19]. The availability and activity of renin is the rate limiting step in the RAS. Therefore, this is the most obvious target for blood pressure regulation.

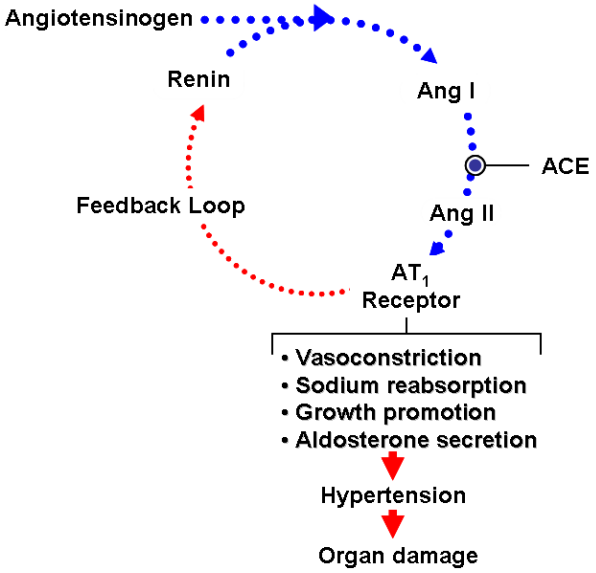

Figure 2. The renin-angiotensin system (RAS).

Angiotensinogen is cleaved by renin to produce angiotensin I (AngI), which is further converted to angiotensin II (AngII) by the angiotensin converting enzyme (ACE). AngII binds to the angiotensin II type 1 receptor (AT1) and increases blood pressure.

The classical circulating RAS is complemented by additional local RAS in diverse tissues. A prerequesite for the existence and functionality of a local RAS is the production of the individual RAS components in the tissue or alternatively, an uptake of the soluble proteins such as renin or angiotensinogen from the circulation. Since the site of expression of renin is exclusively in the kidney, a mechanism for the uptake of renin from the circulation into tissue is still under investigation. A local RAS is described for the heart, blood vessels, retina and kidney [20, 21].

2.2.2. Prorenin und renin

Renin is a specific aspartyl protease which exclusivly uses angiotensinogen as a substrate. Renin folds in predominatly β-sheet conformation, typical for the aspartic proteinase family (Figure 3B). The active cleft in the renin molecule contains two catalytically active aspartyl residues, aspartic acid 38 and 226 [22].

Recently, the crystal structure of human angiotensinogen was solved alone (Figure 3 A) and in complex with renin (Figure 3 B). It was shown that the processing of angiotensinogen by renin is modulated by a redox switch in angiotensinogen protein. Reduced angiotensinogen does not interact with renin that is bound to the PRR, whereas oxidized angiotensinogen is converted with a 4-fold increase after binding to renin [23].

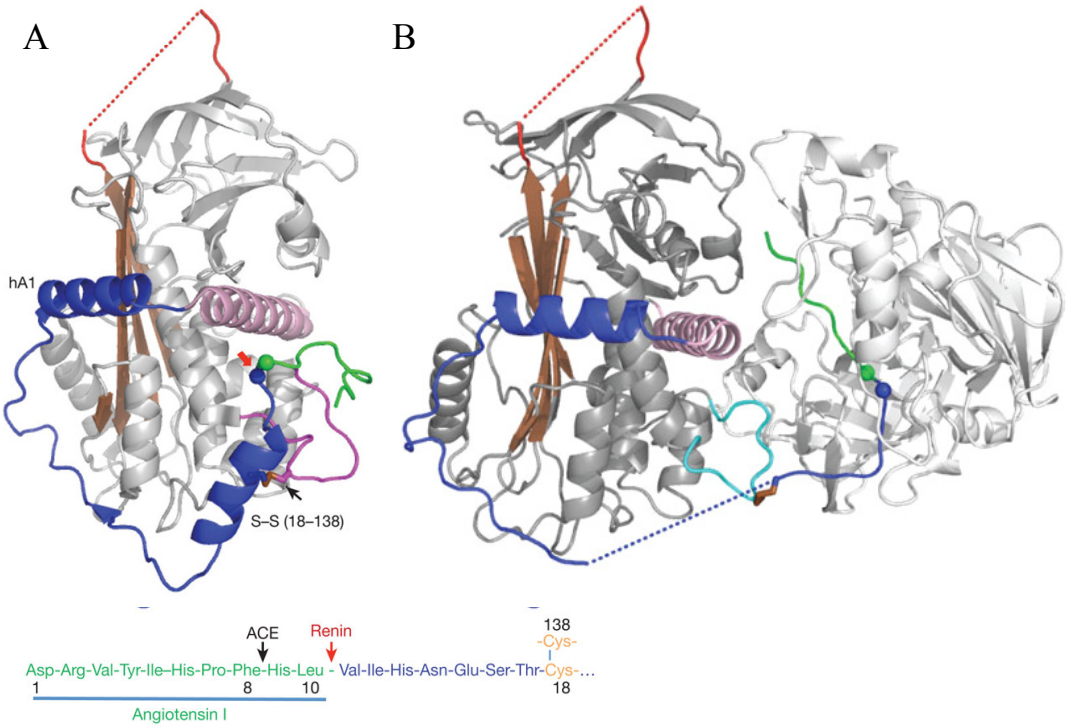

Figure 3. Crystal structure of human angiotensinogen and renin.

A) Crystal structure of human angiotensinogen alone. The N-terminus contains two unique helices (blue), the angiotensin peptide is shown (green) and the renin cleavage site (blue and green balls). B) Human angiotensinogen (grey) with renin (light grey) showing the displacement of the angiotensin peptide. The figures are taken from Zhou et al. [23].

Prorenin contains an additional 43 N-terminal amino acids. This propeptide is hypothesised to cover renins enzymatic cleft and prevent the binding and cleavage of angiotensinogen. No structural information for prorenin is available.

Prorenin can be activated proteolytically or non-proteolytically [24]. *In vivo,* proconvertase I [25] and cathepsin B [26] proteolytically remove the prosegement. This happens exclusively in the juxtaglomerular cells. *In vitro,* activation of prorenin can occur by addition of trypsin or plasmin. The reversible, non-proteolytic activation of prorenin occurs under non-

physiological conditions such as low pH (~ pH 3.3) and reduced temperature (~4ºC) [27, 28]. Under these conditions, the propeptide is thought to no longer cover the active cleft of prorenin.

For a long time, it was assumed that prorenin was *only* the inactive precursor of renin [2, 29]. However, recent findings suggest that prorenin could have important physiological or pathophysiological functions. Under physiological conditions, less than 2% of cirulating prorenin is in the active, uncleaved conformation [29]. In healthy patients, the plasma prorenin:renin ratio is approximately 10 to 1. Prorenin is constitutively secreted into the plasma, whereas renin is stored in secretory vesicles and released only after certain stimuli. The site of renin expression is only in the juxtaglomerular cells of the kidney, whereas prorenin is also produced in the eye, adrenal gland, placenta, testis and ovaries [30]. Under certain circumstances, the plasma prorenin concentration can rise. During pregnancy, prorenin levels are increased and they are used as a marker for the onset of microalbuminuria in diabetic patients [31, 32]. Microalbuminuria describes the onset of kidney failure, because the kidney leaks small amounts of albumin into the urin. Its defined by elevated albumin concentrations between 30-300 mg/l urin [33].

For years, it was supposed that a binding partner for renin or prorenin exists. An intracellular renin binding protein (Rbp) was found to bind renin and inactivate it [34], but deletion of this gene did not result in any change in blood pressure or the RAS [35]. In 2001, Saris et al discovered that renin and prorenin bind with high affinity to the mannose-6-phosphate/insulin-like growth factor II receptor [36, 37]. After binding, the ligand is internalised and degraded. Therefore, this receptor is thought to be solely responsible for renin and prorenin clearance, and has no influence on angiotensin I formation [38]. As mentioned above, in 2002 Nguyen *et al* described the binding of renin and prorenin with the PRR [1].

2.2.3. PRR and RAS

Nguyen showed in 1996 that renin binds specifically to human mesangial cells [39]. A mesangial cell line without an expression contruct of PRR DNA shows a specific binding to renin or prorenin. Binding to PRR increases the activity of renin five-fold and unexpectedly, prorenin is also non-proteolytically activated thereby resulting in the production of angiotensin I (Figure 4) [1]. Batenburg et al showed that renin binds PRR with a kD of 20 nM and prorenin with a kD of 7 nM, concluding that prorenin is the endogenous binding partner

of PRR [40]. PRR is expressed ubiquitously in all cell types. Especially high levels are found in the heart, brain, placenta and hematopoetic cells and lower levels in the kidney and liver [1].

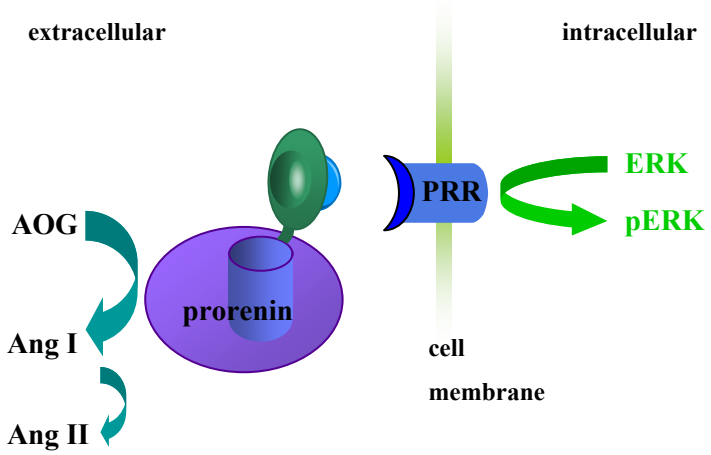

Figure 4. RAS-dependent function of the PRR.

The PRR binds renin and prorenin. Upon binding, prorenin is activated non-proteolytically and processes angiotensiongen (AOG) to angiotensin I (Ang I). Also, the ERKinase becomes phosphorylated and activates the MAP kinase pathway.

Several signal transduction pathways and effector mechanisms are triggered in an angiotensin II independent manner upon binding of renin or prorenin to the PRR. To analyze PRR mediated signal transduction, cells were pretreated with AT1R blockers to exclude angiotensin II induced effects, and then stimulated with renin or prorenin. These experiments show that the mitogen activated protein kinase (MAPK), Erk1/2, is activated *in vitro* in monocytes [41], mesangial cells [1, 42], vascular smooth muscle cells [43-45] and endothelial cells [46] after stimulation with renin or prorenin. This stimulation induced an increase in the transforming growth factor β [42, 47, 48], which in turn stimulated the expression of the profibrotic genes plasminogen activator inhibitor 1 [42, 44, 47], fibronectin [42], collagen I [42] and inflammatory associated proteins such as cyclooxygenase 2 [49], interleukin 1 [50, 51] and tumor necrosis factor α [51]. Interaction with renin or prorenin also induced cell proliferation in mesangial cells [1]. Another study shows in cardiomyoctes, prorenin induced angiotensin II independent activation of the p38 MAP kinase. Thus, a role for the PRR in this signal transduction pathway is likely [52]. A yeast two-hybrid screen identified the transcription factor promyelotic zincfinger (PLZF) as a new binding partner for the PRR. After activation of the PRR by renin, PRR was shown to interact with PLZF which then translocates into the nucleus and inhibits the expression of PRR [53, 54].

It is hypothesized that PRR is directly involved in pathology because of its involvement in several signalling pathways resulting in the expression of inflammatory and fibrotic genes. Additionally, a polymorphism in the PRR gene was shown to be associated with blood pressure in Japanese men [55]. This was also confirmed by another group studying a Caucasian cohort, who has an identical phenotype [55, 56]. Also a transgenic rat overexpressing the PRR develops elevated blood pressure levels after 6 month of age [57]. Another group reported glomerulosclerosis in a similar animal model [58]. Both animal models had a moderately mild phenotype with a late onset arguing for a rather marginal role of the PRR in cardiovascular pathology.

Since its discovery, discussion has centered on the development of PRR inhibitors which would block the angiotensin II mediated effects of PRR and therefore be beneficial antihypertensive therapies. Ichihara *et al* designed a decapeptide inhibitor (handle region peptide, HRP) which mimicked some of the amino acids of the prosegment of prorenin called the "handle" region. This region was shown to be important for the non-proteolytic activation of prorenin [59]. Since prorenin becomes activated by binding to the PRR, this peptide is proposed to competitivly inhibit the binding of prorenin to the PRR. However, several conflicting studies arose with this putative PRR inhibitor. In diabetic animals, HRP prevents the formation of glomerulosclerosis [51]. HRP treatment in spontanous hypertensive rats results in reduced cardiac fibrosis, proteinuria and glomerulosclerosis [59, 60]. Also in diabetic AT1R KO mice, HRP prevents the formation of glomerulosclerosis [61]. Based on these results, it is proposed that PRR has pathologic actions *via* an angiotensin II independent pathways. Beneficial effects of HRP treatment are also shown in pathologies such as retinal neovascularization and ocular inflammation [62]. For all of these studies, only prorenin is considered as a binding partner for the PRR. In contrast to these findings, several other publications could not confirm the beneficial effects of HRP. Susic *et al* found in their model of spontanous hypertensive rats that HRP does not ameloriate cardiac hypertrophy [63]. Several other animal models also do not confirm the observed beneficial effects of HRP. In double transgenic animals overexpressing renin and angiotensinogen [43], as well as in Goldblatt hypertensive animals [64], no ameliorated cardiac or renal factors are observed upon treatment with HRP. These studies suggest that the efficiency of HRP as a therapeutic compound for renovascular damage needs further examination. So far no other inhibitor for the PRR has been described. Without further knowledge about the detailed cellular function of PRR it remains controversial as to whether PRR should be seen as a drug target. The angiotensin II

independent functions of the PRR are still not completely understood, and the consequences of blocking them are not clear. Another aspect is the direct inhibition of renin, as this will result in higher renin levels. Renin might not longer be able to process angiotensinogen, but an interaction with the receptor is likely and the induction of its signal transduction [65].

2.3. RAS-independent functions of the PRR

2.3.1. vacuolar H^+-ATPase (vATPase)

As previously mentioned, when PRR was first discovered it was found to be associated with the vATPase [7]. The vATPase is an ATP-dependent proton pump. Its main function is the regulation of pH in intracellular compartments and extracellular fluids, which is essential for a variety of cellular processes [66].

2.3.1.1. Structure of the vATPase

vATPase is structurally and mechanistically related to F-ATPase, and even more closely to archaebacterial ATPase. vATPase is a rotary proton pump which hydrolyses ATP. In contrast to F-ATPase, vATPase is not able to synthesise ATP [67]. vATPase is divided into two domains. It consists of a cytoplasmic 650 kDa V_1 domain where ATP hydrolysis occurs and a 260 kDa membrane V_0 domain responsible for proton translocation (see Figure 5) [66, 68]. All together, vATPase is composed of 14 protein subunits. Additionally, different isoforms of these subunits are described for several tissues and cellular locations, further increasing the complexity of this pump. The V_1 complex contains 8 subunits: *A, B, C, D, E, F, G, H*. Three copies of each of the *A* and *B* subunits are present, which form an alternating hexamer with three catalytic sites in the *A* subunit for ATP hydrolysis, and three nucleotide binding sites at the *AB* interface. Surrounding the *AB* ring are two copies of the *G* and *E* subunits, which form heterodimers. Further present in the complex are 1 or 2 copies of the *H* subunit, and a single copy of all other subunits. Functionally, a peripheral stalk, composed of the *C, E, G, H* subunits, and a central stalk, composed of the *D* and *F*, subunits are defined. The central stalk provides the energy to the rotation necessary for proton transport, whereas the peripheral stalk is hypothesized to prevent rotation of the *AB* hexamer. The peripheral stalk, the *AB* complex, and subunits *a* and *e* of the V_0 domain, form the stationary part of vATPase called the “stator”.

The V_0 domain consists of the subunits *a, c, c′, c′′, d* and *e*. Subunit *a* has eight or nine transmembrane regions with one buried arginine residue that connects the V_1 and V_0 complex

and is absolutely necessary for proton translocation. The *c, c´* and *c´´* subunits form the so-called proteolipid ring. These highly hydrophobic subunits all possess a single buried glutamate residue, which is also important for proton transport. The *d* subunit sits atop of the proteolipid ring and connects the V_0 domain with the central stalk of the V_1 domain. The function of the highly hydrophobic *e* subunit has so far not been described [68].

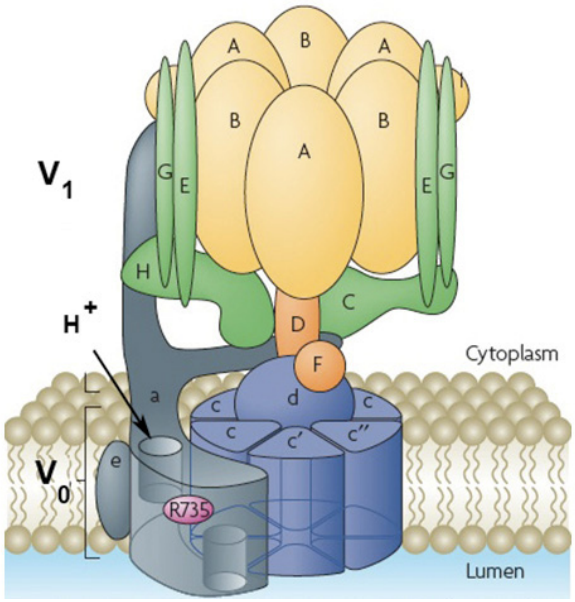

Figure 5. Schematic representation of the structure of vATPase.
vATPase is composed of the V_1 (orange and green) and the V_0 domain (blue) and its subunits (*A-H* (V_1) and *a-e* (V_0)). The V_1 domain is responsible for ATP hydrolysis, while the V_0 domain translocates the protons across the membrane. For details see text. The figure is taken from Forgac [68].

The correct assembly and targeting of vATPase is critical for its function in certain tissues and cellular compartments. The V_1 domain is able to self-assemble, whereas the V_0 domain requires the support of several endoplasmatic reticulum assembly factors such as VMA (vacuolar membrane ATPase activity) 21, VMA 12, VMA 22 and Pkr1[69-71]. The targeting of vATPase to its site of activity is mediated by several isoforms. Four isoforms of the *a* subunit have been described, which all differ in the cell type in which they are expressed and the cellular location in which they function. Multiple isoforms of the same subunit are also possible in one cell [68, 72]. For example, the *a1* subunit is found in presynaptic nerves, in synaptic vesicles and on the plasma membrane [73]. The *a2* subunit is expressed in renal proximal tubule cells in the apical endosomes [74]. In contrast, the *a3* subunit is localised on the plasma membrane of osteoclasts [75], whereas *a4* is located in the apical membrane of renal intercalated cells [76]. Most of the other V_0 subunits have two isoforms, where one isoform is

ubiquitously expressed and the second isoform is only expressed in a specific cell type or tissue [68]. PRR is not thought to be directly involved in the formation of vATPase complex, but is associated to the V_0 domain. Therefore, PRR might play role in assembly of the V_0 domain.

2.3.1.2. Proton transport of the vATPase

Protons are translocated after ATP hydrolysis via an active transport mechanism, through the rotation of the proteolipid ring, subunits *D*, *F* and *d* [77]. Protons enter from the cytoplasmic side of the membrane through a hemi-channel of subunit *a*, and protonate the buried glutamate in the *c, c´* or *c´´* subunit. Following ATP hydrolysis, the proteolipid and accessory subunits rotate, thereby displacing the protons. The protonated glutamate then interacts with the buried arginine in the *a* subunit [66]. This arginine becomes protonated and releases the proton into the lumen of the vesicular compartment or the extracellular fluid [78]. The stoichiometry for this process is between 1:2 and 1:3. Three, since there are three ATP binding sites in the AB hexamer and 6-10 protonable sites in the proteolipid, depending on the amount of proteolipids in the ring [68].

Bafilomycin and concanamycin are inhibitors for vATPase and are proposed to block proton transport by circumventing the helical rotation around their own axes of the proteolipids. This helical swivelling is important for the rotation and the proton transport of the proteolipid ring [79-82].

2.3.1.3. Regulation of vATPase activity

Since pH is crucial for many cellular processes, vATPase activity is highly regulated. Several mechanisms are described for the regulation of vATPase activity. One mechanism is the reversible dissociation of the domains V_1 and V_0. This mechanism is best understood in yeast and insect cells, but also occurs in mammalian cells [68]. In yeast, it was shown that after depletion of glucose, which consequently resulted in a reduction of ATP consumption, the two domains of vATPase dissociated [83]. This process is reversible, but dissociation and assembly are regulated differently. Assembly in yeast requires a protein complex called RAVE [84], whereas dissociation is not dependent on this complex. The mechanism for the reversible dissociation is not fully understood, but it is hypothesized that the non-homologous region of the *A* subunit plays a role in dissociation [85]. Also, the RAS/cAMP/protein kinase A pathway has been described to be involved in the dissociation of vATPase [86]. A role for PRR

in assembly or dissociation of vATPase is possible. Because of its transmembrane localization, an interaction with the V_0 domain appears feasible. Thus, regulation of vATPase activity could be mediated *via* an interaction between the V_0 domain and the PRR. The first evidence for an involvement of PRR in vATPase assembly and function came from Kinouchi *et al*. They showed that deletion of the PRR results in a downregulation of the V_0 subunits and affect the stability and assembly of the V_0 subunits, thereby compromising vesicular acidification [87].

Besides reversible dissociation, another regulatory mechanism of vATPase activity is the endocytosis or exocytosis of vATPase at the plasma membrane. In this case, vATPase is stored in vesicles close to the plasma membrane in renal epithelial cells and is transported to the membrane upon induction by a glucose stimulus. The complex is internalised and trafficked to intracellular storage compartments if proton transport is reduced [88].

A third hypothesized mechanism for the regulation of vATPase activity is the increase/decrease of the coupling efficiency of ATP hydrolysis and proton translocation. This mechanism is controlled by the different *a* subunit isoforms. Different yeast homologs for the *a* subunit showed altered coupling efficiency suggesting a tighter coupling of proton transport and ATP hydrolysis [72]. A special mechanism to regulate the activity of vATPase is the formation of a reversible disulfide bond in the subunit *a*, causing a disruption of the catalytic function of the ATPase [89].

A tight regulation of vATPase activity is important for cellular function and is achieved by these various processes. A role for the PRR in these mechanisms is possible, but needs further investigation.

2.3.2. PRR and vATPase

It has been shown that PRR is associated to vATPase [7]. Another link between PRR and vATPase was shown by Advani *et al*, where PRR was demonstrated to co-localize with the *B* subunit of vATPase in the kidney [90]. Additionally, Cruciat *et al* showed that PRR co-immunoprecipitated with transmembrane subunits of vATPase [16]. All of these effects were first shown *in vitro,* until recently where support for a link between PRR and vATPase came from *in vivo* studies. The first conditional knock-out of PRR in cardiomyocytes resulted in lethal heart failure accompanied with impaired autophagic degradation [87]. The authors explain

these phenomena by the defective acidification of intracellular compartments, which is necessary for protein degradation. They showed that malfunction of this acidification was due to a disordered assembly of vATPase; evidenced by deletion of PRR reducing protein levels of subunits of transmembrane vATPase [87]. Furthermore, conditional KO of PRR in podocytes also caused a defect in protein degradation and autophagy [91, 92]. Podocytes form the main filtration barrier in the kidney and deletion of PRR in this cell type resulted in kidney failure and early lethality. Additionally, similar to the phenotype observed in cardiomyocytes, the authors observed a block in podocyte lysosome processing, which they propose could be due to defective vATPase function and impaired acidification [91]. Another group described the same podocyte model with a similar phenotype. They confirmed again that deletion of PRR suppressed expression of the *c* subunit of the V_0 domain of vATPase, resulting in deacidification of intracellular vesicles [92]. All of these studies point towards PRR having an important role in the function and regulation of vATPase *in vivo*.

2.3.3. Physiological and pathophysiological function of the vATPase

vATPase is involved in a variety of cellular processes where acidification is necessary. Depending on its cellular localization it is involved in different functions. For example, vATPase is found in cellular compartments such as endosomes, lysosomes, Golgi-derived vesicles, clathrin-coated vesicles, secretory vesicles and the central vacuoles of plants and fungi. In these compartments, vATPase is engaged with protein trafficking including processes such as clathrin-mediated endocytosis, receptor recycling, lysosomal degradation and secretion. In clathrin-mediated endocytosis, ligand-receptor complexes are clustered in clathrin-coated pits which then bud off from the plasma membrane as clathrin-coated vesicles and form early- or sorting-endosomes. Sorting endosomes are then acidified by vATPase and the internalised ligand-receptor complex dissociates. The receptor is then shuttled back to the cell surface and the ligand is further trafficked to the lysosome. In lysosomes, proteases are only active at low pH and thus acidification by vATPase is essential for the degradation of proteins [68]. Not only for protein degradation, but also for the processing of proteins vATPase is necessary. In secretory vesicles, vATPase is essential for the activation of proteases at low pH cleaving prohormones, such as in pancreatic beta cells, where proinsulin is converted to insulin [93]. Additionally, vATPases provide the membrane potential or pH gradient required to drive the transport of neurotransmitters in secretory vesicles [94]. Previously, it was shown that PRR is expressed in the brain and plays a role in the neural control of cardiovascular

functions [95]. Besides the acidification in intracellular compartments, the vATPase is also involved in development in *Xenopus* embryos [96].

vATPase is also found on the plasma membrane of a variety of cells. Mutations in subunits of vATPase are involved in several pathophysiologies. In particular, cell surface vATPase in the kidney is important for several processes. Alpha-intercalated cells in the kidney have a large amount of vATPases in their apical membrane, which acts to secrete protons into the lumen of the distal tubule and collecting duct. This mechanism is important for the acid/base homeostasis of the urine [97], and a mutation in the *B* subunit of the vATPase results in an inherited form of distal renal tubule acidosis [98]. Osteoclasts are another cell type in which vATPase has an important role. At the plasma membrane, vATPase creates an acidic pH necessary for the activity of digestive enzymes that degrade the bone. A mutation in vATPase subunit *a3* in osteoclasts results in osteopetrosis [99]. This disease is characterized by thickening of the bone, due to malfunctioning of the bone degradation machinery. Interestingly, this same mutation in the *a3* subunit additionally results in a decreased insulin secretion in beta cells in the pancreas [75]. vATPase is also critical for sperm maturation in the vas deferens. Here, the epididymal clear cells secrete protons into the lumen of the epididymus to generate an acidic pH required for the development and maintenance of sperm [100]. Additionally, vATPase plays a crucial role for maintaining the homeostasis of neutrophils and macrophages when they are recruited to sites of inflammation. At these sites there is often an acidic pH, and thus, these immune cells require a functional vATPase at the plasma membrane in order to maintain their neutral intracellular pH [101]. vATPase also influences angiogenesis of endothelial cells, especially in migration, invasion and tumor metastasis. In the case of tumor cells, vATPase acidifies the extracellular surrounding, thereby promoting invasion by providing the low pH required for cathepsins to digest the extracellular matrix [102]. These studies highlight that vATPase is important for several pathophysiological processes.

Besides the above described diseases associated with vATPase, a role for vATPase in bacterial and viral infections is also known. Several viruses and toxins enter the cell with the help of vATPase. One example is the influenza virus, which is able to infect the cell due to the low pH in the endocytosed viral vesicles which facilitates fusion of the viral and endosomal membranes, resulting in the release of viral RNA into the host cell [103]. The low pH in intracellular vesicles additionally aids the entry of bacterial toxins such as anthrax or diphtheria into the cell [104]. vATPases are also hypothesized to play a role in infection by HIV.

In this case, the virus enters the cell *via* the CD4 receptor on T cells, within endosomes. Acidification by vATPase is crucial for the intracellular release of the virus. Additionally, the *H* subunit of vATPase has been shown to interact with the virus protein NEF and regulate CD4 internalization so as to prevent multiple infections [105].

Taken together, these facts show that vATPase is involved in several diseases and is also crucial for physiological processes. This makes vATPase an important complex for the maintenance of cellular function. Therefore, the function of the PRR and its importance for vATPase, *in vitro* and *in vivo,* should be elucidated further.

2.3.4. WNT/β-catenin pathway

A recent publication described PRR as an important protein involved in WNT/β-catenin signalling [17]. The WNT/β-catenin canonical signalling pathway has an essential role in cell proliferation, stem cell maintenance, cell fate decision, organized cell movements and the establishment of tissue polarity. It is frequently deregulated in human cancer and degenerative disease [106]. Besides the canonical WNT pathway, non-canonical WNT pathways exist, among them the planar cell polarity pathway [107].

The canonical WNT pathway depends on the presence of WNT (see Figure 6). WNT is a secreted signalling molecule and binds to its cell surface receptor Frizzled. Upon binding to Frizzled, the complex interacts with the membrane-bound co-receptor LRP6 (low-density lipoprotein receptor-related protein 6). In the next step, Dishevelled is recruited to the receptor complex and becomes activated. Dishevelled is another key component of the canonical WNT pathway and inhibits the destruction complex. This destruction complex is composed of the proteins axin, glycogen synthase kinase 3 (GSK3), adenomatous polyposis coli (APC) and casein kinase 1 (CK1). The destruction complex promotes the proteolytic degradation of β-catenin. Dishevelled destroys this complex, but the mechanism for this is not clear. In turn, β-catenin accumulates in the cytoplasm and translocates into the nucleus where it interacts with the transcription factor family TCF/LEF to induce gene expression. After interaction of β-catenin with TCF, groucho dissociates and target gene transcription starts. In the absence of WNT, β-catenin is complexed with the destruction complex, where it is phosphorylated by GSK3 which then targets it to the β-TrCP E3 ligase. This complex promotes the ubiquitinylation of β-catenin, subsequently resulting in the proteolytic degradation of β-catenin by the proteasome [107, 108].

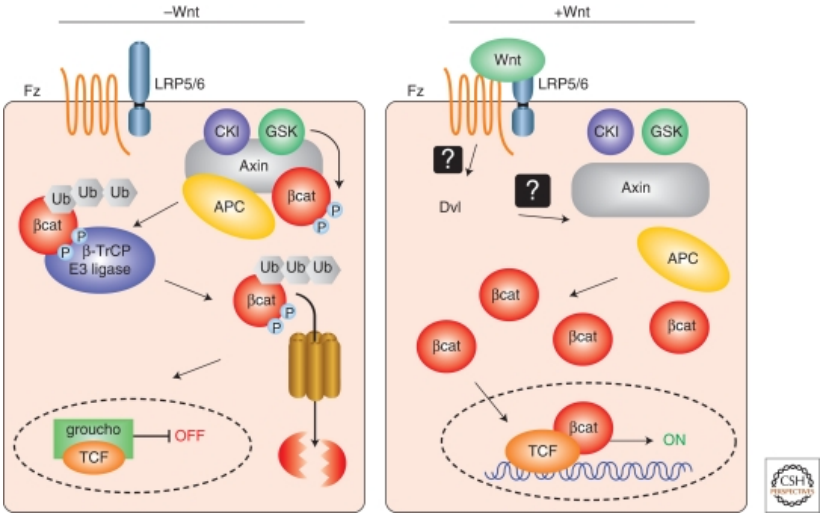

Figure 6. Schematic representation of the canonical WNT/β-catenin pathway.
In the absence of Wnt signal, β-catenin is recruited into the APC/Axin/GSK3/CKI complex, and is phosphorylated by GSK3. Phosporylated β-catenin binds to β–Trcp E3 ligase of the proteosome machinery and is targeted for degradation. Wnt binds to its frizzled Fz receptor and LRP5/6 co-receptor and activates dishevelled (Dvl), leading to the inhibition of APC/Axin/GSK3 mediated β-catenin degradation. Stabilized β-catenin forms a transcriptional complex with LEF/TCF and activates downstream targets. The figure is taken from Cardigan and Pfeiffer [108].

There are also several non-canonical pathways, such as the planar cell polarity (PCP) pathway. The biggest difference between the non-canonical and the canonical-pathways is the independence of β-catenin. The PCP pathway is best understood in *Drosophila* and only a little is know about these pathways in mammalian cells [106]. Frizzled and dishevelled form a complex that binds and activates small Rho GTPases and JNK (c-Jun N-terminale kinase) [106]. In this thesis, I will focus on the canonical-WNT pathway.

2.3.5. PRR and WNT signalling

A new function of PRR was proposed by Cruciat *et al* in 2010, where they describe PRR as a component of the WNT receptor complex [17]. They show that PRR binds to WNT receptors Frizzled and LRP6 and hypothesize that PRR in combination with vATPase, influences LRP6 phosphorylation and activation. This phosphorylation process may only occur under acidic conditions mediated by vATPase. Additionally, they describe a PRR knock down in *Xenopus* that results in body morphogenesis and pigmentation defects displaying a similar phenotype as already described for zebrafish. All these functions are renin-independent [17].

In the same year, two other publications confirmed the importance of PRR for non-canonical WNT signalling. They both show in *Drosophila* that PRR interacts with Frizzled [109, 110]. The authors hypothesize that the complex of vATPase and PRR, contributes to the function and signalling of Frizzled and thereby mediates non-canonical WNT (PCP) signalling. They also report that a knock down of PRR in *Xenopus* results in a defective PCP signalling phenotype, similar to previously published ones [109]. Thus, PRR is not only involved in the canonical WNT pathway described by Cruciat *et al* [17], but also plays a role in the non-canonical WNT pathway. It has been hypothesized that PRR is a conserved modulator of both non-canonical and canonical WNT pathways bridging the WNT receptors with vATPase [17, 109].

2.3.6. WNT/β-catenin signalling in development and disease

The canonical WNT pathway is highly conserved in evolution and is a fundamental signalling pathway in all species [111]. The impact of WNT signalling on development and disease is described in the following.

The use of gain-of-function and loss-of-function mutations of WNT components in animal models have helped to obtain insight into the diverse functions of the WNT pathway in development [112]. The WNT pathway has an enormous role in stem cell fate and proliferation [108]. It has also been shown that WNT signalling is critical for the proliferation of intestinal epithelial cells [113] and hair follicle stem cells [114]. WNT signalling also controls differentiation of mesenchymal stromal stem cells and regulates the self-renewal of hematopoietic stem cells [112]. For example a gain-of-function mutation that results in constitutive active β-catenin in hematopoetic precursors results in impaired self renewal of these cells [115, 116].

In terms of disease, the WNT pathway is implicated in cancer progession. A large number of mutations in WNT pathway related genes are associated with leukaemia, colon cancer and a variety of other cancers [111]. APC is a tumour suppressor gene and allelic mutations, resulting in loss of both functional alleles, is present in almost 80 % of all sporadic colorectal cancers. Mutation of APC results in an over-activation of the canonical WNT pathway, resulting in β-catenin being no longer bound to the degradation complex and thereby inducing the uncontrolled proliferation of intestinal epithelial cells [117]. Some colon cancers are linked to a loss of function mutation of Axin, which in turn are correlated to hepatocellular carcinomas [111].

A deregulated WNT pathway is involved in several additional diseases. Skeletal disorders and bone formation are linked to deregulated WNT components. Expression of gain-of-function LRP5 in mice results in high bone density and elevated numbers of active osteoblasts, while loss-of-function of LRP5 leads to reduced bone mass in animal models [111]. Interestingly, vATPase is also involved in bone formation; mutations in vATPase subunit *a3* in osteoclasts results in osteopetrosis [99]. Disturbed WNT/β-catenin signalling is as well involved in neuronal disorders, like Alzheimers disease and, moreover, in wound healing and cardiovascular disease [107]. Mice models with defective WNT signalling are more prone to infarct rupture after induction of myocardial infarction and neovascularisation of the infarct area is influenced [118]. The contribution of PRR to these diseases that are associated with a deregulated WNT/ β-catenin pathway is yet to be determined.

2.4. T cells

T cells are a specialised type of immune cell which play a central role in cell mediated immunity. Their main function is the recognition of intracellular pathogens and activation of B cells [119]. To become a functional T cell, they undergo several steps of maturation in the thymus for which the canonical WNT signalling pathway is essential [120]. PRR is ubiquitously expressed and shows a high level of gene expression in hematopoietic tissue (*personal communication*, M. Andrade, MDC, Berlin, Germany). As described above, PRR is proposed to be an adaptor between the WNT receptors and vATPase, and thus, might be important in T cell maturation [17].

2.4.1. T cell function

The immune system is composed of several cell types originating from pluripotent hematopoetic stem cells from the bone marrow. These hematopoetic stem cells separate into common myeloid progenitors that give rise to granulocytes, macrophages, dendritic cells and erythrocytes and into common lymphoid progenitors. The common lymphoid progenitors give rise to B and T cells, which are both components of the adaptive immunity, and to natural killer cells [119].

T cells are defined by their maturation in the thymus and their expression of a T cell receptor (TCR). The TCR is a cell surface receptor responsible for the recognition of antigens and the activation of T cells. The TCR is a heterodimer consisting of a α- and β-chain or a γ- and δ-chain. The γδ T cells are engaged in early and late immune responses, and function as effector

cells and immune regulators. Because γδ T cells are the first T lymphocytes to arise in ontogeny, it seems likely that they play an important role in immune protection early in development [121].

The majority of T cells express the CD3 TCR that is composed of α- and β-chains, which play a major role in cell-mediated immunity. These T lymphocytes are further separated into T helper cells, cytotoxic T cells and regulatory T cells. T helper cells express the CD4 protein on their cell surface, whereas cytotoxic T cells express CD8 on their surface and therefore they are known as $CD4^+$ and $CD8^+$ T cells, respectively. CD4 and CD8 are co-receptors for the TCR that are required to bind to the major histocompatibility complex (MHC) present on all antigen presenting cells, such as dendritic cells or macrophages. CD4 binds to MHC class II, whilst CD8 interacts with MHC class I. This interaction is important for antigen recognition and T cell response [119]. For activation of T cells, signalling *via* the TCR MHC complex is essential, but also co-stimulatory signals are required. The best known signal is the CD28-mediated co-stimulus. In response to this, T cells clonally expand and become activated [122]. $CD8^+$ T cells are responsible for the killing of pathogen infected cells. The $CD8^+$ cells induce formation of a pore and activate apoptotic pathways. $CD4^+$ T cells are not directly involved in cell apoptosis, instead they assist to activate $CD8^+$ T cells or macrophages, and effect the maturation of B cells [119]. Upon activation, the $CD4^+$ T cells differentiate into several subtypes expressing diverse cytokines, thereby modulating the immune response. For example, Interleukin 12 induces the development of Th1 cells that secrete interferon γ and support the cellular immune response. In contrast interleukin 4 stimulates the expansion of Th2 cells affecting the humoral immune response [123]. Th17 cell development is triggered by the presence of TGF β, interleukin 6 and 21. These cells are characterized by the expression of interleukin 17. Th17 cells are important in clearing pathogens during host defence reactions and inducing tissue inflammation in autoimmune disease [124, 125]. The last T cell subtype is regulatory T cells. These are induced by TGF β and are supposed to have suppressor and regulatory functions for the immune system [126]. Most of these cells die within 1 or 2 weeks after activation, and only a small subset survives as effector memory T cells or central memory T cells [123].

2.4.2. T cell development

For the existence and function of T cells, their maturation process is crucial. The WNT/β-catenin pathway plays a key role in their development and thus the role of the PRR in this process should be analyzed closer.

T cell maturation is a highly regulated and complex procedure. Initially, common lymphoid progenitors migrate to the thymus. They do not express the TCR or the co-receptor CD4 and CD8 and are therefore called double negative (DN; $CD4^-/CD8^-$) cells. These DN cells are further characterized by the expression of the two surface markers CD44 and CD25, corresponding to the α-chain of the interleukin-2 receptor. In the first DN stage, the cells are negative for CD25 and positive for CD44 and are also referred to as DN1 ($CD25^-/CD44^+$) (Figure 7). During the next maturation step (DN2; $CD25^+/CD44^+$) the cells downregulate the hematopoetic stem cell marker cKIT and upregulate CD25. With this, they lose their potential to form other cells, such as B cells and natural killer cells and are committed to the T cell lineage [127]. Until this point the cells are moderately proliferating, whilst during the DN3 ($CD25^+/CD44^-$) stage they stop proliferation and downregulate CD44. During the following rearrangement of the β-chain, the TCR gene is genetically recombined to recognize different antigens. Cells which successfully rearranged their β-chain, present the pre-TCR on their surface; cells that do not rearrange successfully undergo apoptosis. The pre-TCR is composed of a β-chain and a non-rearranged α-chain. This point is the first important stage for T cell maturation called the "β-selection checkpoint" [128, 129]. β-catenin deletion results in a developmental block at the DN3 stage to DN4, pointing towards an important role of WNT/β-catenin signalling in the β-selection checkpoint [120]. When cells further proceed with their next maturation process (DN4; $CD25^-/CD44^-$), they downregulate CD25 and start to express the CD4 and CD8 co-receptors, therefore becoming double positive cells (DP; $CD4^+/CD8^+$). More then 90 % of the cells die at this stage during a positive selection process. Only cells that moderately bind to MHC class I or II complexes are chosen, whereas non-functional T cells are eliminated by "death by neglect", because they do not obtain important signals for their further survival. The surviving cells start to express high levels of the TCR with a rearranged TCR α-chain, whilst the pre-TCR is downregulated. Between 5-10 % of the remaining cells are negatively selected because they bind to self antigens and undergo apoptosis. Only 2 % of T cells survive these selection rounds and transit from a DP cell, to a single positive (SP) mature $CD4^+$ (helper) or $CD8^+$ (cytotoxic) cells. These cells then move from the thymus to the blood stream. [128]. The T cell repertoire is established during early

years, as the thymus shrinks during adolescence. However, T cell production remains continuous [127]

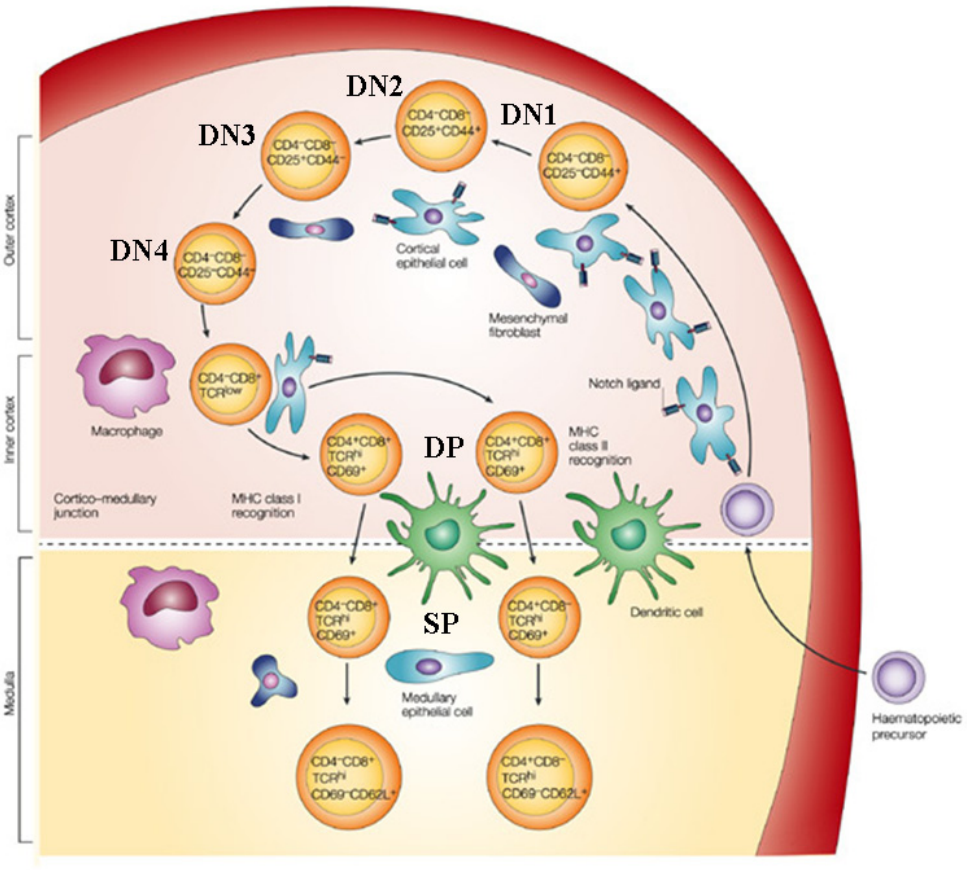

Figure 7. Overall scheme of T cell development in the thymus.

The hematopoetic precursors migrate from the bone marrow to the thymus. The double negative (DN) cells are characterized by the absence of $CD4^-/CD8^-$. These cells can be further subdivided into DN1-DN4 cells characterized by the expression of CD25 and CD44. Thereafter DN cells start to express the $CD4^+/CD8^+$ antigen (DP) and finally develop into single positive $CD4^+$ or $CD8^+$ cells. For details see text. The figure is adapted from Zúñiga-Pflücker [130]

2.4.3. T cells and PRR

A role for PRR in T cells has not been described before, but as WNT/β-catenin signalling and vATPase are involved in T cell function and development a role for PRR is likely.

β-catenin is the central mediator of WNT signalling and a conditional deletion in T cells results in an impaired T cell development [120]. The authors showed that the amount of T cells was drastically reduced in lymphoid tissues and the circulation, while B cells were not affected. The lack of β-catenin did not result in an increased apoptosis or in a dramatic changed proliferation rate, thus concluding that the maturation in the thymus is affected. A

block in development was shown by analyzing the thymocytes. The pre-TCR signalling seems to be dependent on functional WNT signalling [120].

Another publication implicates that vATPase also plays an important role for T cell development. Pua *et al* published that autophagy is critical for lymphocyte development and function and suggest an essential role for survival and proliferation. Autophagy is an intracellular degradation process depending on acidification. Mice that are deficient for ATG5 had reduced numbers of T cells with a dramatically increased number of dead cells and a proliferation defect [131]. vATPase was shown to play a role in the infection of HIV. It helps the virus to enter the CD4+ T cell and prevents multiple infections of the same cell [105, 132] Acidification of the lytic granules of the cytotoxic T cell is dependent on vATPase and therefore necessary for their function [133]. All these observations point to an important role of vATPase and WNT/β-catenin signalling for T cell function and maturation and therefore imply a fundamental role for PRR for T cells. Additionally T cell subtypes are important to cardiovascular function and target-organ damage [134] .

A better understanding of the function of the PRR for these cells would give insight into T cell regulation. Additionally, this cKO model would provide knowledge about the *in vivo* implication of PRR for vATPase and WNT/β-catenin pathway.

2.5. Objectives of the work

The aim of this thesis was to characterize the PRR. This characterization might help in the future to obtain a better understanding of the role of the PRR for the RAS, WNT/β-catenin pathway and the vATPase, both *in vitro* and *in vivo.*

No structural data is available for the soluble region of PRR. Therefore, the first aim of my thesis was to obtain structural information by protein X-ray crystallography of the soluble region of PRR. With the help of structural data, additional information about possible binding sites to renin or prorenin or other interaction partners could be analyzed and would give insights into the function of the soluble region of PRR.

Specific aims therefore were to find soluble, truncated proteins of PRR that could be purified in high amounts and quality in an *E.coli* expression system. These constructs were then analyzed for their secondary structure to obtain information about their folding. Next, binding to renin or prorenin of these constructs was analyzed. In addition these PRR proteins were analyzed for their oligomerization behaviour. All constructs were used for crystallization trials.

The second aim of my thesis was to analyse the role of the PRR in an *in vivo* system, using a conditional knockout approach. The hypothesis tested that the deletion of PRR in T cells would result in phenotype similar to that of a β-catenin knockout, displaying a maturation defect at the DN3 to DN4 cell stage. With this, the possible link of PRR to WNT/β-catenin pathway should be analyzed to understand the function of the PRR.

In this project it was analyzed if PRR deletion results in a decrease of T cells in peripheral lymphoid tissue. Furthermore it was determined what kind of T cells, $CD4^+$ or $CD8^+$ cells, are reduced in this cKO model. To explain the reduction of T cell it was further analyzed if this is due to a developmental defect. For that reason, T cells were examined during their maturation process in the thymus. The proportion of typical cellular stages of thymus maturation, double negative, double positive and single positive $CD4^+$ or $CD8^+$ T cells, was determined. The double negative cell subset was further analyzed for the proportion of DN3 and DN4 cells to draw conclusion for possible blocks in the distinct developmental steps.

3. Materials and methods

3.1. Materials

3.1.1. Chemicals

Chemicals were obtained from the following companies: Karl Roth GmbG & Co. KG (Karlsruhe, Germany), Jena Bioscience (Jena, Germany), Merck KGaA (Darmstadt, Germany), Sigma-Aldrich GmbH (Hannover, Germany), Amersham-Pharmacia (Freiburg, Germany), Qiagen (Hilden, Germany), GE Healthcare (Munich, Germany), BD Bioscience (Heidelberg, Germany) and Miltenyi Biotec GmbH (Bergisch Gladbach, Germany).

3.1.2. Enzymes

KOD DNA Polymerase	Novagen (Darmstadt, Germany)
PFU DNA Polymerase	Roboklon (Berlin, Germany)
T4 DNA Polymerase	New England Biolabs (Frankfurt a.M., Germany)
DNase I	Roche (Mannheim, Germany)
Restriction Nucleases (BamHI, XhoI, EcoRI, NotI, DpnI)	New England Biolabs (Frankfurt a.M., Germany)
Prescission Protease	GE Healthcare (Munich, Germany)
Trypsin, Chymotrypsin, Thermolysin, Subtilisin	Sigma Aldrich (Hannover, Germany)
Superscript III Reverse Transkriptase	Invitrogen (Darmstadt, Germany)
Proteinase K	Roth GmbG & Co. KG (Karlsruhe, Germany)

3.1.3. Clones

cDNA clones for the human (*Homo sapiens*), mouse (*Mus musculus*), zebrafish *(Danio rerio*) and frog (*Xenopus laevis*) PRR were purchased from imaGenes (Berlin, Germany).

3.1.4. Kits and standards

Kits

QIAgen Plasmid Purification (Mini) Kit	Qiagen (Hilden, Germany)
QIAquick Gel Extraction Kit	Qiagen (Hilden, Germany)
Rneasy Kit	Qiagen (Hilden, Germany)
DNAse Digest	Qiagen (Hilden, Germany)
Superscript III cDNA Synthesis Kit	Invitrogen (Darmstadt, Germany)
NuPageNovex Bis Tris precast gel system	Invitrogen (Darmstadt, Germany)

Kits

TaqMan® Fast Universal PCR Master Mix	Applied Biosystems (Carlsbad, USA)
CytoFix/CytoPerm Solution Kit	BD Bioscience (Heidelberg, Germany)
Bradford Protein Assay	BioRad (Munich, Germany)
$CD4^+$ T Cell Isolation Kit II	Miltenyi Biotec (Bergisch Gladbach, Germany)
CellTrace™ CFSE Cell Proliferation Kit	Invitrogen (Darmstadt, Germany)
mouse T cell activation and expansion Kit	Miltenyi Biotec (Bergisch Gladbach, Germany)

Standards

2-log, 100bp and 1kb DNA ladder	New England Biolabs (Frankfurt a.M., Germany)
Mark12 protein marker	Invitrogen (Darmstadt, Germany)
Unstained Protein Molecular Weight Marker	Fermentas GmbH (St.Leon-Rot, Germany)

3.1.5. Bacterial Strains

Strain	Genotype	
E. coli TG1 K12	*supE, hsdΔ5, thi, Δ(lac-proAB), F'[traD36, proAB+, lacIq, lacZΔM15]*	Promega (Mannheim, Germany)
E.coli Rosetta 2DE3	*F–, ompT, hsdSB(rB– mB–), gal dcm, (DE3), pRARE*	Novagen (Darmstadt, Germany)
E.coli Lemo21 (DE3)	*fhuA2 [lon] ompT gal (λ DE3) [dcm]* Δ*hsdS/ pL*emo(Cam^R)	New England Biolabs (Frankfurt, Germany
E.coli BL21(DE3) pLysS	*F–* omp*T* hsd*SB(rB–, mB–)* gal dcm *(DE3) pLysS (Cam^R)*	Invitrogen (Darmstadt, Germany)
E.coli SoluBl21	Optimized *E. coli* BL21 strain for expressing insoluble proteins in soluble form	Genlantis, (SanDiego, USA)
E.coli RosettaGami™ 2(DE3)	Δ(*ara-leu*)*7697* Δ*lacX74* Δ*phoA Pvu*II *phoR araD139 ahpC galE galK rpsL* (DE3) F′[lac^+ $lacI^q$ *pro*] *gor522*::Tn*10 trxB* pRARE2 (Cam^R, Str^R, Tet^R)	Novagen (Darmstadt, Gerrmany)

3.1.6. Media and antibiotics

Antibiotics	Concentration
Kanamycin	25 µg/mL
Chloramphenicol	34 µg/mL
Carbenicillin	60 µg/mL
Ampicillin	100 µg/mL

Antibiotics	Concentration
Streptomycin	50 µg/mL
Tetracyclin	15 µg/mL

Media	Composition
Luria Bertani (LB)	10 g/l Bactotryptone, 10 g/l NaCl, 5 mM NaOH, 5 g/l yeast extract
Terrific Broth (TB)	purchased from Roth GmbG & Co. KG (Karlsruhe, Germany), 12 g/l BactoTryptone, 24 g/l Bacto-yeast-extract, 4 g/l glycerol, 17 mM, 72 mM K_2HPO_4
Autoinduction Medium (AIM)	purchased from Novagen (Darmstadt, Germany)
M9 Minimal Medium	10 mL/L trace elements, 1mM $MgSO_4$, 0.3 mM $CaCl_2$, 100 ml/l M9 salt, 2 g/l Glucose, 1.5 mg/L Thiamine, 1.5 mg/l Biotin, 0,5 g/l NH_4Cl
M9 salt (10x)	64 g/l Na_2PO_4, 20 g/l KH_2PO4, 5 g/l NaCL, pH 7.2-7.3
M9 trace elements	5 g/l EDTA , 500 mg/l $FeSO_4$, 50 mg/l $ZnCl_2$, 10 mg/l $CoSO_4$, 10 mg/l $CuCl_2$, 10 mg/l H_3BO_3 , 1mg/l $MnCl_2$

3.1.7. Buffers

2x SDS sample loading buffer	100 mM Tris/HCl pH 6.8, 20 % Glycerol (v/v), 4 % SDS (w/v), 200 mmM DTT, 0.04 % (w/v) Bromphenol Blue
Lysis buffer for test expression	20 mM Hepes/NaOH pH 7.5, 150 mM NaCl, 1 µg/mL DNaseI, 0.1 mM Pefabloc, (2 mM DTT or 2 mM β-ME), 1 mg/mL Lysozyme I (Roth) or 1 Volume of BugBuster Lysis Buffer (Merck)
Lysis buffer for protein purification	20 mM Hepes/NaOH pH 7.5, 150 mM NaCl, 1 µg/mL DNaseI, 0.1 mM Pefabloc, (2 mM DTT or 2 mM β-ME)
Equilibration/ Wash buffer	20 mM Hepes/NaOH pH 7.5, 150-300 mM NaCl, (2 mM DTT or 2 mM β-ME)
Elution buffer for His fusion proteins	20 mM Hepes/NaOH pH 7.5, 150 mM NaCl, 150-300 mM Imidazol, (2 mM β-ME)
Elution buffer for GST fusion proteins	20 mM Hepes/NaOH pH 7.5, 150 mM NaCl, 20 mM glutathione , (2 mM DTT)
Gel filtration buffer	20 mM Hepes/NaOH pH 7.5, 150 mM NaCl, 0,2 µM filtered, degassed
SDS running buffer	25 mM Tris, 192 mM Glycine, 1 % (w/v) SDS
Coomassie fixation solution	10 % (v/v) Acetic acid, 50 % (v/v) Ethanol
Coomassie staining solution	10 % (v/v) Acetic acid, 0.025 % (w/v) Coomassie G250
TAE buffer	40 mM Tris, 20 mM acetic acid, 1 mM EDTA
PBS	Purchased from Invitrogen (Darmstadt, Germany)

FACS buffer	PBS + 0.1 % (v/v) FCS
Lysis buffer for genomic DNA isolation	50 mM Tris, 100 mM EDTA, 0.5 % (w/v) SDS

3.1.8. Plasmids

Plasmid	Properties	
pSKB2LNB2	Prokaryotic expression vector for high-level expression of N-terminally His_6-tagged fusion protein, PreScission cleavage site, Kan^R	Oliver Daumke, MDC
pGex6p1	Prokaryotic expression vector for high-level expression of N-terminally GST-tagged fusion proteins, PreScission cleavage site, Amp^R	GE Healthcare (Munich, Germany)

3.1.9. Constructs and mutants

The following is a list of all constructs generated for expression in E .coli.

Construct	Vector	*E.*coli strain	Remarks
hsPRR (15-288)	pSKB2LNB2	*Rosetta 2DE3*	not soluble
	pGex6p1	*Rosetta 2DE3*	low amount soluble, precipitates
hsPRR (15-300)	pSKB2LNB2	*Rosetta 2DE3*	not soluble
	pGex6p1	*Rosetta 2DE3*	low amount soluble, precipitates
		Lemo21 (DE3)	low expression, low amount soluble
		SoluBl21	low expression, low amount soluble
hsPRR (15-278)	pGex6p1	*Rosetta 2DE3*	not soluble expressed
hsPRR (15-257)	pGex6p1	*Rosetta 2DE3*	not soluble expressed
hsPRR (32-288)	pGex6p1	*Rosetta 2DE3*	not soluble expressed
hsPRR (32-278)	pGex6p1	*Rosetta 2DE3*	not soluble expressed
hsPRR (32-257)	pGex6p1	*Rosetta 2DE3*	not soluble expressed
hsPRR (170-303)	pGex6p1	*Rosetta 2DE3*	**soluble expressed**, precipitates
	pSKB2LNB2	*Rosetta 2DE3*	not soluble expressed
hsPRR (62-303)		*Rosetta 2DE3*	not soluble expressed
hsPRR (62-288)	pGex6p1	*Rosetta 2DE3*	not soluble expressed
hsPRR (62-300)	pGex6p1	*Rosetta 2DE3*	not soluble expressed
hsPRR (62-278)	pGex6p1	*Rosetta 2DE3*	not soluble expressed
hsPRR (62-257)	pGex6p1	*Rosetta 2DE3*	not soluble expressed
hsPRR (73-303)	pGex6p1	*Rosetta 2DE3*	not soluble expressed
hsPRR (73-288)	pGex6p1	*Rosetta 2DE3*	not soluble expressed

Construct	**Vector**	***E*.coli strain**	**Remarks**
hsPRR (73-300)	pGex6p1	*Rosetta 2DE3*	not soluble expressed
hsPRR (73-257)	pGex6p1	*Rosetta 2DE3*	not soluble expressed
hsPRR (140-302)	pGex6p1	*Rosetta 2DE3*	not soluble expressed
hsPRR (101-302)	pGex6p1	*Rosetta 2DE3*	not soluble expressed
hsPRR (15-177)	pGex6p1	*Rosetta 2DE3*	not soluble expressed
hsPRR (32- 177)	pGex6p1	*Rosetta 2DE3*	not soluble expressed
hsPRR (62- 177)	pGex6p1	*Rosetta 2DE3*	not soluble expressed
hsPRR (101-257)	pGex6p1	*Rosetta 2DE3*	**soluble expressed, GST co-purified with PRR**
	pGex6p1	*BL21(DE3) pLysS*	**soluble expressed**
	pSKB2LNB2	*Rosetta 2DE3*	**soluble expressed, highest yield**
hsPRR(101-257) S104G	pGex6p1	*Rosetta 2DE3*	**soluble expressed, GST sticks to PRR**
	pSKB2LNB2	*Rosetta 2DE3*	**soluble expressed**
hsPRR (132-257)	pGex6p1	*Rosetta 2DE3*	not soluble expressed
hsPRR (140-302)	pGex6p1	*Rosetta 2DE3*	not soluble expressed
hsPRR (132-302)	pGex6p1	*Rosetta 2DE3*	not soluble expressed
hsPRR (101-302)	pGex6p1	*Rosetta 2DE3*	not soluble expressed
hsPRR (106-257)	pGex6p1	*Rosetta 2DE3*	not soluble expressed
hsPRR (106-278)	pGex6p1	*Rosetta 2DE3*	not soluble expressed
hsPRR (106-288)	pGex6p1	*Rosetta 2DE3*	not soluble expressed
hsPRR (106-302)	pGex6p1	*Rosetta 2DE3*	not soluble expressed
hsPRR (101-278)	pGex6p1	*Rosetta 2DE3*	not soluble expressed
hsPRR (101-288)	pGex6p1	*Rosetta 2DE3*	not soluble expressed
hsPRR(15-300)S104G	pGex6p1	*Rosetta 2DE3*	not soluble expressed
hsPRR (32-278) S104G	pGex6p1	*Rosetta 2DE3*	not soluble expressed
hsPRR (62-288) S104G	pGex6p1	*Rosetta 2DE3*	not soluble expressed
hsPRR(101-302) S104G	pGex6p1	*Rosetta 2DE3*	not soluble expressed
hsPRR (120-257)	pSKB2LNB2	*Rosetta 2DE3*	not soluble expressed
		BL21(DE3) pLysS	not soluble expressed
	pGex6p1	*Rosetta 2DE3*	not soluble expressed
		BL21(DE3) pLysS	very low amount soluble
hsPRR (141-257)	pSKB2LNB2	*Rosetta 2DE3*	no over expression
		BL21(DE3) pLysS	no over expression
	pGex6p1	*Rosetta 2DE3*	no over expression
		BL21(DE3) pLysS	no over expression

Construct	**Vector**	***E*.coli strain**	**Remarks**
hsPRR (166-257)	pSKB2LNB2	*Rosetta 2DE3*	**soluble expressed, highest yield**
		BL21(DE3) pLysS	**soluble expressed**
	pGex6p1	*Rosetta 2DE3*	**soluble expressed**
		BL21(DE3) pLysS	**soluble expressed**
hsPRR (166-269)	pSKB2LNB2	*Rosetta 2DE3*	soluble expressed, dirty
hsPRR (174-257)	pSKB2LNB2	*Rosetta 2DE3*	soluble expressed, dirty
hsPRR(170-302) SER KQAK284-287 AAAA	pSKB2LNB2	*Rosetta 2DE3*	not soluble expressed
hsPRR(101-257) SER EE120/121 AA	pGex6p1	*Rosetta 2DE3*	low overexpression, not soluble expressed
hsPRR(101-257) SER EE 131/132 AA	pGex6p1	*Rosetta 2DE3*	low overexpression, not soluble expressed
hsPRR(15-300) SER KE 55AA	pSKB2LNB2	*Rosetta 2DE3*	not soluble expressed
hsPRR(15-300) SER EE120/121 AA	pSKB2LNB2	*Rosetta 2DE3*	not soluble expressed
hsPRR(15-300) SER EE 131/132 AA	pSKB2LNB2	*Rosetta 2DE3*	not soluble expressed
hsPRR(15-300) SER KQAK284-287 AAAA	pSKB2LNB2	*Rosetta 2DE3*	not soluble expressed
hsPRR(166-257) 201 AAAAAAA 207	pSKB2LNB2	*Rosetta 2DE3*	soluble expressed, high yield higher expression w/o mutation
mm PRR (16-288)	pSKB2LNB2	*Rosetta 2DE3*	not soluble expressed
	pGex6p1	*Rosetta 2DE3*	not soluble expressed
mm PRR (16-300)	pSKB2LNB2	*Rosetta 2DE3*	not soluble expressed
	pGex6p1	*Rosetta 2DE3*	not soluble expressed
mm PRR (101-257)	pSKB2LNB2	*Rosetta 2DE3*	not soluble expressed
mm PRR (166-257)	pSKB2LNB2	*Rosetta 2DE3*	low amount of soluble protein
xl PRR (98-254)	pSKB2LNB2	*Rosetta 2DE3*	no expression
xl PRR (163-254)	pSKB2LNB2	*Rosetta 2DE3*	low amount of soluble protein
xl PRR (14-286)	pSKB2LNB2	*Rosetta 2DE3*	low expression, not soluble
	pGex6p1	*Rosetta 2DE3*	no expression
xl PRR (14-298)	pSKB2LNB2	*Rosetta 2DE3*	no expression
	pGex6p1	*Rosetta 2DE3*	no expression

Construct	**Vector**	***E*.coli strain**	**Remarks**
dr PRR (99-255)	pSKB2LNB2	*Rosetta 2DE3*	low amount of soluble protein
dr PRR (164-255)	pSKB2LNB2	*Rosetta 2DE3*	**soluble expressed**
dr PRR (15-287)	pSKB2LNB2	*Rosetta 2DE3*	not soluble expressed
	pGex6p1	*Rosetta 2DE3*	not soluble expressed
dr PRR (15-299)	pSKB2LNB2	*Rosetta 2DE3*	not soluble expressed
	pGex6p1	*Rosetta 2DE3*	not soluble expressed
hs Renin (23-407)	pSKB2LNB2	*Rosetta 2DE3*	low expression, not soluble
		RosettaGami	no expression
	pGex6p1	*Rosetta 2DE3*	not soluble expressed
		RosettaGami	no expression
hs Prorenin (66-407)	pSKB2LNB2	*Rosetta 2DE3*	low expression, not soluble
		RosettaGami	no expression
	pGex6p1	*Rosetta 2DE3*	not soluble expressed
		RosettaGami	no expression
mm Renin2 (86-425)	pSKB2LNB2	*Rosetta 2DE3*	no expression
	pGex6p1	*Rosetta 2DE3*	not soluble expressed
mm Prorenin2 (48-425)	pSKB2LNB2	*Rosetta 2DE3*	no expression
	pGex6p1	*Rosetta 2DE3*	not soluble expressed
rn Renin (64-403)	pSKB2LNB2	*Rosetta 2DE3*	low expression, not soluble
	pGex6p1	*Rosetta 2DE3*	not soluble expressed
rn Prorenin (26-403)	pSKB2LNB2	*Rosetta 2DE3*	low expression, not soluble
	pGex6p1	*Rosetta 2DE3*	not soluble expressed
coexpression			
hs Renin (23-407) +	pGex6p1	*Rosetta 2DE3*	no expression
hs PRR (15-300)	pSKB2LNB2		
hs Renin (23-407) +	pGex6p1	*Rosetta 2DE3*	low expression PRR, not soluble,
hs PRR (15-288)	pSKB2LNB2		no expression Renin
hs Prorenin (66-407) +	pGex6p1	*Rosetta 2DE3*	low expression PRR, not soluble,
hs PRR (15-300)	pSKB2LNB2		no expression Renin
hs Prorenin (66-407) +	pGex6p1	*Rosetta 2DE3*	low expression PRR, not soluble,
hs PRR (15-288)	pSKB2LNB2		no expression Renin

3.1.10. Antibodies and staining reagents for flow cytometry

Specificity	Conjugate	Manufacturer
mCD3	APC cy7	BD Bioscience (Heidelberg, Germany)
mCD4	Cy5	BD Bioscience (Heidelberg, Germany)
	biotinylated	DRFZ (Berlin, Germany)
mCD8a	PE	BD Bioscience (Heidelberg, Germany)
	biotinylated	DRFZ (Berlin, Germany)
mCD25	PE	BD Bioscience (Heidelberg, Germany)
mCD44	Cy5	BD Bioscience (Heidelberg, Germany)
mCD45	FITC	BD Bioscience (Heidelberg, Germany)
mCD45R	biotinylated	BD Bioscience (Heidelberg, Germany)
Streptavidin	PerCP	BD Bioscience (Heidelberg, Germany)
Annexin V	Cy5	BD Bioscience (Heidelberg, Germany)

3.1.11. Recombinant proteins

Recombinant human Renin, 6xHisRenin and 6xHisProrenin were provided by Actelion Pharmaceuticals Ltd. (Allschwil, Switzerland).

3.1.12. Animals

The animals used for this work were bred under pathogen free conditions in the animal care unit of the MDC.

Strain	Genotype	Obtained from
C57/BL6	floxed PRR	Genevieve Nguyen, College de France, Paris
C57/BL6	LcK Cre	Achim Leutz, MDC, Berlin

3.1.13. Primers and oligonucleotides

Primers and oligonucleotides were synthesised by Biotez (Berlin, Germany)

Genotyping primer

Name	Sequence (5´-3´)
PRR 1 fw(Lf)	5´ AGC ACT CTC TTC CAG GTA TGT TGT G 3´
PRR 2 fw (Ef)	5´CTG GAT CCC GGA GCA TGG GTA AAG G 3´
PRR rev (Er)	5´ GCT GTC CAAAGA AAC CAG AGC C 3´
Lck cre fw	5´GCT GCC ACG GCC AAG TG 3´
Lck cre rev	5´TCG GCA TCT TCC AGC AG 3´

The primer and oligonucleotides for real-time PCR were designed using Primer Express®ABI PRISM software to be species specific (except for the eukaryotic18s primer and probe) and exon overlapping.

Name	Sequence 5´-3´
r18s fw	5´ ACATCCAAGGAAGGCAGCAG 3´
r18s rev	5´ TTTTCGTCACTACCTCCCCG 3´
r18s probe	5´ FAM-CGCGCAAATTACCCACTCCCGAC-TAMRA 3´
mmPRR fw	5' CCAGTTTGTTGTCTCGTCATAAGC 3'
mmPRR rev	5' ACCTGCCAGCTCCAATGAAT 3'
mmPRR probe	5' FAM-TCTAGCCAAGGACCATTCACCCGACTT-TAMRA 3'

3.1.14. Hardware

NanoDrop®ND1000	PEQLAB Biotechnologie GMBH (Erlangen, Germany)
7500 Fast Real-Time PCR System	Applied Biosystems (Carlsbad, USA)
FACSCanto	BD Bioscience (Heidelberg, Germany)
Viscotek 270 Dual detector	Malvern Instruments Ltd. (Worcestershire, UK)
Microfluidiser	Microfluidics (Newton, USA)
XL-A type analytical ultracentrifuge	Beckman Coulter (Palo Alto, USA)
Jasco L-720 spectropolarimeter	Jasco Corp. (Hachioji, Japan)
Hydra plus one crystallization robot	Thermo Scientific (Karlsruhe, Germany)

3.1.15. Software

7500 Fast System Software	Applied Biosystems (Carlsbad, USA)
Primer Express®ABI PRISM	Applied Biosystems (Carlsbad, USA)
Netprimer	PREMIER Biosoft International (Palo Alto,USA)
OmniSec	Malvern Instruments Ltd. (Worcestershire, UK)
Bioedit	IbisBiosciences (Carlsbad, USA)
GraphPadPrism	GraphPad Software, Inc. (San Diego, USA)
FlowJo	Tree Star, Inc. (Ashland, USA)
FACS Diva	BD Bioscience (Heidelberg, Germany)
Sedfit	Peter Schuck [135]
Sedphat	Peter Schuck [135]

3.1.16. Statistics

All experiments were analysed for at least n=5 for the WT groups and n=3 (spleen) or n=4 (thymus) for the KO group. All statistical tests were performed using GraphPadPrism. The data were analyzed for Gaussian distribution by using the Kolmogorov-Smirnov-test. Because of the low amount of animals per KO group, a Gaussian distribution could not be confirmed for all of the KO groups. Therefore, the Mann-Whitney-test was used to test for significance between the WT and KO group. For the analysis of the different cell subsets in the thymus, a one-way-ANOVA with Tukey post-hoc test was used. Results were considered significant if the p-value was $(p) < 0.05$.

3.2. Molecular biology methods

3.2.1. Construct design

The constructs were designed based on sequence alignments program (ClustalW algorithm [136]) and a secondary structure predictions (Jpred3 [137]). The sequence alignment is in the appendix.

3.2.2. Polymerase chain reaction (PCR)

Amplification of DNA fragments was performed using *Pfu* DNA polymerase (Roboklon) following standard protocols described in Sambrook et al. [138].

3.2.3. Restriction digest

Plasmid DNA and PCR fragments were digested with restriction enzymes obtained from New England Biolabs, according to the manufacturer's protocol.

3.2.4. Agarose gel electrophoresis

Agarose gel electrophoresis was performed according to standard procedures [138].

3.2.5. DNA gel extraction

PCR fragments or digested Plasmid DNA were first run on an agarose gel. Fragments of the expected size were cut from the gel and subsequently purified with the QIAquick Gel Extraction kit (Qiagen), according to the manufacturer's protocol. The quality and quantity of purified DNA was determined with a Nanodrop spectrophotometer (Peqlab) at a wavelength of 260 nm.

3.2.6. Ligation

Ligation was performed overnight at 4°C using 12 ng of digested vector and a 12 molar excess of the purified insert after addition of T4 DNA ligase (New England Biolabs).

3.2.7. Transformation

Ligation products were cloned into the *TG1 K12 E.coli* strain according to the heat shock method of Sambrook et al. [138]. For protein expression, purified and sequence verified plasmids were transformed into *Rosetta 2DE3*, *BL21 (DE3) pLysS, Lemo21 (DE3)* or *SoluBl21 E.coli* strains using standard protocols.

3.2.8. Preparation of heat competent *E.coli* cells

Competent cells were prepared according to the protocol of Chung et.al. [139]. Bacteria were grown at 37°C in 200ml of LB medium from a 2 ml overnight pre-culture, until an OD_{600nm} of 0.4-0.5 was reached. The cells were incubated for 20 min on ice, then centrifuged for 5 min at 1,200 *g* and 4°C, and then the pellet was resuspended in 20 ml of ice-cold sterile TSS buffer (85% LB medium without NaOH, 10% PEG8000 or 3350, 5% DMSO, 50 mM MgCl2, pH 6.5). *E.coli* cells were then aliquoted, flash frozen and stored at -80°C.

3.2.9. Plasmid purification

Plasmids were purified from 5mL overnight cultures with the Plasmid Purification Mini Kit (Qiagen), according to the manufacturer's protocol. Quality and quantity of purified DNA was determined with a Nanodrop spectrophotometer (Peqlab) at a wavelength of 260 nm.

3.2.10. Site directed mutagenesis

Mutagenesis of plasmids was performed using a site directed mutagenesis PCR kit, using KOD DNA polymerase (Novagen), followed by digest with Dpn1 (New England Biolabs) and transformation into the *TG1 K12 E.coli* strain. All steps were performed according to the Quick Change protocol (Stratagene).

3.2.11. Bacterial storage

E.coli transformed with the desired plasmid were grown overnight and glycerol stocks were prepared according to standard procedures and then stored at -80 °C.

3.2.12. RNA isolation

Cells or tissues were homogenized in a Precelly24 homogenater (Peqlab) by adding Qiazol lysis reagent (Qiagen) and 2.8 mm ceramic beads (Peqlab). After centrifugation the aqueous RNA phase was applied onto spin columns of RNAeasy Kit (Qiagen). An on-column DNAse digest (Qiagen) was performed after first washing the bound RNA once. All other steps were performed according to the RNAeasy manual. The quality and quantity of the RNA was determined with a Nanodrop spectrophotometer at a wavelength of 260 nm.

3.2.13. cDNA transcription

2 µg of purified RNA was transcribed to cDNA using the Superscript III cDNA Synthesis Kit (Invitrogen) according to the manufacturer's protocol.

3.2.14. Real-Time PCR

Real-Time PCR was performed on a 7500 Fast Real-Time PCR System using TaqMan® Fast Universal PCR Master Mix (both Applied Biosystems) according to the manufacturer's protocol. Per sample, 0.2 ng cDNA was used and all samples were measured in triplicate. Data was evaluated with the 7500 Fast System Software (Applied Biosystems) and the samples were normalized against a housekeeper gene, 18s.

3.2.15. Mouse genotyping

Isolation of genomic DNA from tail cuts was performed with the direct PCR Tail lysis reagent (Peqlab), following the manufacturer's protocol .The genomic DNA was amplified with the REDTaq® ReadyMix™ PCR Reaction Kit (Sigma Aldrich) according to the manual. Fragments were analyzed on an agarose gel.

3.2.16. Isolation of genomic DNA

DNA was isolated from different organs and cells with Phase Lock Gel™ tubes (5Prime, Hamburg, Germany) and a phenol/chloroform extraction of nucleic acids was performed according to the manufacturer's protocol.

3.3. Biochemical methods

3.3.1. SDS-polyacrylamide gel electrophoresis (SDS-PAGE)

SDS-PAGE was performed for the separation of proteins of different molecular weight based on the standard protocol described by Laemmli et al. [140]. Alternatively, purchased gradient gels NuPAGE® Novex 4-12 % Bis-Tris (Invitrogen) were used according to the manufacturer's protocol. Samples were mixed with a 2x SDS sample loading buffer (see 3.1.7.), boiled for 5 min at 95 °C and then loaded onto the gel.

3.3.2. Coomassie staining

SDS-polyacrylamide gels were first fixed in coomassie fixation solution (see 3.1.7.) for at least 15 minutes, and then stained in coomassie staining solution for a minimum of 15 min. Gels were then washed with water until the background went clear.

3.3.3. Determination of protein concentration

Protein concentration was determined using a Nanodrop spectrophotometer (Peqlab) at a wavelength of 280 nm. The concentration was calculated according to the Beer-Lambert equation using the respective molecular weight and the extinction coefficient [141]. Additionally, the Bradford Protein Assay (Roth) was used according to the manufacturer's protocol [142].

3.3.4. Small-scale over-expression and solubility test

For small-scale over-expression and solubility test, respective plasmids were transformed into the required *E.coli* expression strains (see 3.1.5. and 3.2.7.). These test inductions were performed with an auto induction media (AIM) (Novagen). AIM enables the growth of IPTG-inducible expression strains and induces target protein expression automatically. This is achieved as follows: The media contains a limited concentration of glucose. By depletion of glucose during mid to late log growth phase, lactose is taken up and converted into allolactose. Allolactose induces expression of the T7 RNA polymerase and its target proteins [143]. Fresh overnight colonies were used to inoculate 1 ml of AIM in 24-well plates. The 24-well plates were then incubated for 8 hours at 37°C and 900 rpm on a thermomixer (Eppendorf). Afterwards, the temperature was lowered to 20 °C and cultures were incubated overnight. After approximately 18-20 hours, bacterial cells were harvested by centrifugation for 15 min at 4 °C and 5000 rpm. To aid with lysis, the cell pellet was first frozen at -80 °C

for at least 30 min or quickly frozen in liquid nitrogen. The pellet was then resuspended in 300 µL of lysis buffer (see 3.1.7.) and incubated for 30 min at 15 °C and 350 rpm on a thermomixer. An aliquot was taken from the lysate for analysis of the induced sample by SDS-PAGE. The lysate was then centrifuged for 20 min at 4 °C and 13000 rpm. A sample from the supernatant was taken for analysis of the soluble proteins by SDS-PAGE. All samples for SDS-PAGE were then mixed with 2x SDS sample loading buffer and then loaded on to the gel. After Coomassie staining, the gel was scrutinized for the presence of soluble recombinant protein. Positive clones with relatively high soluble expression were then used for large scale expression and purification (see 3.3.5. and 3.3.6.). In some cases, small-scale affinity purification was performed. Here, the supernatant was incubated with 50µl of Talon resin or GSH sepharose. The beads were washed once, and then the protein was eluted with the respective buffer (see 3.1.7.)

3.3.5. Large-scale over-expression

A fresh overnight culture in LB media was used to inoculate (1:100) 5 to 10 L of TB media including antibiotics. Cultures were incubated at 37 °C under constant shaking until an OD_{600nm} of 0.4-0.5 was reached. Cells were then cooled to 18 °C and protein expression was induced by the addition of Isopropyl-β-D-thiogalactopyranosid (IPTG; 40µM). Proteins expression was induced overnight. Bacteria were harvested by centrifugation for 15 min at 4°C and 5000 rpm. Pellets were then resuspended in lysis buffer (see 3.1.7.) and used directly for large scale purification or stored at -30°C. For NMR experiments and over-expression in *SoluBl21*, cells were grown in minimal media under the same conditions.

3.3.6. Large-scale purification

3.3.6.1.Cell lysis and sample preparation

Frozen cells were first thawed in cold water. DNase I was then added and the cells were lysed with a microfluidiser (Microfluidics, Newton, USA). The lysate was centrifuged for 30-45 min at 35000rpm and 4°C. The supernatant was then passed through a 0.45 µM or 0.2 µM filter to prevent obstruction of the purification columns. Aliquots of the induced lysate and lysate supernatant fractions were removed for subsequent analysis on SDS-PAGE.

3.3.6.2.Affinity chromatography

The supernatant was applied onto an equilibrated affinity chromatography column with a flow rate of 1-2 ml/min. Depending on the expression vector and the corresponding tag, these

columns were either a 5-10ml Talon cobalt affinity column (Clontech, Saint-Germain-en-Laye, France) or a 10-20 ml reduced glutathione (GSH)-Sepharose column (GE Healthcare). The columns were then washed with at least 15 column volumes of washing buffer (see 3.1.7.). The GSH column was furthermore treated with a washing buffer with high salt (300mM) conditions. Bound protein was then eluted in 5 ml fractions with the corresponding elution buffer (see 3.1.7.). The GSH elution buffer was additionally incubated for 5 to 10 min with the column material before elution. The eluted fractions were analyzed with Bradford Reagent (Roth) for protein content. Aliquots for flow through, wash and elution fractions were taken for analysis on SDS-PAGE.

3.3.6.3.Tag cleavage

The protein concentration of the elution fractions were determined and analyzed for purity on SDS-PAGE. The fractions with the highest yield and purity were then pooled. Tag cleavage was performed overnight at 4°C with approximately 10µg of Prescission Protease per 1mg of eluted protein. As the protease is active under reducing conditions, if the elution buffer did not contain a reducing reagent, 2 mM DTT or 2mM β-ME were added. All samples were first dialysed overnight at 4°C against the gel filtration buffer (see 3.1.7.) to dilute the imidazol or gluthathione concentration. In some cases, the GST-tagged proteins were directly cleaved on the column material. Here, the GST remains bound to the column whilst the un-tagged protein is washed out after cleavage. Analysis of cleavage success was analysed by SDS-PAGE.

3.3.6.4.Removal of Prescission Protease

All samples were passed over a 1ml GSH column to remove the GST tagged Prescission Protease and the cleaved GST tag (for GST-tagged proteins). All His-tagged proteins were additionally passed over a Talon column again to remove any contaminating proteins.

3.3.6.5.Size-exclusion chromatography

The final purification step was size exclusion chromatography. The protein was first concentrated with amicon filters (Millipore) and centrifuged for 10 min at 4°C and 13000 rpm to remove precipitate. Depending on the molecular weight and the amount of protein, the concentrated sample was then run on either a Superdex 200 or Superdex 75 in 16/60 or 26/60 gel filtration columns (GE Healthcare). The elution fractions were analyzed on SDS-PAGE and the fractions corresponding to the respective protein were pooled.

3.3.7. Protein storage

Purified protein samples were concentrated with amicon filters (Millipore) and the concentration was determined (3.3.3.). Small aliquots were flash frozen in gel filtration buffer (see 3.1.7.) liquid nitrogen and stored at -80°C.

3.3.8. GST pull-down assay

For GST pull-down assays, the GST tag was not cleaved from the recombinant PRR proteins. Recombinant human renin or prorenin was then incubated with equimolar amounts of GST-tagged PRR proteins. The mixture was incubated overnight at 4°C with GSH Sepharose. The next day, unbound proteins were washed from the beads and the bound protein was eluted with elution buffer (3.1.7.). Aliquots from the unbound and bound fraction were then analyzed by SDS-PAGE.

3.3.9. Limited proteolyis assay

During this assay, protein samples are incubated with low concentrations of proteases. Flexible regions within the protein structure are preferentially cut by the proteases, thereby the stable structural region of the protein can be identified. This then allows the design of more stable proteins, which would be more likely to crystallise. The proteins were incubated with the following proteases: Trypsin, Thermolysin, Subtilisin and Chymotrypsin at two dilutions (1:100, 1:1000). The samples were incubated for 20 min either at 4°C or 37°C. Proteolysis was stopped by the addition of 2x SDS loading buffer, and the samples were then analyzed by SDS-PAGE. The protein fragments were cut from the SDS-PAGE and digested with trypsin for identification by mass spectrometry. Mass spectroscopy experiments and data analysis were performed by Gunnar Dittmar (MDC).

3.3.10. Chemical cross-linking

Chemical cross-linking was performed to examine if the proteins formed dimers or higher oligomers. Bis[sulfosuccinimidyl] suberate (BS^3) (Thermo Scientific) contains an amine-reactive *N*-hydroxysulfosuccinimide (NHS) ester that reacts with primary amines at pH 7-9 to form stable amide bonds. All cross linking experiments were performed according to the manufacturer's protocol. After cross-linking samples were analyzed on SDS-PAGE.

3.4. Biophysical methods

3.4.1. Right-angle light-scattering (RALS)

Right-angle light-scattering measures the intensity of the scattered light to determine the average molecular weight (Mw) of a protein. With this method it is therefore possible to obtain information about the monomeric or oligomeric state of a protein [144]. A refractive index and UV detector were coupled to a RALS system (Viscotek 270 Dual detector, Malvern Instruments). All detectors were connected in line with an analytical (Superdex 200 or Superdex 75, 10/300) gel filtration column (GE Healthcare) at 4°C. The whole system was equilibrated for at least 3 column volumes at a flow rate of 0.5ml/min with gel filtration buffer (see 3.1.7.). The protein samples were first filtered through a 0.2µm filter and then loaded onto the column. For each sample, 100 µl of a 0.5 -10 mg/ml solution was used. Data was analyzed with the OmniSec software (Malvern).

3.4.2. Circular dichroism (CD)

Circular dichroism (CD) spectroscopy measures the difference in the absorbance of right- and left-circularly polarized light. CD is monitored between 260 and 180 nm for analysis of protein secondary structure. Alpha-helix, beta-sheet, and random coil structures each give rise to a characteristic CD spectrum. Alpha-helical proteins typically have peaks of negative ellipticity at 222nm and 208 nm, whilst predominantly beta-sheet proteins have a single peak of negative ellipticity at 218nm [145-149].

CD spectra were recorded on Jasco L-720 spectropolarimeter (Jasco Corp.) or on a Chirascan Circular Dichroism Spectrometer (Applied Photophysics). The samples were routinely measured at 20ºC (unless indicated) with a resolution of 1nm over the wavelength range of 180-260nm. Samples in NaCl buffer were dialysed into buffer containing NaFl, because Cl interferes with the measurement. Samples were diluted to 0.2mg/ml and transferred to 1mm cuvettes. To estimate the percentage of alpha-helical, beta-sheet or random-coil secondary structure, the data was analyzed with a protocol established by Sandro Keller (University Kaiserslautern). The specific melting temperature (Tm) of each protein was determined by heating the samples 1°C per minute from 4°C to 94°C. A CD signal at 222nm was obtained at every temperature interval. A full CD spectrum (180-260nm) was also measured before and after the Tm analysis, to monitor if the proteins had precipitated during the experiment.

3.4.3. Analytical Ultracentrifugation (AUC)

All experiments were performed in a XL-A type analytical ultracentrifuge (Beckman) equipped with UV absorbance optics.

3.4.3.1.Sedimentation velocity

Sedimentation velocity is an analytical ultracentrifugation (AUC) method that measures the rate at which molecules move in response to centrifugal force. The time course of sedimentation provides information about the molecular mass and the shape of molecules that is described by the sedimentation coefficient, Svedberg (S) [135, 150, 151].

Sedimentation velocity experiments were carried out in two-channel cells with a total volume of 360µL for each sample. The concentration of the protein samples were chosen to have an optimal absorbance at 280nm between OD 0.1-1. Samples were centrifuged at 40000 rpm and 20°C. Sedimentation velocity profiles were analyzed with the program SEDFIT [135], using a model for continuous c(s) distribution.

3.4.3.2.Sedimentation equilibrium

Sedimentation equilibrium is the analysis of the steady-state dispersion of a protein in a centrifugal cell, achieved when the rate of sedimentation of the protein is equal to the opposing rate of diffusion. Thereby, sedimentation equilibrium is insensitive to the shape of the macromolecule and directly reports the molar mass.

Sedimentation equilibrium experiments were carried out using six-channel cells with a 12 mm optical path length and a total volume for each sample of 70 µl. Molecular mass studies of hsPRR 166-257 were performed at several different protein concentrations (0.25, 0.5, 0.75, 1, 1.5, 2 mg/mL). The samples were centrifuged at 20000, 25000 and 35000 rpm until equilibrium was reached (overnight). Radial scans with a step size of 0.001 cm was recorded at equilibrium and the data was analyzed with the programs SEDFIT and SEDPHAT [135] using the species analysis model.

3.4.4. Protein crystallization trials

Proteins can form crystals under certain conditions. Nucleation is the starting point for crystallization and happens at high levels of supersaturation. A crystal is a regular and periodic arrangement of proteins in a three dimensional manner and is the basis for protein x-ray crystallography. Crystallization trials were performed with the hsPRR(170-303), hsPRR(101-257), hsPRR(166-257), hsPRR(166-257) $_{201AAAAAA207}$ and drPRR(164-255). Commercially available crystal screens such as pHClear, pHClear II, Classics, Classics II,

ClassicsLite, JCSG, JBS, JBS/JCSG, PEGs and PEGs II, from Qiagen, Hampton Research and Jena Bioscience were used for initial screens. Protein concentrations ranged from 5-40mg/mL. Crystallisation drops for the various screens were pipetted with the Hydra plus one robot (Thermo Scientific), using the sitting-drop vapour-diffusion method. In each trial, 300 nl of protein and 300 nl crystallization buffer were spotted onto the crystal plate (Crystal Quick 96 well plates, Greiner BioOne) with an additional 75 µl of reservoir solution. For the hsPRR 166-257 and the hsPRR 101-257 additional manual screens using the hanging-drop vapour-diffusion method were made. In these cases, 24-well plates (SuperClear Pregreased 24-well plates, Crystalgen) were used for the screens with a reservoir volume of 750µL. 1µl of protein and 1µL of crystallization buffer were mixed on a coverslip, which was then suspended over the resorvoir. Different precipitants (PEGs, isopropanol, ammonium sulfate, MPD), buffer (pH ranging from 4.5-9) and salt (48 different ions) conditions were successively tested. The best conditions were considered for the design and preparation of the following screen. In both the screens and manual trials, plates were stored at 4°C or 20°C.

3.4.5. Nuclear magnetic resonance (NMR) spectroscopy

Solution-state nuclear magnetic resonance (NMR) spectroscopy is a method which is used to obtain structural and functional information about molecules; ranging from small chemical compounds up to proteins with a maximal molecular weight of ~35 kDa. Only isotopes with an odd number of neutrons and protons have a spin. The spin is required to be observable in NMR. Therefore it is necessary to isotopically label the protein with ^{13}C and ^{15}N. The naturally occurring isotope ^{12}C is not NMR active. In $^{1}H–^{15}N$ heteronuclear single-quantum correlation spectroscopy (HSQC) the frequencies for the $^{1}H–^{15}N$ are correlated. This method gives one peak per pair of bonded nuclei. Thus, for every amino acid, one signal for the backbone amide group (except proline) should be detected.

For the HSQC experiment hsPRR (166-257) was single labelled with ^{15}N isotopes (see 3.3.5.). The sample was then measured at a concentration of 1 mM in 100 mM NaCl and 50 mM phosphate buffer pH 7.5 at 20 °C (AV750, spectrophotometer, Bruker). All NMR experiments were performed in collaboration with Peter Schmieder (FMP, Berlin).

3.5. Cell biological methods

3.5.1. Isolation of lymphocytes from blood

Blood was isolated from 6-8 week old mice using heparinised syringes. 1 volume of blood was incubated with 9 volumes of erythrocyte lysis buffer (155mM NH_4Cl, 10mM $NaHCO_3$, 1mM EDTA) for 5 min at 37°C. The reaction was stopped by the addition of 1 volume of ice cold PBS + 0.1% FCS and the lymphocytes were then washed twice with PBS + 0.1% FCS. Purified cells were counted with the Countess Automated Cell Counter (Invitrogen) and analyzed for cell vitality with trypan blue staining.

3.5.2. Isolation of single cell suspensions from spleen and thymus

Splenocytes were isolated from 6-8 week old mice and thymocytes were isolated from 4-6 week old mice. Tissues were kept in ice cold PBS + 0.1% FCS and all steps were performed on ice. Spleen and thymus samples were first passed through a 70µM cell strainer (BD Bioscience) and were then washed twice with PBS + 0.1% FCS. Purified cells were counted and analyzed for cell vitality.

3.5.3. $CD4^+$ cell isolation

$CD4^+$ cells were isolated from spleen and lymph node cell suspensions of 6-8 week old mice. $CD4^+$ cells were purified using the $CD4^+$ T Cell Isolation Kit II (Milteny) according to manufacturer's recommendation. Purity of the cell isolation was confirmed by staining the cells with a $CD4^+$ antibody and analyzing by flow cytometry (see 3.5.5).

3.5.4. Isolation of $CD4^-/CD8^-$ double negative lymphocytes

$CD4^-/CD8^-$ double negative lymphocytes were isolated from the thymus using magnetic cell sorting (MACS). First, thymocytes were separated (see 3.5.2.) and erythrocytes were lysed (see 3.5.1.). Then, $CD4^+$, $CD8^+$ single or double positive cells were stained and removed by MACS, thereby enriching the $CD4^-/CD8^-$ double negative lymphocytes that pass through the column. The cells were pre-incubated for 10 min with a blocking reagent (Fcγ, RZPD) and then stained with biotinylated $mCD4^+$ and biotinylated $mCD8^+$ antibodies (1:100) for 10 min at 4°C. After washing, the thymocytes were then incubated with anti Biotin Microbeads (Milteny) for 15 min and isolated with a QuadroMACS separator and LS columns (Milteny), according to the manufacturer's protocol.

3.5.5. Flow cytometry

Flow cytometry is a method where the size and phenotype of single cells are characterized as they pass through a laser beam. The scattered light provides information simultaneously about size and granularity of cells, whilst the fluorescence emission gives information about the cellular expression of membrane bound or intracellular proteins that were first stained with fluorescently labelled antibodies. All experiments were performed on FACSCanto (BD Bioscience) and data was analyzed using the programs FACSDiva and FlowJo software.

For extracellular staining, $1x10^6$ cells in 100 µL of FACS buffer were incubated with the desired fluorescently labelled antibodies for 15 min at 4°C in the dark. If necessary, the cells were incubated with a second antibody after a single washing step. For intracellular staining, the cells were first permeabilized using the CytoFix/CytoPerm Solution Kit (BD Bioscience), according to the manufacturer's protocol. Antibody incubation of permeabilized cells was performed as for extracellular staining protocol.

3.5.6. Apoptosis staining

When cells undergo apoptosis, phosphatidylserine translocates from the intracellular to the extracellular side of the cell membrane. Annexin V binds to phosphatidylserine and is detectable on the cell surface. Purified and prestained (CD4, CD8) cells were stained with Cy5 labelled Annexin V (BD Bioscience) according to the manufacturer's protocol and analyzed by flow cytometry (see. 3.5.5)

4. Results

4.1. Expression and design of recombinant PRR proteins

4.1.1. Protein test-expression and solubility

One aim of this thesis was to structurally and biochemically characterize PRR. As it has been previously found that the full-length PRR (containing the transmembrane region) could not be purified (*personal communication*, G. Nguyen, College de France), the focus was set on the expression on the soluble, extracellular domain (Figure 8). The first step for the structural and biochemical characterisation of a protein is the production of sufficient amounts of recombinant protein of high purity. An *E.coli* expression system was used, because high amounts of protein can be purified and the system is time and cost efficient. *E.coli* was also suitable because no post-translational modifications such as glycosylation are known for PRR. These are limitations for bacterial expression systems.

The constructs were designed based on sequence alignments (ClustalW algorithm [136]) and secondary structure predictions (Jpred3 [137]) (see Appendix).

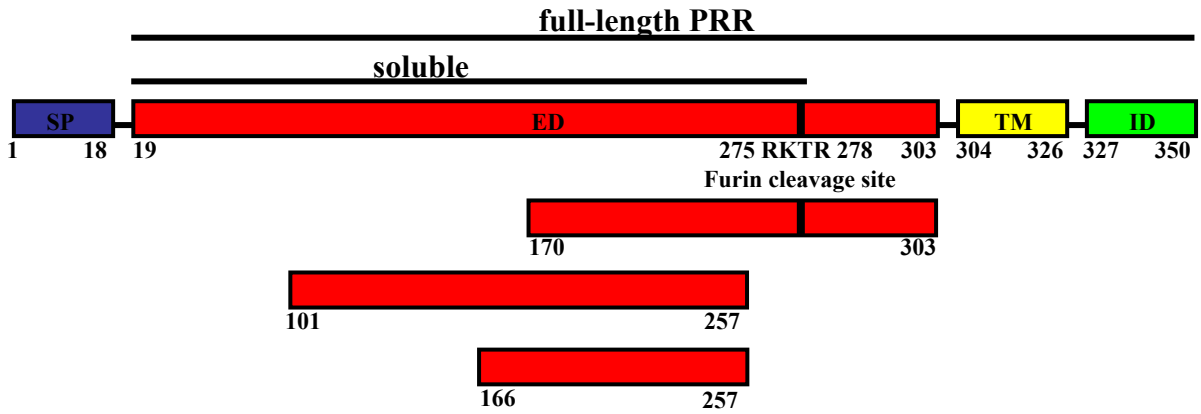

Figure 8. Schematic representation of human PRR and its domains.

PRR consists of a short intracellular (ID), a transmembrane (TM) and an extracellular (ED) domain. Also shown is the PRR signalpeptide (SP) and the furin cleavage site (RKTR) in the extracellular domain. The soluble human PRR proteins purified in this project are depicted below.

To find a soluble construct, test-expressions for all constructs were carried out, as described in section 3.3.4. Figure 9 shows an example of a typical test-expression. The protein was over-expressed and, after cell lysis, the insoluble (in) and soluble fractions (SN) analysed by SDS-PAGE. In this example, the human (hs) PRR (166-257) was over expressed and tested for

solubility. Clones in lane a and b did not express hsPRR (166-257), but in lane c and d the protein is highly expressed and a large proportion was found in the soluble fraction.

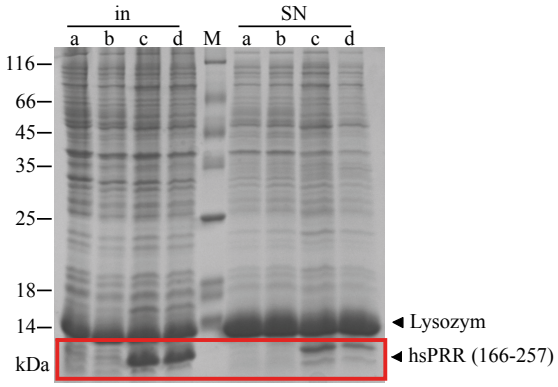

Figure 9. Test-expression of the hsPRR (166-257) constructs.

Different expression clones were tested for soluble protein (a-d). Sample a and b show no overexpression while c and d are overexpressing the protein, which is also soluble. In this example the induced and soluble fractions of hsPRR(166-257) are shown. The red box indicates the over expressed (in) and the soluble fraction (SN). Lysozyme was added to the lysis buffer.

During these expression and solubility tests more then 50 PRR constructs were screened from various species (*Homo sapiens, Mus musculus, Danio rerio, Xenopus laevis*), in two different expression vectors, with either a 6xHis or GST-tag. In addition, to achieve better amounts of soluble protein surface entropy reduction mutations using the SERp server were introduced [152]. This server recognizes clusters of flexible, solvent-exposed residues and replaces them with residues with lower conformational entropy to enhance a proteins ability to be crystallized. Furthermore, I tested different *E.coli* expression strains to test if this would enhance solubility. As it is known that co-expression of the binding partner can improve the solubility of the protein [153], co-expressing renin or prorenin together with the respective PRR construct was tested. For hsPRR (15-300), which showed weak soluble expression of the protein, the purification conditions were attempted to be improved, by changing the amount of salt, pH, adding detergent or using different buffers. None of these efforts resulted in soluble protein in sufficient amount and quality. All attempts are summarized in the construct table (see methods section, 3.1.9).

Only a few proteins were found to be soluble and their expression was then scaled up in order to purify protein in sufficient amount and quality. These were hsPRR (170-303), hsPRR (101-257) and hsPRR (166-257) (Figure 9) and the mmPRR (166-257), xlPRR (163-254), drPRR

(99-255) and drPRR (164-255). The purification and characterization of these soluble PRR proteins is described in the following sections.

4.1.2. Expression of hsPRR (170-303)

Hs PRR (170-303) was found to be soluble only when fused to a GST-tag (Figure 10 A, SN lane). The first purification step for this protein was therefore a GSH-Sepharose column. Following a series of washes to remove non-specifically bound proteins (Figure 10 A, lane W), Prescission protease digestion was then performed directly on the column. On-column digestion was chosen to prevent the GST-tag from non-specifically binding to the untagged protein (data not shown). The eluted, untagged protein was then additionally purified by size-exclusion chromatography.

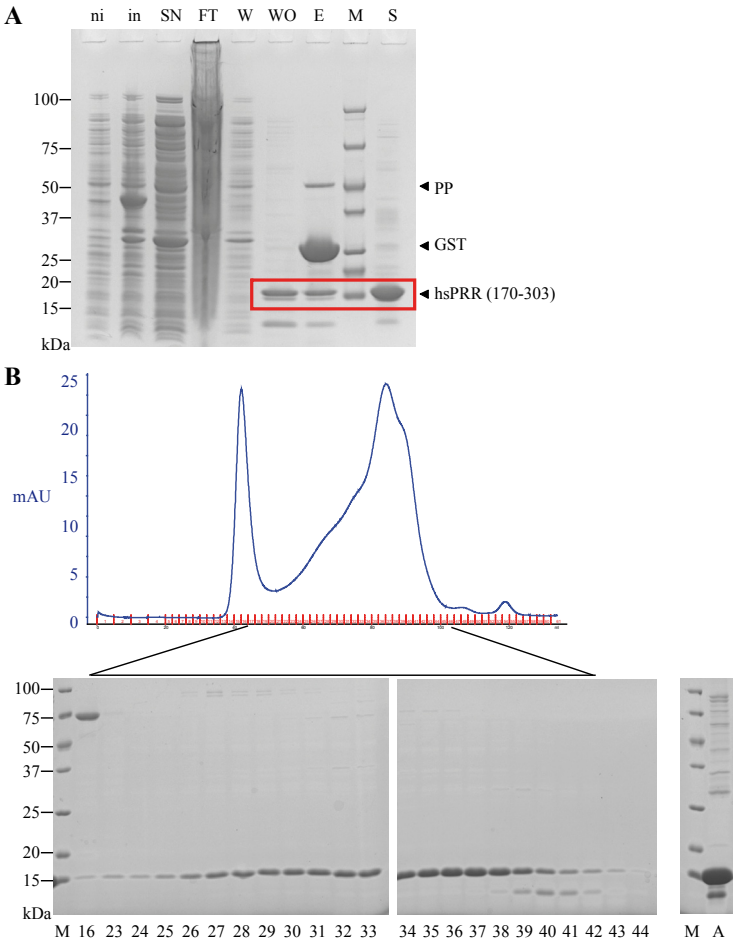

Figure 10. Purification of GST-tagged hsPRR (170-303).

A) SDS-PAGE analysis of GSH-sepharose purification step. Lane contents: ni, uninduced cell lysate; in, induced cell lysate; SN, supernatant/soluble fraction; FT, GSH-sepharose flow-through; W, first wash; WO, wash-out (untagged hsPRR) fraction; E, eluate (of GST-tag); S, purified protein; M, marker. Arrows indicate bands

corresponding to the Prescission protease (PP), free GST-tag, and hsPRR (170-303). (B) Chromatogram of the hsPRR (170-303) run on a Superdex200 column. Below the trace a SDS-PAGE analysis of the corresponding fractions was performed (indicated by numbers). On the right, SDS-PAGE analysis of the final purified protein (A, pooled fractions 30-39) is shown**.**

The elution profile of the Superdex 200 gel filtration column is shown in Panel B (Figure 10 B). The elution profile was very broad, making the removal of contaminating proteins difficult. As a result, the pooled protein had several higher molecular weight contaminants and was estimated to be only 80 % pure (Figure 10 B, lane A). Typical yields of hsPRR (170-303) were ~0.5 mg protein per 1 L of bacterial culture.

4.1.3. Expression of hsPRR (101-257)

Because hsPRR (170-303) was only 80 % pure and the yield was low, screening for soluble proteins was continued. The hsPRR (101-257) was found to be soluble in test-expressions.
The first purification step for 6xHis hsPRR (101-257) was an immobilized metal ion affinity column (IMAC) (Figure 11 A). After extensive washing of the column (lane w), the bound protein was eluted with 150 mM imidazol (lane E) and the 6xHis tag was subsequently cleaved overnight (lane +PP). During the overnight cleavage, the sample was dialyzed against buffer without imidazol. In the second purification step, the cleaved hsPRR (101-257) was applied again onto the Talon column in combination with a GSH column. The untagged hsPRR (101-257) (in buffer without imidazol) passed through the column (lane 2. FT.), while contaminating proteins (lane E2) and GST Prescission Protease (lane E1) bound to the column.

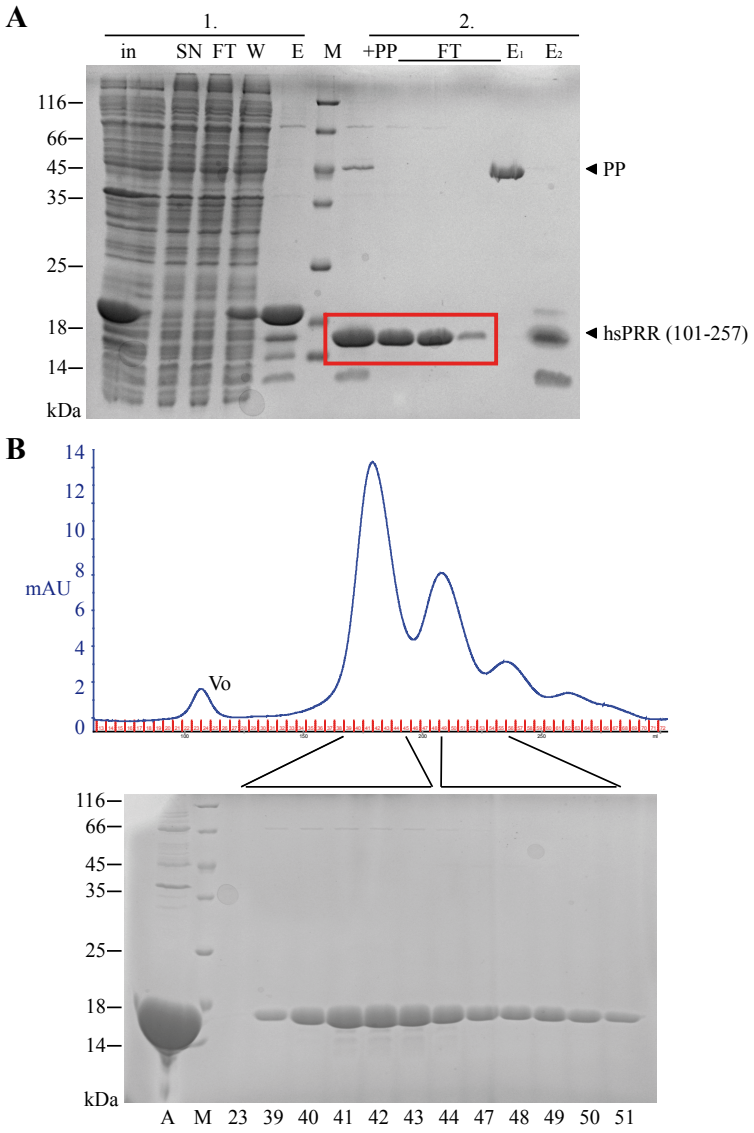

Figure 11. Purification of the 6xHis-tagged hsPRR (101-257).

A) SDS-PAGE analysis of IMAC purification. Lane contents: in, induced cell lysate; SN, supernatant/soluble fraction; FT, flow-through; W, wash fraction; E, eluate of hsPRR (101-257); M, marker; +PP, Prescission protease digest; 2. purification step, FT flow through fraction after cleavage, E_1 elution from GSH column (control), E_2 elution from the Talon column (control). Arrows indicate bands corresponding to the Precission Protease (PP) and hsPRR (101-257). (B) Chromatogram of the hsPRR (101-257) run on a Superdex200 column. Directly below the trace SDS-PAGE analysis of the corresponding fractions (indicated by numbers) is shown. On the left SDS-PAGE analysis of the final purified protein (A, pooled fractions 30-39) is shown.

The last purification step was a gel filtration column (Figure 11 B). The sample eluted with two distinct peaks, however when analysed by SDS-PAGE these were found to consist only of hsPRR (101-257), indicating that the hsPRR (101-257) forms two different oligomeric

species. The protein was about 90 % pure and gave yields of about 2 mg per 1 L bacterial culture.

4.1.4. Limited proteolysis of hsPRR (101-257)

Conditions which favour homogenous and stable protein populations are most favourable for crystallization. To identify the structurally stable regions of soluble PRR, a limited proteolytic digestion approach was used. As flexible loops are more accessible by proteases and are thus preferentially cut, limited proteolysis can remove these flexible regions, creating shorter, stable constructs. The hsPRR (101-257) was incubated with several proteases (thermolysin, subtilisin, chymotrypsin and trypsin) at different dilutions and temperatures. Interestingly, digestion with all four proteases resulted in the appearance of a ~ 14 kDa fragment. Of the four proteases, most distinct results were obtained with digestion with chymotrypsin 1:1000 at 37 °C (Figure 12), where a second band of ~10 kDa was observed. The two observed bands (Figure 12, red box, arrows 1 and 2), were then cut from the gel and identified by mass spectrometry. The mass spectrometry data of the two samples (Figure 12, arrow 2) identified a hsPRR fragment with a molecular weight of approximately 12 kDa. The sequence coverage was around 90 %. The mass spectrometry data was compared with the secondary structure prediction analysis (described above) and the known peptide cleavage site, and on the basis of this, three new constructs covering this fragment were designed.

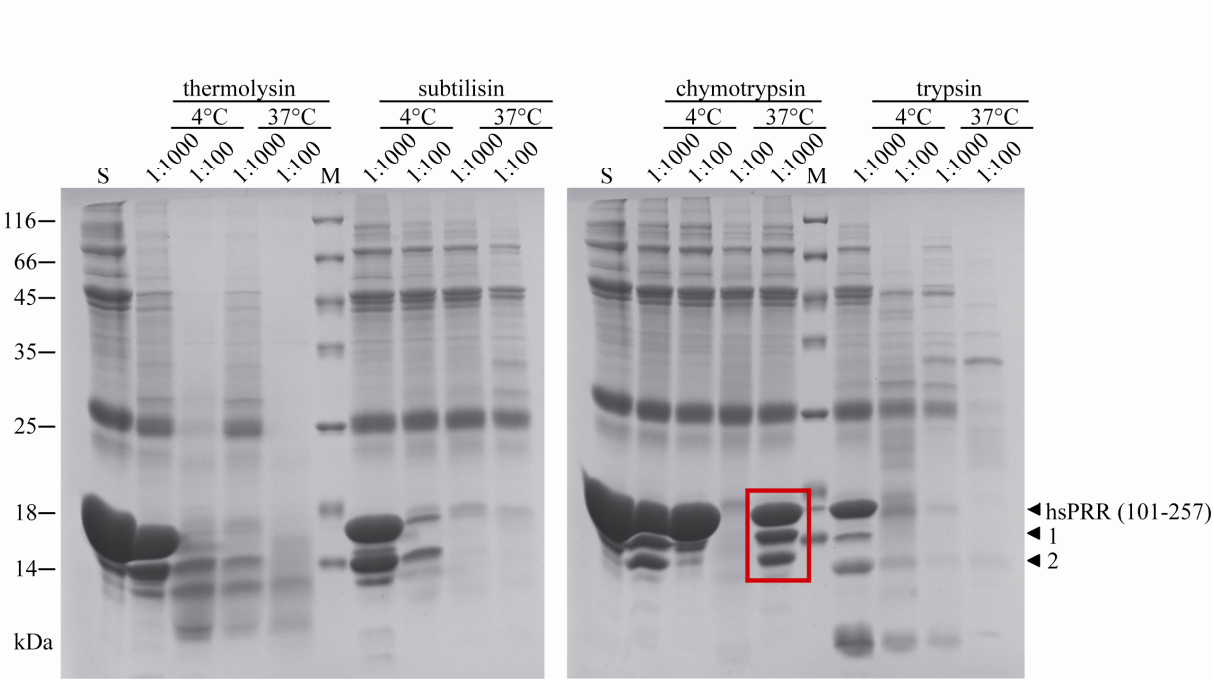

Figure 12. Proteolytic digestion of hsPRR (101-257).

SDS-PAGE analysis of hsPRR (101-257) incubated with the four different proteases (thermolysin, subtilisin, chymotrypsin, trypsin). Digestion with chymotrypsin 1:1000 at 37 °C resulted in two stable fragments (red box, arrows 1 and 2). These were subsequently analyzed by mass spectrometry. S untreated sample, M marker

4.1.5. Expression of hsPRR (166-257)

Based on the limited proteolysis experiment, three new constructs were cloned. Only one of these, hsPRR (166-257), was found to be soluble and thus only expression of this protein was scaled up.

The 6xHis hsPRR (166-257) was purified by an IMAC. The bound protein was eluted and the tag was cleaved overnight and dialyzed against buffer without imidazol. To remove the GST-tagged Prescission protease and contaminating proteins, the sample was applied again on the Talon column in combination with a GSH column (Figure 13 A). The sample was applied on a gel filtration column (Figure 13 A) and eluted in one distinct peak. The protein was about 95 % pure and gave yields of about 8 mg per 1 L bacterial culture.

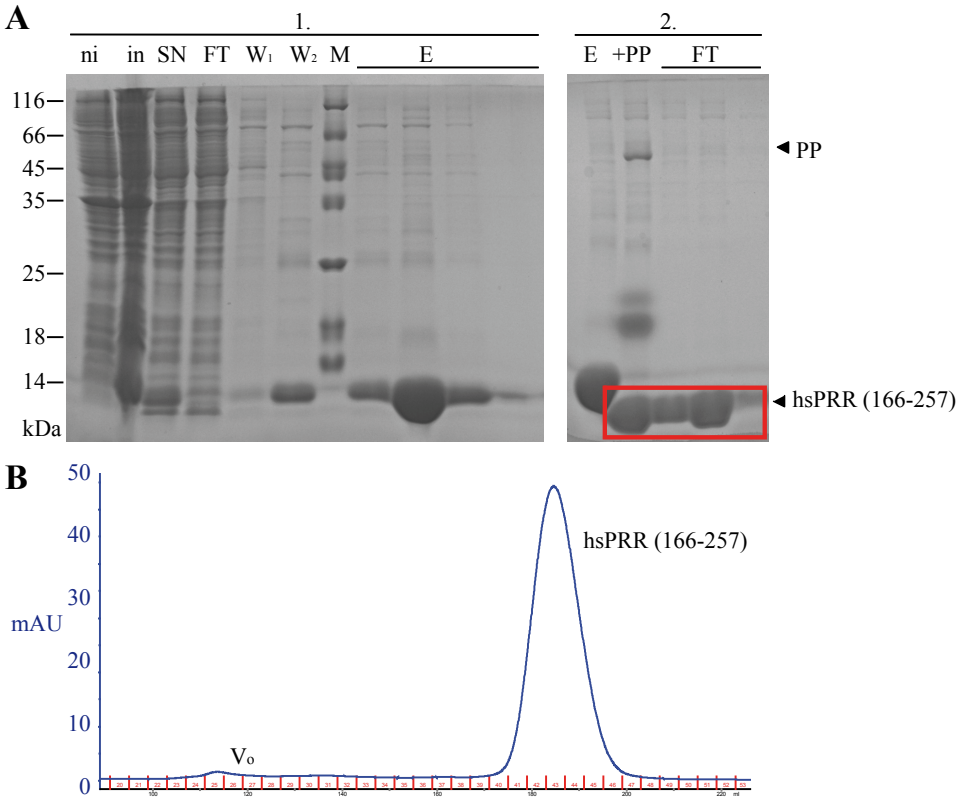

Figure 13. Purification of the 6xHis-tagged hsPRR (166-257).

A) SDS-PAGE analysis of IMAC purification. Lane contents: in, induced cell lysate; SN, supernatant/soluble fraction; FT, flow-through; W1, wash fraction; W2, wash fraction with 10mM imidazol E, eluate of hsPRR (166-

257); M, marker; +PP, Prescission protease digest; 2. purification step, FT flow through fraction after cleavage, Arrows indicate bands corresponding to the Precission Protease (PP) and hsPRR (166-257). (B) Chromatogram of the hsPRR (166-257) run on a Superdex75 column.

4.1.6. Expression of PRR proteins from different species

Consequently, the human constructs 101-257 and 166-257 were tried to adopt to the different available species by using the amino acid alignment results described previously. During test expressions only a few of these constructs were soluble. MmPRR (166-257), xlPRR (163-254), drPRR(164-255) and drPRR(99-255) were expressed and purified. All of these proteins gave rather low amounts of protein (approximately 0.5 mg per 1 L bacterial culture), and protein preparation were only 70-80 % pure.

4.2. Characterization of purified hsPRR proteins

4.2.1. Characterization of hsPRR (170-303)

4.2.1.1. Secondary structure determination of hsPRR (170-303)

hsPRR (170-303) could be purified in mg amounts. The correct fold of a protein is necessary for its function. Therefore, the secondary structure of hsPRR (170-303) was analyzed by circular dichroism (CD). Figure 14 A shows the CD spectrum for hsPRR (170-303) measured at four different temperatures. At room temperature, the spectrum reflects a typical alpha helical fold, with minima at 222 nm and 208 nm. The data was fitted with an algorithm provided by Sandro Keller (TU Braunschweig, Germany) to estimate the percentages of folds (alpha-helical, beta-sheet, random coil; Figure 14 A table). This analysis showed that the hsPRR (170-303) has an almost exclusively alpha helical fold. At 4 °C and 20 °C the alpha helical content was 84 % and 65 %, respectively. Analysis of the structural stability of the protein was also performed. Figure 14 B shows the melting curve of hsPRR (170-303). The ellipticity of the protein was monitored at a wavelength of 222 nm with a constant increase in temperature of 1 °C per minute. The calculated melting temperature is 45.3 °C, which is relatively low [154]. Above this temperature, the protein unfolds and precipitates.

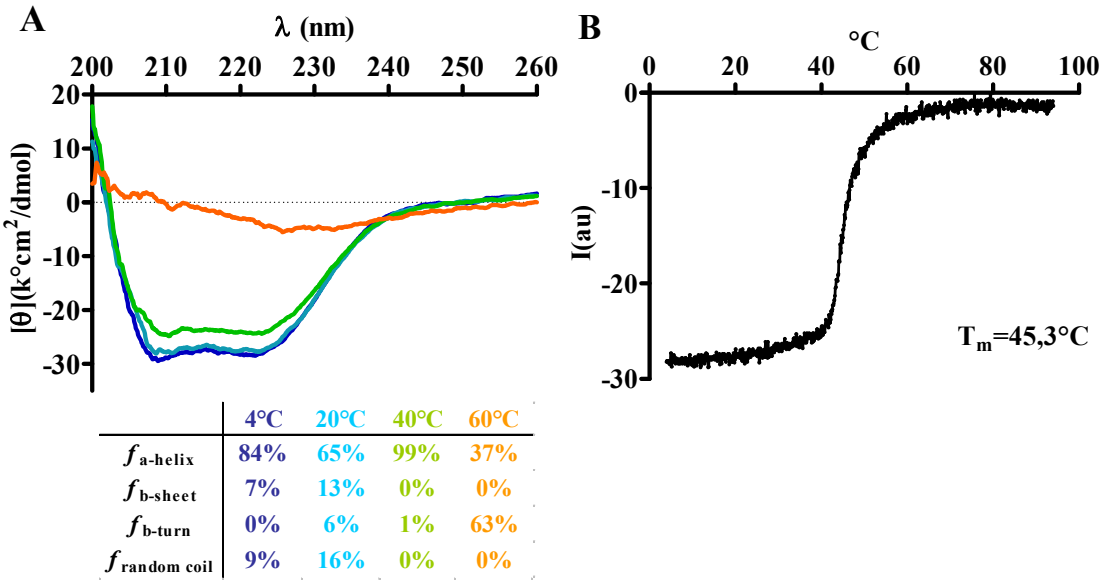

	4°C	20°C	40°C	60°C
$f_{a\text{-helix}}$	84%	65%	99%	37%
$f_{b\text{-sheet}}$	7%	13%	0%	0%
$f_{b\text{-turn}}$	0%	6%	1%	63%
$f_{random\ coil}$	9%	16%	0%	0%

Figure 14. Secondary structure analysis of hsPRR (170-303) by circular dichroism (CD) spectrometry.
A) The CD spectra of the hsPRR(170-303) was measured at four different temperatures (4 °C blue, 20 °C light blue, 40 °C green, 60 °C orange). The proportion of α-helix, β-sheet, β-turn and random coil were estimated and are listed in the table. (B) Melting curve analysis at 222nm with temperature increments of 1 °C per minute.

4.2.1.2. Interaction of hsPRR (170-303) with (pro)renin

Next it was investigated if hsPRR (170-303) bound to its known ligands. It was previously published that full-length PRR binds to renin and with even higher affinity to prorenin [1, 40]. The (pro)renin binding site has not yet been identified, except that it is located on the extracellular domain. Human renin or prorenin was incubated in equimolar amounts with GST-tagged PRR (170-303). The two supposed interaction partners were then incubated with GSH sepharose. The unbound protein was washed from the GSH material and the bound protein was eluted. Figure 15 shows that neither renin (A) or prorenin (B) was pulled-down with the PRR construct, indicated by the lack of visible bands in the bound fraction. This suggests that in this assay, renin and prorenin do not bind with high affinity to GST-tagged hsPRR (170-303).

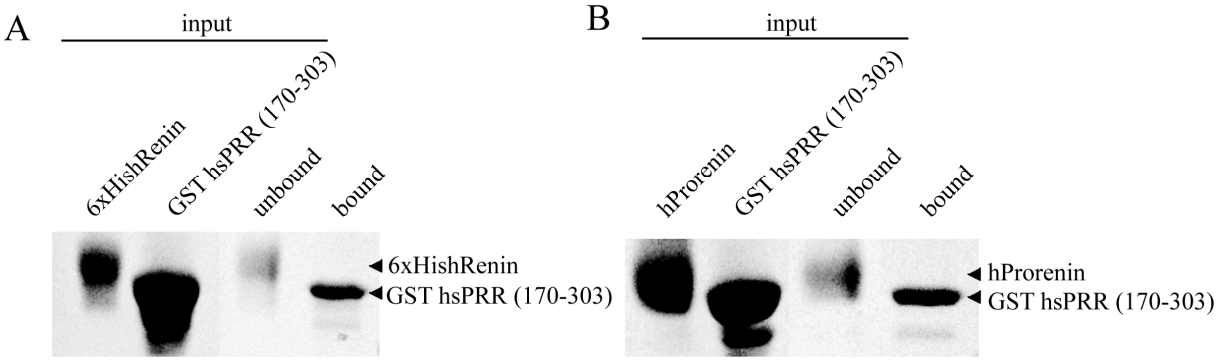

Figure 15. Interaction study of GST hsPRR (170-303) with renin or prorenin.

SDS-PAGE analysis of the pull-down assay. On the left side of the SDS-PAGE the controls 6xHis renin (A) or prorenin (B) and the GST hsPRR (170-303) (input) are shown. On the right side are the bound and unbound samples. Arrows indicate the position of GST hsPRR (170-303) and renin or prorenin.

4.2.2. Characterization of hsPRR (101-257)

4.2.2.1. Secondary structure determination of hsPRR (101-257)

hsPRR (101-257) was of good solubility and could be purified to high amounts and quality. The secondary structure of hsPRR (101-257) was also analyzed by circular dichroism. Since hsPRR (170-303) revealed an overall alpha helical fold, it was of interest to see if this protein gave similar results. Figure 16 A shows the CD spectra for hsPRR (101-257) with a typical alpha helical fold, with minima at wavelengths of 222nm and 208 nm. For temperatures between 4 °C and 44 °C the percentage of alpha helices is between 62 % and 92 % (Table 16 A). With increasing temperatures, the composition changes from an overall alpha helical fold to a higher percentage of random coil structure Table A. After first heating the sample to 94 °C and decreasing the temperature back to 4 °C, the protein seems to be predominantly structured (Figure 16 A purple line), indicating that it is able to re-fold after thermal denaturation. However, the calculated percentages of the folds in this sample are quite different when compared to the spectra collected at 4 °C and 24 °C, and shows a relatively high content of random coil. Since the melting curve displayed an almost linear increase instead of a typical sigmoidal curve, the melting point could not be determined. These results indicate that hsPRR (101-257) has increased thermal stability.

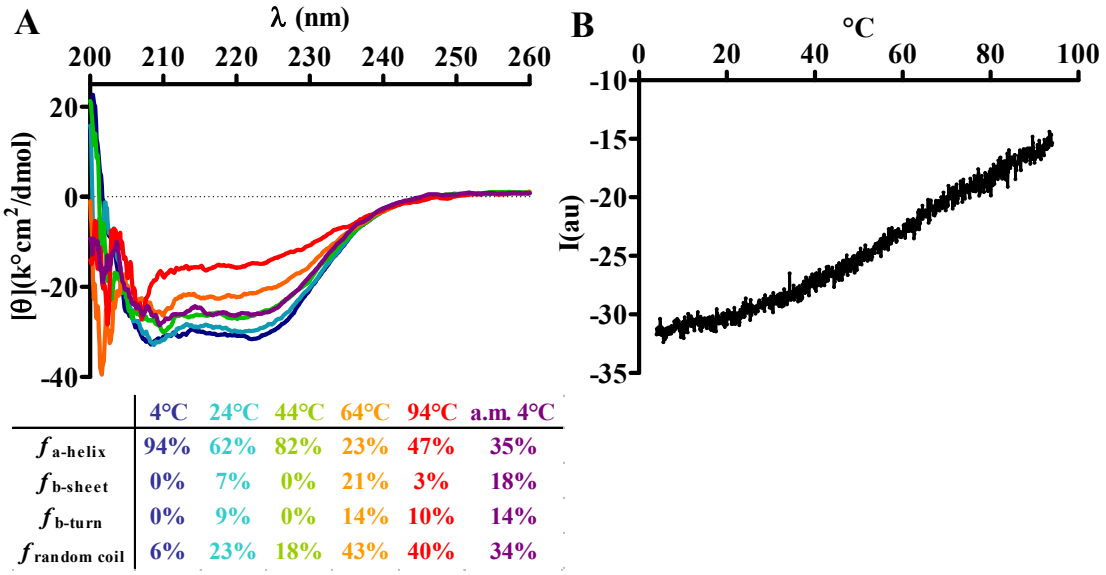

	4°C	24°C	44°C	64°C	94°C	a.m. 4°C
$f_{\text{a-helix}}$	94%	62%	82%	23%	47%	35%
$f_{\text{b-sheet}}$	0%	7%	0%	21%	3%	18%
$f_{\text{b-turn}}$	0%	9%	0%	14%	10%	14%
$f_{\text{random coil}}$	6%	23%	18%	43%	40%	34%

Figure 16. Secondary structure analysis of hsPRR (101-257) by circular dichroism (CD) spectrometry.
A) CD spectra of the hsPRR (101-257) were measured at 6 different conditions (4 °C blue, 24 °C light blue, 44 °C green, 64 °C orange, 94 °C red, 4 °C after melting purple). The proportion of α-helix, β-sheet, β-turn and random coil were estimated and are listed in the table. (B) Melting curve analysis at 222 nm with temperature increments of 1°C per minute is shown.

4.2.2.2. Interaction study of hsPRR (101-257) with (pro)renin

Next it was asked whether hsPRR (101-257) can bind to renin or prorenin. To address this, the same GST pull down approach as described before was used. Human renin and prorenin were incubated with GST-tagged hsPRR (101-257), thus allowing the complex to be pulled down with GSH sepharose. Figure 17 shows the result of the pull-down.

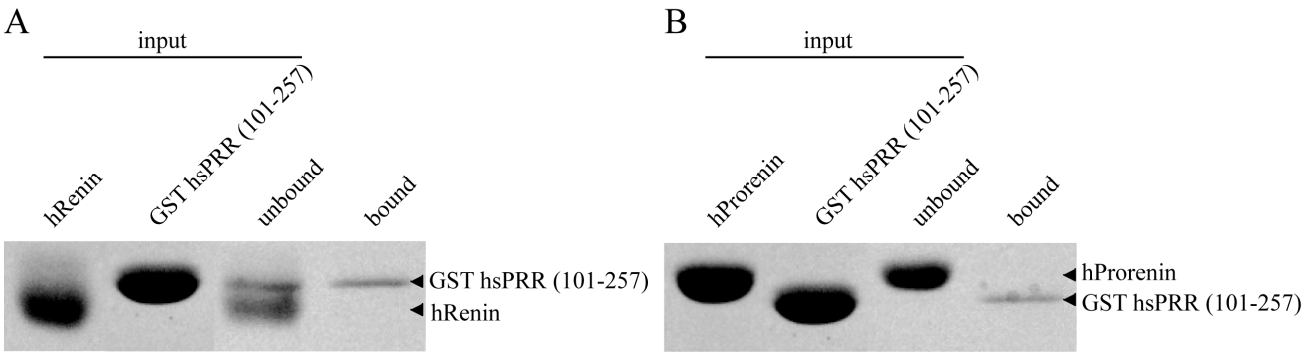

Figure 17. Interaction study of GST hsPRR (101-257) with renin or prorenin.
SDS-PAGE analysis of the pull-down assay. On the left side of the SDS-PAGE are the controls renin (A) or prorenin (B) and the GST hsPRR 101-257 (input). On the right side are the bound and unbound samples. Arrows indicate the position of GST hsPRR (101-257) and renin or prorenin.

Renin (A) and prorenin (B) were found solely in the unbound fraction, and GST-tagged hsPRR (101-257) in the bound fraction. This result indicates that under these conditions, this short construct is not able to bind to renin or prorenin.

4.2.2.3. Analysis of the oligomerization of hsPRR (101-257)

Results from the purification of hsPRR (101-257) showed that this protein eluted in two peaks from gel filtration column. SDS-PAGE revealed that these peaks only contain hsPRR (101-257) and do not consist of contaminating proteins (see 3.1.3.). This suggests the presence of two oligomeric species in the sample. To analyze the molecular weight of the sample right-angle light-scattering (RALS) was used. In this experiment, a refractive index, UV and a RALS detector are set-up in-line with a gel filtration column (Superdex 200 10/300). With this, the average molecular weight of the sample can be estimated. The calculated molecular weight (Figure 18, black line) shows two different plateaus for the two peaks, reflecting different molecular weights. Closer analysis showed that the first peak has a calculated average molecular weight of 96 kDa. As hsPRR has a theoretical molecular weight of 18.44 kDa, this peak represents an oligomer of 5-6 subunits (pentamer or hexamer). This experiment was repeated five times, resulting in an average molecular weight of 102 ± 11 kDa. The second peak was estimated by RALS to have an average molecular weight of 26 kDa. In five different experiments this peak had an average molecular weight of 23 ± 5 kDa. This peak therefore seems to be predominantly monomeric. By re-applying the concentrated fractions of either peak 1 or peak 2, the protein still eluted in two distinct peaks, each having the same average molecular weights as calculated previously. Also, when analysed at different concentrations varying from 2 to 10 mg/ml, two peaks were observed. These results indicate that hsPRR (101-257) forms a monomer and an oligomer in solution, which are in equilibrium.

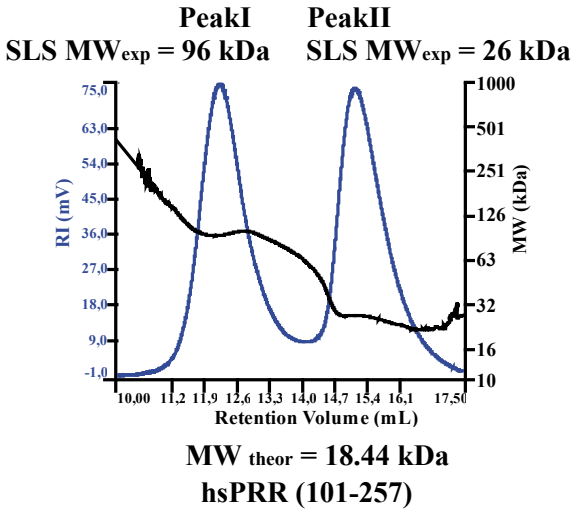

Figure 18. Right angle light scattering (RALS) analysis of the hsPRR (101-257).

200µg of hsPRR (101-257) was used for analysis. The refractive index (blue line) and the calculated molecular weight (black line) are depicted. (A) HsPRR (101-257) eluted in two peaks with different apparent molecular weights. Single analysis of the first peak giving a calculated MW of 96 kDa and single analysis of the second peak with a determined MW of 26 kDa

To further investigate the oligomerization of hsPRR (101-257), analytical ultracentrifugation was used. Sedimentation velocity is an analytical ultracentrifugation experiment, which measures the rate at which molecules move in response to the centrifugal force. The time course of sedimentation provides information about the molecular mass and the shape of molecules that is described by the sedimentation coefficient, Svedberg (S). Figure 19 shows a typical sedimentation time course and the fitted data.

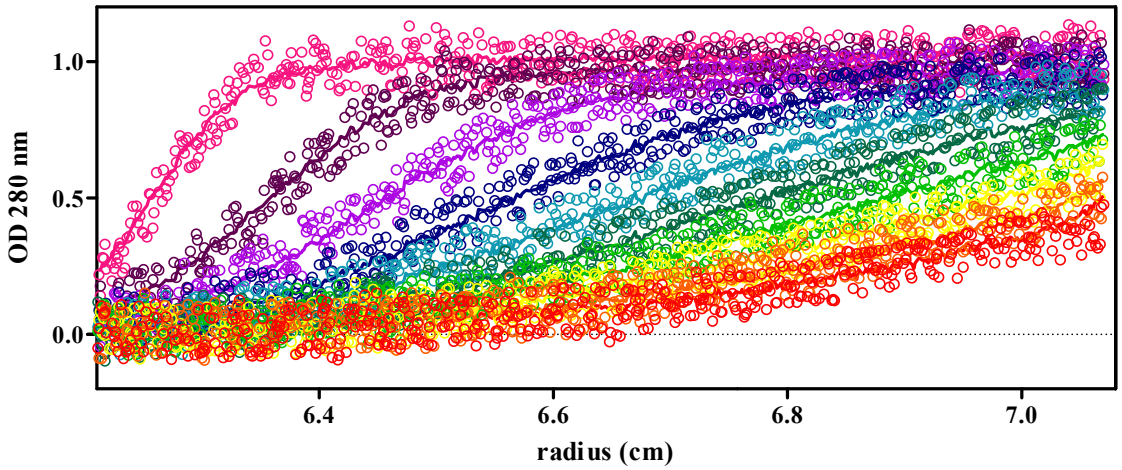

Figure 19. Sedimentation velocity analysis of hsPRR (101-257).

Sedimentation velocity of 2 mg/mL hsPRR (101-257) with radial scans collected in 10 min intervals (circles) and theoretical fits of the data (lines). For clarity, only every fourth scan is shown.

Figure 20 shows the sedimentation coefficient distribution for hsPRR (101-257). At concentrations of 1 and 0.5 mg/ml, only one species is present in solution with a sedimentation coefficient between 2.5 S and 2.6 S. This was estimated to correspond to a molecular mass between 26 and 29 kDa using the program SEDFIT, indicating that predominantly monomers are present in solution. At a concentration of 2 mg/ml, an additional peak was observed in the distribution. This corresponds to an oligomeric species with a sedimentation coefficient of 4.04 S and an estimated molecular mass of 56 kDa. These results are in agreement with the RALS results, where the existence of a monomer and an oligomer was observed. Although the estimated molecular weight for the oligomeric peak measured with RALS was around ~100 kDa. Sedimentation velocity analysis does not take into account the shape of a molecule, which might influence its sedimentation behaviour; therefore the RALS results are more reliable. But sedimentation velocity analysis gave additional information about the concentration dependence of the oligomerisation of hsPRR (101-257) below 2 mg/ml, as the RALS experiments were only performed at concentrations of 2 mg/ml and above.

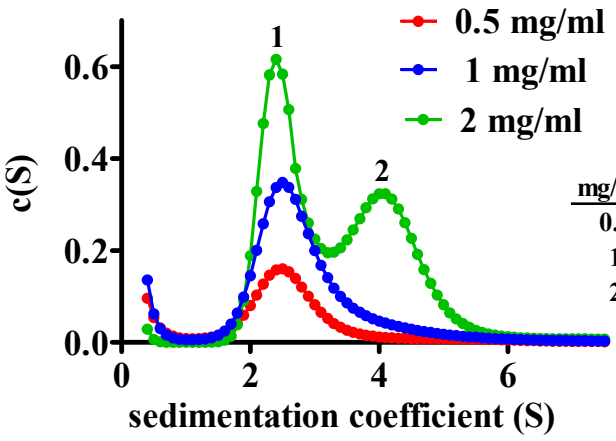

mg/mL		Svedberg (S)	molecular mass (kDa)
0.5		2.55	28.28
1		2.66	29.12
2	peak 1	2.50	26.54
	peak 2	4.04	56.11

Figure 20. Sedimentation coefficient distribution of hsPRR (101-257) at different protein concentrations. The hsPRR (101-257) was analyzed at 0.5 (red line), 1 (blue line) and 2 mg/mL (green line). The average sedimentation coefficient and molecular mass of the peaks are shown in the table.

For protein structure determination, a homogenous sample is favourable because the presence of several different species in the sample reduces the likelihood of crystallization. As shown in Figures 18 and 20 above, at protein concentrations above 2 mg/ml hsPRR (101-257) exists in a monomer/oligomer equilibrium. As high protein concentrations are needed for structural studies, this heterogeneous equilibrium condition is not likely to results in crystal formation. To investigate if buffer conditions affect the oligomerization of hsPRR (101-257), sedimentation velocity experiments were performed at different pHs. The protein sample was

at a concentration of 2 mg/mL in a buffer containing 150 mM NaCl and 20 mM of the respective buffer. Figure 21 shows the sedimentation coefficient distributions for hsPRR (101-257) at each different pH. For improved clarity, the six different conditions are shown in two graphs. At pH 6 the protein precipitated, indicated by a loss in adsorption of the sample (data not shown), therefore this condition could not be measured. At pH 6.5 (MES buffer), a broad distribution was observed. This probably reflects the beginning of sample precipitation. At pH 7 and pH 7.5 (both in HEPES), the expected monomer/oligomer peaks, as described in Figure 20 above, were seen. However, above pH 8 (Tris pH 8, Tris pH 8.5 and Glycine pH 9) only one peak was visible. The sedimentation coefficient for this peak varied from 2.28 to 2.37 S, which represents a molecular mass of approximately 24 kDa. Therefore, under these conditions (i.e. above pH 8) hsPRR (101-257) appears to be predominantly monomeric.

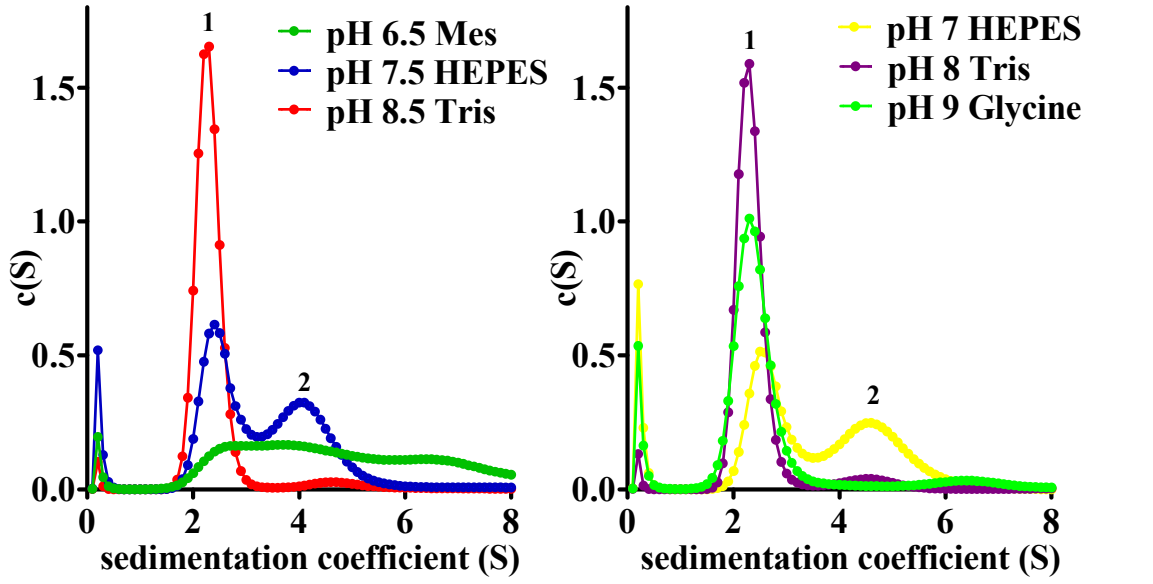

Buffer		Svedberg (S)	molecular mass (kDa)
Mes pH 6.5		n.a.	n.a.
HEPES pH 7.5	peak 1	2.5	26.54
	peak 2	4.04	56.11
Tris pH 8.5		2.28	23.31

Buffer		Svedberg (S)	molecular mass (kDa)
HEPES pH 7	peak 1	2.66	28.78
	peak 2	4.6	41.96
Tris pH 8		2.3	23.65
Glycine pH 9		2.37	24.77

Figure 21. Sedimentation coefficient distributions of hsPRR (101-257) at different pH values.

Left panel: pH 6.5 (pink), pH 7.5 (purple), pH 8.5 (green). Right panel: pH 7.0 (purple), pH 8 (blue), pH 9 (green). The average sedimentation coefficients and molecular mass of the peaks are shown in the table. Because of the broad distribution at pH 6.5 these parameters could not be determined (n.a.) For clarity, data are depicted in two graphs.

The effect of buffer composition on the oligomerization of hsPRR (101-257) was also investigated. Figure 22 shows the sedimentation coefficient distribution for hsPRR (101-257) at pH 8 in Tris and HEPES buffer. Under both conditions, hsPRR (101-257) sedimented as one peak with an average sedimentation coefficient of 2.3 S and 2.45 S for Tris and HEPES, respectively. This indicates that under these conditions, hsPRR (101-257) is predominantly monomeric and that the oligomerization observed is dependent on the pH of the buffer, and not on the composition. Above pH 8 it, exists as a monomer, while below pH 7.5 it exists in a monomer/oligomer equilibrium.

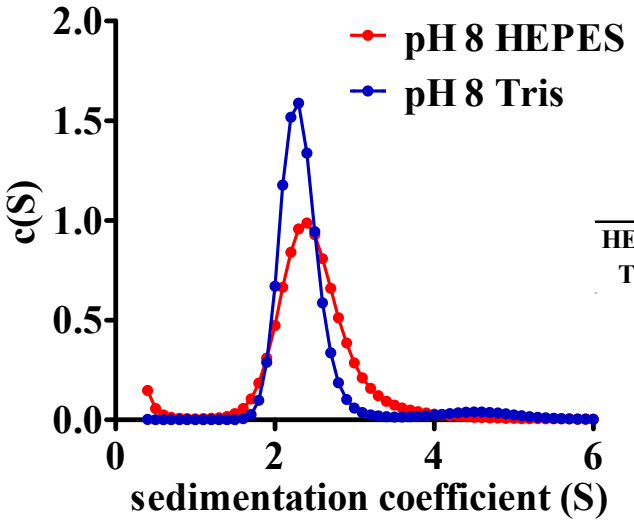

Buffer	Svedberg (S)	molecular mass (kDa)
HEPES pH 8	2.45	26.35
Tris pH 8	2.30	23.65

Figure 22. Sedimentation velocity analysis of hsPRR (101-257) at pH 8 in HEPES (red) or Tris (blue) buffer. The average sedimentation coefficients and molecular mass of the peaks are shown in the table.

As shown above, changing the pH resulted in a drastic shift from a single monomer in solution to monomer/oligomer equilibrium. One possibility is that this pH change induces the protein to unfold. Therefore, secondary structure of hsPRR (101-257) was analyzed in different buffers (20 mM buffer, 150 mM NaFl), varying from pH 6.5 to pH 8 using CD spectroscopy (Figure 22). Under all conditions, hsPRR (101-257) had a predominantly alpha-helical fold, of approximately 73 % to 76 %. This indicates that changing the pH and the buffer composition has no dramatic effect on the secondary structure of hsPRR (101-257).

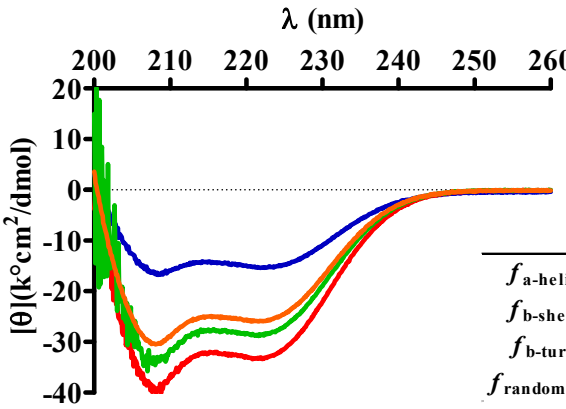

	Mes pH6.5	HEPES pH 7.5	HEPES pH 8	Tris pH 8
$f_{\text{a-helix}}$	73%	73%	76%	73%
$f_{\text{b-sheet}}$	0%	0%	0%	0%
$f_{\text{b-turn}}$	6%	0%	0%	0%
$f_{\text{random coil}}$	20%	26%	24%	26%

Figure 23. Secondary structure of hsPRR (101-257) in different buffer conditions.
CD spectra of hsPRR (101-257) were measured at 20 °C with different buffers (20 mM) and pH (Mes pH 6.5 in blue, HEPES pH 7.5 in red, HEPES pH 8 in green, HEPES pH 8 in orange). The amount of α-helix, β-sheet, β-turn and random coil were estimated and are listed in the table.

4.2.3. Characterization of hsPRR (166-257)

HsPRR (166-257) was designed after performing a limited proteolysis experiment (section 3.1.4). This protein could be purified to high purity and yield.

To analyze if this protein is folded, secondary structure determination of hsPRR (166-257) was performed by circular dichroism. Figure 24 A shows that all spectra have a typical alpha helical shape with two minima. The hsPRR (166-257) has an alpha helical fold content of approximately 80 %. The melting temperature was determined to be 53.7 °C (B). The hsPRR (166-257) was able to reversibly refold after thermal unfolding and had almost the same alpha helical composition as before unfolding. These results indicate that hsPRR (166-257) has a very high thermal stability.

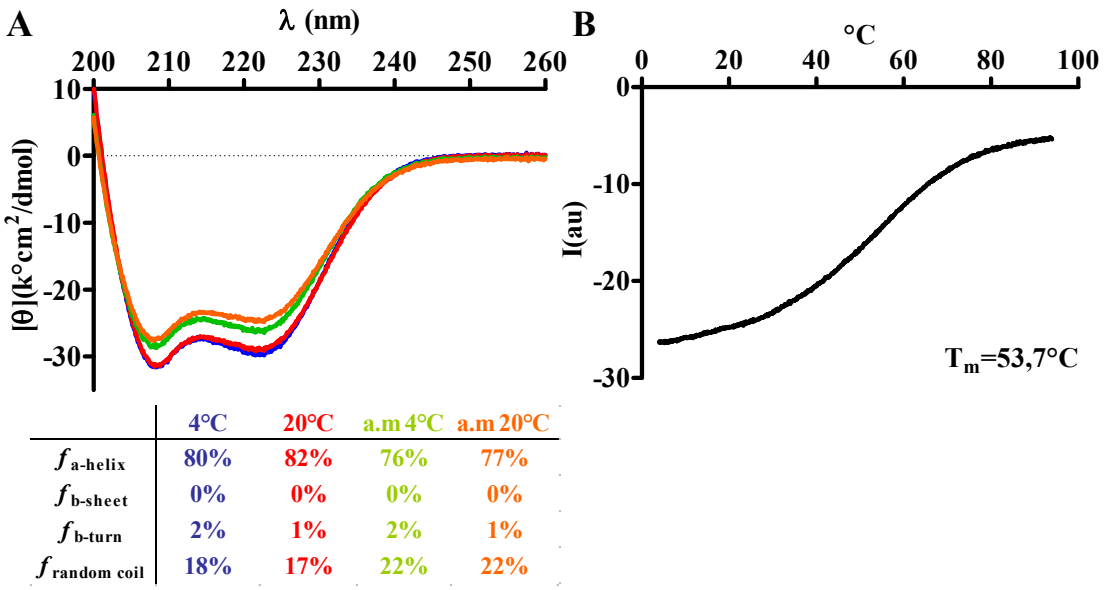

	4°C	20°C	a.m 4°C	a.m 20°C
$f_{\text{a-helix}}$	80%	82%	76%	77%
$f_{\text{b-sheet}}$	0%	0%	0%	0%
$f_{\text{b-turn}}$	2%	1%	2%	1%
$f_{\text{random coil}}$	18%	17%	22%	22%

Figure 24. Secondary structure analysis of hsPRR (166-257) by circular dichroism (CD) spectrometry.
A) CD spectra of hsPRR (166-257) were measured at 4 different conditions (4 °C blue, 20 °C red, 4 °C after melting green, 20 °C after melting orange). The proportion of α-helix, β-sheet, β-turn and random coil were estimated and are listed in the table. (B) Melting curve analysis at 222 nm with temperature increments of 1 °C per minute.

As hsPRR (101-257) was found to be in a monomer/oligomer equilibrium in solution, it was of interest to analyse the molecular weight of the hsPRR (166-257) and to find out if this protein behaved similarly. To determine the molecular weight of this construct, right-angle light-scattering was performed as described previously. Figure 25 A shows that the hsPRR (166-257) eluted in one peak from gel filtration. The theoretical molecular weight is 11.17 kDa while the experimentally observed one by RALS is 18.32 kDa. The calculated molecular weight in this peak ranged from 10 to 27 kDa and the peaks appeared to be unsymmetrical, with a shoulder on one side. Thus, it is possible that in this sample both monomers and dimers are present. To investigate this further, the protein was incubated with a cross-linker, BS3, to covalently cross-link the putative dimer, which could then be analyzed by SDS-PAGE (see 3.3.10.) Figure 25 B shows, in the presence of the cross-linker, the appearance of a dimeric band. By increasing the incubation time for cross-linking, increased amounts of dimeric sample were not observed. Instead higher oligomers appeared that were possibly due to unspecific cross-linking (data not shown).

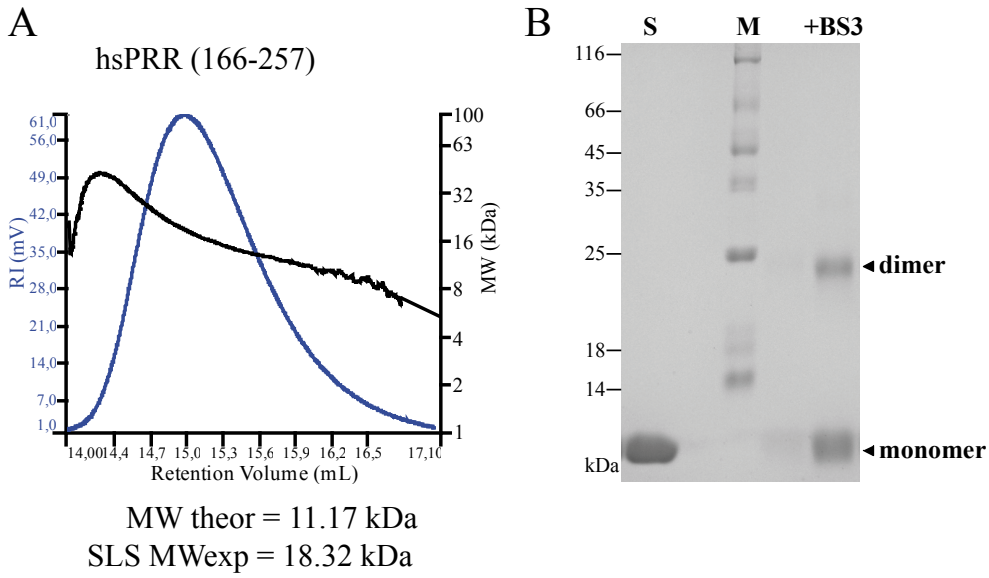

Figure 25. (A) Right-angle light-scattering (RALS) analysis of hsPRR (166-257).

The refractive index (blue line) and the calculated molecular weight (black line) are depicted. (B) Cross-linking of hsPRR (166-257) with BS3. SDS-PAGE analysis of hsPRR (166-257) before and after cross-linking. Arrows mark the position of monomeric and dimeric hsPRR (166-257).

At this point, it was considered that hsPRR (166-257) existed in a monomer/dimer equilibrium. As this condition is not favourable for crystallisation, constructs were designed where potential unstable regions were removed, and an additional helix was added or deleted based on results from the secondary prediction analysis. These constructs were hsPRR (166-269) and hsPRR (174-257). Analysis of the sequence of hsPRR (166-257) revealed a pattern with a high amount of charged amino acids (position 201-207). As charged residues often have a negative influence on crystallization, these amino acids were mutated to alanines (KHLAKDH to AAAAAAA), resulting in the construct hsPRR (166-257) $_{201AAAAAAA207}$. The three new constructs were first analyzed for their molecular weight by right-angle light-scattering. All constructs eluted in a single peak (Figure 26). The hsPRR (166-257) $_{201AAAAAAA207}$ has an average calculated molecular weight of 19.52 kDa (Figure 26 A), hsPRR (166-269) of 19.61 kDa (Figure 26 B) and hsPRR (174-257) of 15.72 kDa (Figure 26 C). For all samples the experimental molecular weight varies for the single peaks from 10 to 30 kDa and the peaks were again non-symmetric, suggesting that these proteins may also be non-homogenous. The theoretical molecular weight is 10.36 kDa for hsPRR (174-257), 10.84 kDa for the hsPRR (166-257) $_{201AAAAAAA207}$ and 12.46 kDa for hsPRR (166-269). Based on the RALS results, it appeared that all three constructs are also in a monomer/dimer equilibrium.

Because of the low purity and quality, working with hsPRR (166-269) and hsPRR (174-257) was stopped.

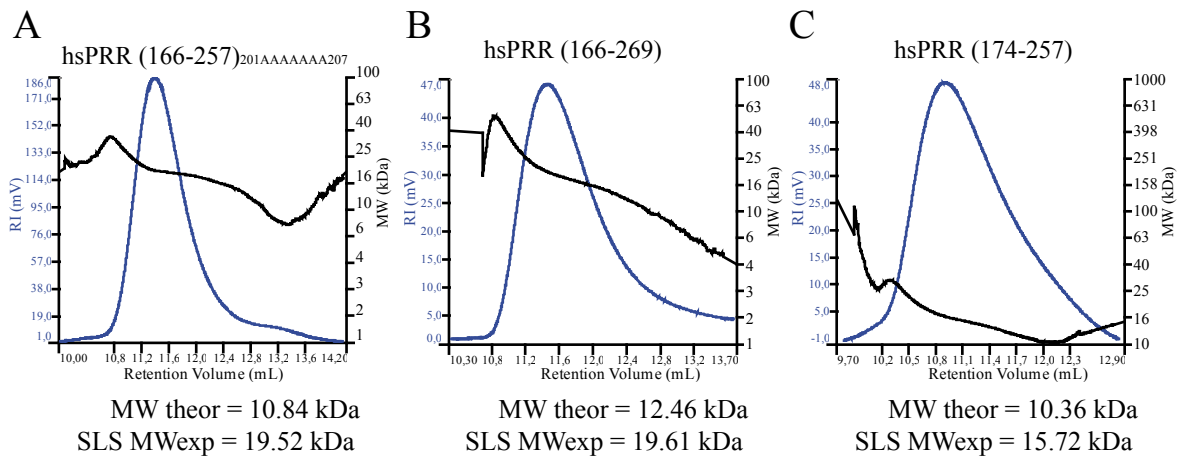

Figure 26. Right angle light scattering (RALS) analysis of hsPRR proteins.

The refractive index (blue line) and the calculated molecular weight (black line) are depicted. (A) The hsPRR (166-257) $_{201AAAAAAA207}$ has an average calculated molecular weight of 19.52 kDa. (B) The hsPRR (166-29) has an average calculated molecular weight of 19.61 kDa and (C) the hsPRR (174-257) has an average molecular weight of 15.72 kDa.

The secondary structure of hsPRR (166-257)$_{201AAAAAAA207}$ was analyzed by circular dichroism. The hsPRR (166-257)$_{201AAAAAAA207}$ has an overall alpha helical fold (Figure 20). Comparison of the wild-type with the mutant construct shows that both have an almost identical protein fold in the CD spectra (alpha helical content of 77 % vs. 80 %).

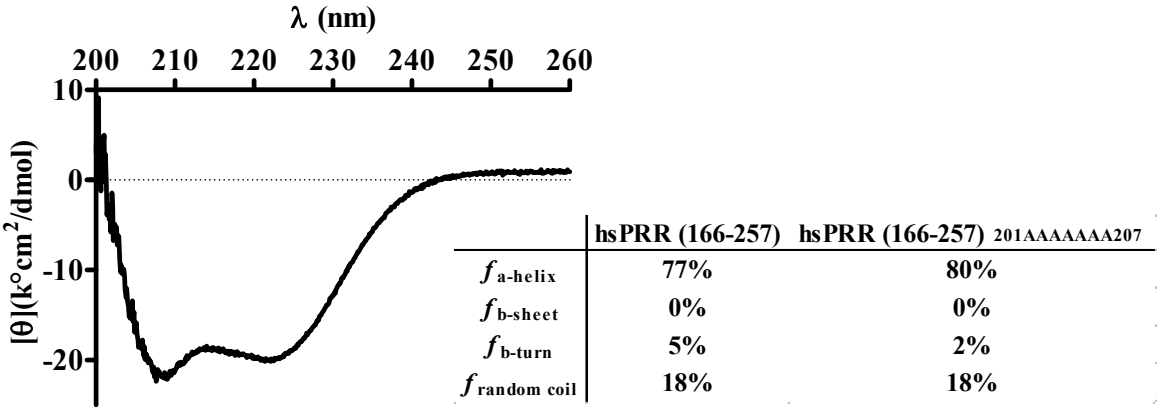

	hsPRR (166-257)	hsPRR (166-257) 201AAAAAAA207
$f_{a\text{-helix}}$	77%	80%
$f_{b\text{-sheet}}$	0%	0%
$f_{b\text{-turn}}$	5%	2%
$f_{random\ coil}$	18%	18%

Figure 27. Secondary structure analysis of hsPRR (166-257)$_{201AAAAAAA207}$ by circular dichroism (CD).

The proportion of α-helix, β-sheet, β-turn and random coil were estimated and are listed in the table. For comparison, the proportions of α-helix, β-sheet, β-turn and random coil of the hsPRR (166-257) are also listed.

To determine if the hsPRR (166-257) proteins have the same molecular mass and form monomers or dimers, the WT and mutant sample were analyzed by sedimentation velocity ultracentrifugation. Figure 28 show that both proteins have similar sedimentation coefficient distributions. The sedimentation coefficient for the WT sample is 2.07 S and for the mutated sample 2.1 S, and the respective estimated molecular mass of 20.39 kDa and 20.91 kDa are almost identical. Insertion of alanines into hsPRR (166-257) did not prevent dimerization, as predicted. Therefore, all following analyses were performed with the WT hsPRR (166-257).

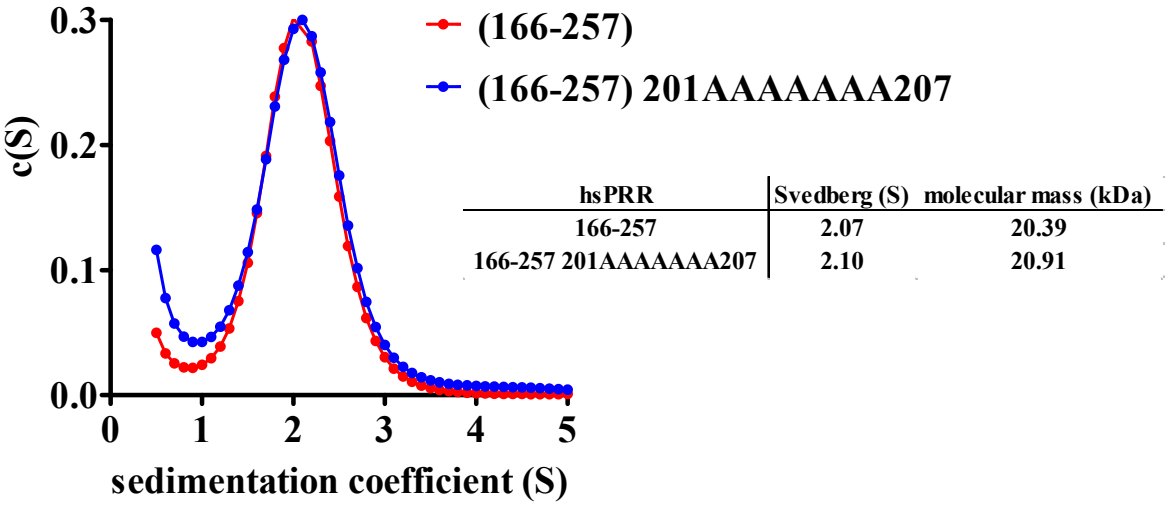

hsPRR	Svedberg (S)	molecular mass (kDa)
166-257	2.07	20.39
166-257 201AAAAAAA207	2.10	20.91

Figure 28. Sedimentation velocity analysis of hsPRR (166-257) (red line) and hsPRR (166-257)$_{201AAAAAAA207}$ (blue line). The average sedimentation coefficients and molecular masses of the peaks are shown in the table.

As decribed above, hsPRR (101-257) oligomerized at concentrations above 2 mg/mL and in a pH dependent (below pH 8) manner. In the next experiments, it was investigated, if the hsPRR (166-257) behaved in a similar fashion. Samples were analyzed by sedimentation velocity centrifugation at different protein concentrations using varying buffer conditions. hsPRR (166-257) was analyzed at concentrations between 0.3 to 1.2 mg/mL. These concentrations were choosen to have the same molar concentration as for the hsPRR (101-257). For all three concentrations, only one peak in the sedimentation coefficient distribution was present (Figure 29). They all have similar sedimentation coefficients between 2.07 and 2.15 S and calculated molecular masses between 20.73 and 21.76 kDa. Thus hsPRR does not oligomerize in a protein-concentration dependent fashion.

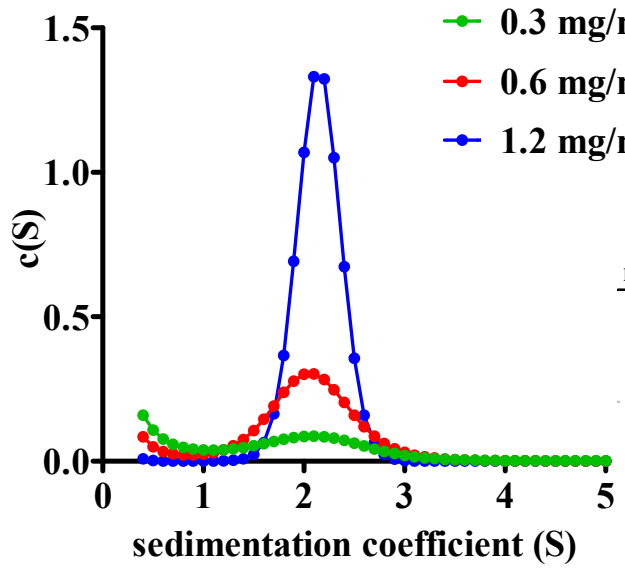

mg/mL	Svedberg (S)	molecular mass (kDa)
0.3	2.08	20.73
0.6	2.07	20.39
1.2	2.15	21.76

Figure 29. Sedimentation velocity analysis of the hsPRR (166-257).

The hsPRR (166-257) was analyzed for 0.3 (green line), 0.6 (red line) and 1.2 mg/ml (blue line). The sedimentation coeffincients and the molecular masses of the peaks were calculated and are depicted in the table.

From sedimentation velocity, right-angle light-scattering and gel filtration experiments it could not accurately be determined if hsPRR (166-257) is either a monomer or a dimer in solution, or if both species are present in equilibrium state. To more accurately determine the oligomerisation state of hsPRR (166-257), sedimentation equilibrium ultracentrifugation experiment was performed. In this analytical ultracentrifugation experiment, the protein reaches a steady-state concentration distribution where the centrifugal force is balanced by the opposing diffusion force. This method is thereby independent of the shape of the protein and directly reports the molar mass of the sample. hsPRR (166-257) was analysed at six different concentrations and at three different speeds. Figure 30 depicts the radial absorbance data (dots) and the fits to the data (lines) at the various concentrations and speeds. The data and fits demonstrate the typical concave distribution of the sample due to it reaching equilibrium.

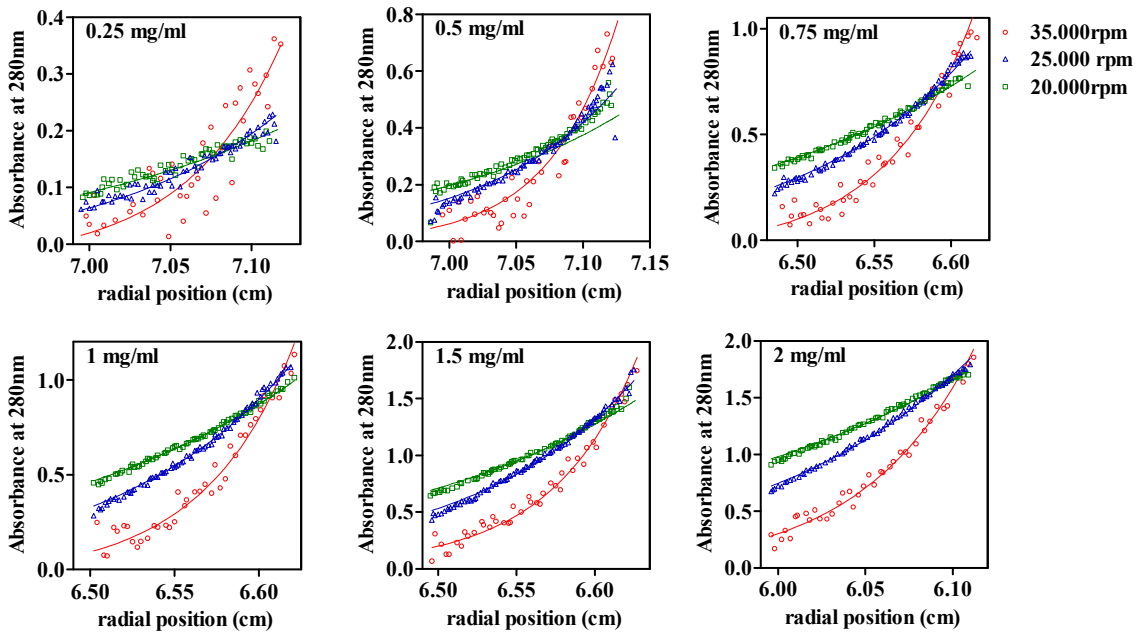

Figure 30. Sedimentation equilibrium centrifugation runs of the hsPRR (166-257).

The hsPRR (166-257) was analyzed for the following concentrations: 0.25, 0.5, 0.75, 1, 1.5, 2mg/ml. Absorbance scans were taken after the sample reached equilibrium at 20,000 (green), 25,000 (blue) and 35,000 (red) rpm. The absorbance data (dots) was fitted (lines) to determine the molar mass of the sample.

By applying a global fit to all data, an apparent average molecular mass of the samples of 17.96 kDa was determined. As the theoretical molecular weight of hsPRR (166-257) is 11.17 kDa, the results from the global fit suggests the presence of both monomer and dimer in solution. Since the applied global fit did not take into account a concentration dependent association, the data was then analyzed separately at each concentration. Figure 31 depicts the calculated molecular mass at each concentration. The black lines indicate the molecular weight of a monomer (11.17 kDa) and a dimer (22.34 kDa). The molecular masses calculated were: 16.6 kDa at 0.25 mg/ml, 18.7 kDa at 0.5mg/ml, 17.9 kDa at 0.75 mg/ml, 19.3 kDa at 1mg/ml, 19 kDa at 1.5 mg/ml and 17.6 kDa at 2 mg/ml. These apparent molecular masses lie in between the calculated monomeric and dimeric molecular weights. It also appears that the molecular mass increases with increasing concentration. Therefore, from this data it was concluded that hsPRR (166-257) exists in a monomer/dimer equilibrium. It would be expected for a real monomer/dimer equilibrium that at lower concentrations the molecular mass of the system would decrease to the molecular weight of the monomer. However, due to the detection limits with this instrument, the concentrations could not be decreased below 0.25 mg/ml.

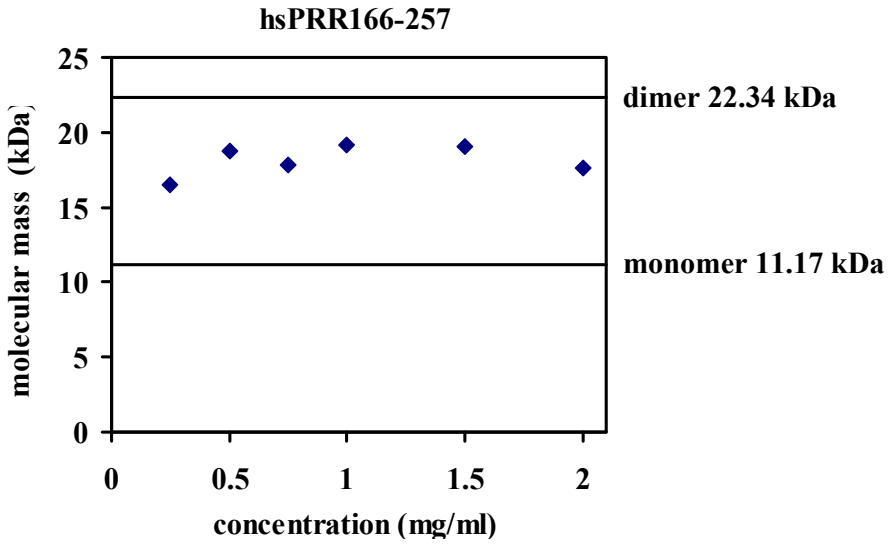

Figure 31. Apparent molecular masses for hsPRR 166-257 calculated by sedimentation equilibrium.
The hsPRR (166-257) was analyzed at protein concentrations at 0.25, 0.5, 0.75, 1, 1.5 and 2mg/ml. The black lines indicate the monomeric and dimeric molecular weight for hsPRR (166-257).

4.2.3.1. Interaction study of hsPRR (166-257) with renin

hsPRR (170-303) and hsPRR (101-257) did not bind to either renin or prorenin in a GST pull-down assay (see Figures 15 and 17). Whilst expressing GST-tagged hsPRR (166-257), the protein was soluble, but during purification the tag showed a tendency to be cleaved from the fusion protein without the use of a protease (data not shown). Thus, a GST pull-down assay was not possible. Instead, the interaction of hsPRR (166-257) with renin was analyzed by sedimentation velocity. The hsPRR (166-257) was incubated in equimolar amounts with renin. Figure 32 shows the sedimentation coefficient distribution hsPRR (166-257) (blue) and renin (green) alone, and when incubated together (red). If the two proteins bound, a shift in the sedimentation coefficient distribution would be expected. Alone, hsPRR (166-257) has a sedimentation coefficient of 2.07 S and renin has a sedimentation coefficient of 3.56 S. These sedimentation coefficients correspond to a molecular mass of 20.39 and 45.17 kDa, respectively (renin has a calculated molecular weight of 42 kDa). When incubated together, no shift in the sedimentation coefficient distribution is observed. The resulting distribution is broad, and overlays the single distribution peaks of the proteins sedimented alone. This indicates that under these conditions, renin does not bind to hsPRR (166-257).

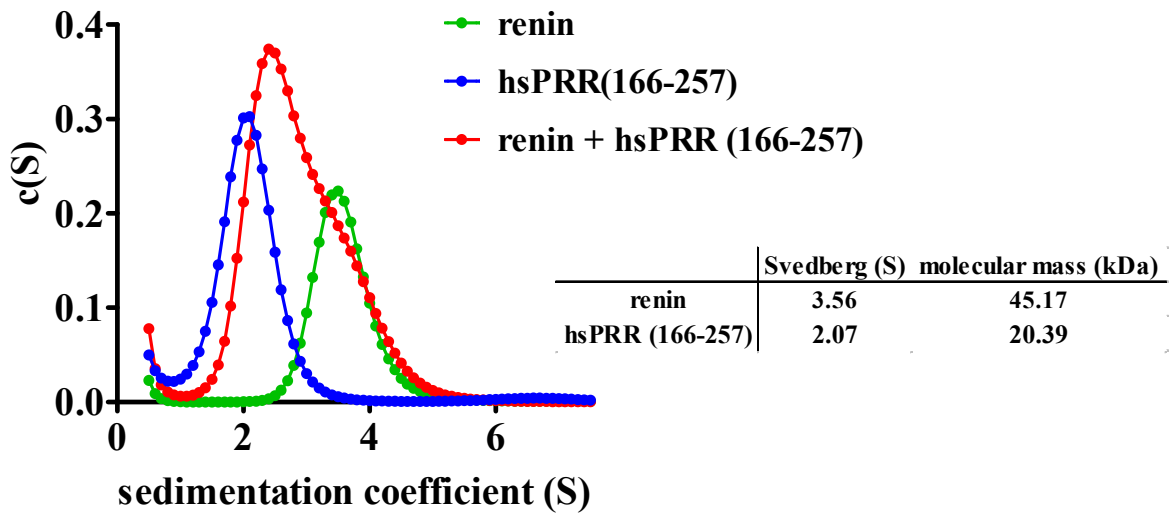

	Svedberg (S)	molecular mass (kDa)
renin	3.56	45.17
hsPRR (166-257)	2.07	20.39

Figure 32. Sedimentation velocity analysis of hsPRR (166-257) incubated with renin.

Both samples are shown alone (renin green, hsPRR (166-257) blue) and when incubated together in equimolar concentration (red). The sedimentation coefficients and molecular mass of renin and hsPRR (166-257) were calculated and are shown in the table.

4.2.4. Characterization of homologous PRR from different species

PRR homologs from other available species, like mouse, zebrafish and frog, were also expressed and purified, using a multiple sequence alignment with the boundaries with the human PRR (101-257) and (166-257). The following proteins were soluble, but could be obtained only in rather low amount and quality: mmPRR (166-257), xlPRR (163-254), drPRR (164-255) and drPRR (99-255). The secondary structure of these proteins was analyzed by circular dichroism. All proteins showed a typical alpha helical CD spectrum (see figure 33). The short proteins from mouse [mmPRR (166-257)], frog [xlPRR (163-254)] and zebrafish [drPRR (164-255)] had ~80% alpha helical content. This is in good agreement with the human proteins; hsPRR (166-257) had ~80% and hsPRR (101-257) had ~70% alpha helical content. The only longer (101-257) construct that was soluble was from zebrafish [drPRR (99-257)] which had a calculated proportion of alpha helical content of 60%, which again is similar to the respective human protein.

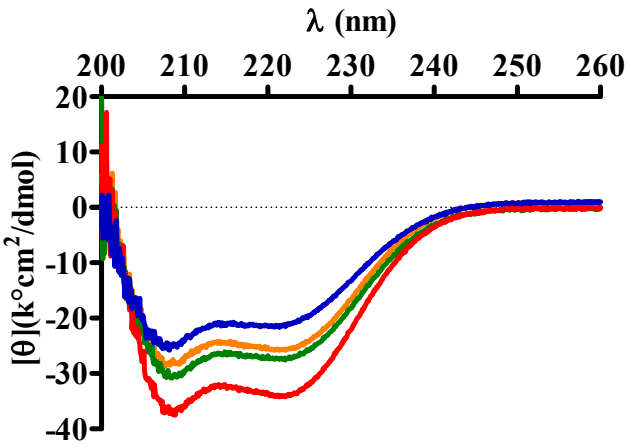

	mmPRR (166-257)	xlPRR (163-254)	drPRR (164-255)	drPRR (99-255)
$f_{\text{a-helix}}$	79%	81%	80%	61%
$f_{\text{b-sheet}}$	0%	0%	0%	7%
$f_{\text{b-turn}}$	2%	1%	2%	2%
$f_{\text{random coil}}$	19%	19%	17%	30%

Figure 33. Secondary structure of different PRR constructs by circular dichroism (CD) spectroscopy.
A) CD spectra measured at 20 °C showing a typical alpha helical for mmPRR (166-257) (orange), xlPRR (163-254) (green), drPRR (164-255) (red) and drPRR (99-255) (blue). The proportion of α-helix, β-sheet, β-turn and random coil structure were estimated and are listed in the table.

As described above, in solution hsPRR (101-257) is in a monomer/oligomer equilibrium and hsPRR (166-257) is in a monomer/dimer equilibrium (Figure 20 and 31). The oligomeric state of the homologous proteins from the different species were also investigated by right-angle light-scattering. Figure 34 shows the elution of the samples in one peak. MmPRR (166-257) (Figure 34 A) had a calculated molecular weight of 54.17 kDa. Taking into account the theoretical molecular weight, this indicates that this protein is a tetramer or pentamer. The xlPRR (163-254) (Figure 34 B) and the drPRR (164-255) (Figure 34 C) both appeared to be dimers, but the data was relatively disperse and the peaks were not homogenous for the dimeric molecular weight. The drPRR (99-257) (Figure 34 D) appeared to have a molecular weight of 32.04 kDa, indicating a dimer.

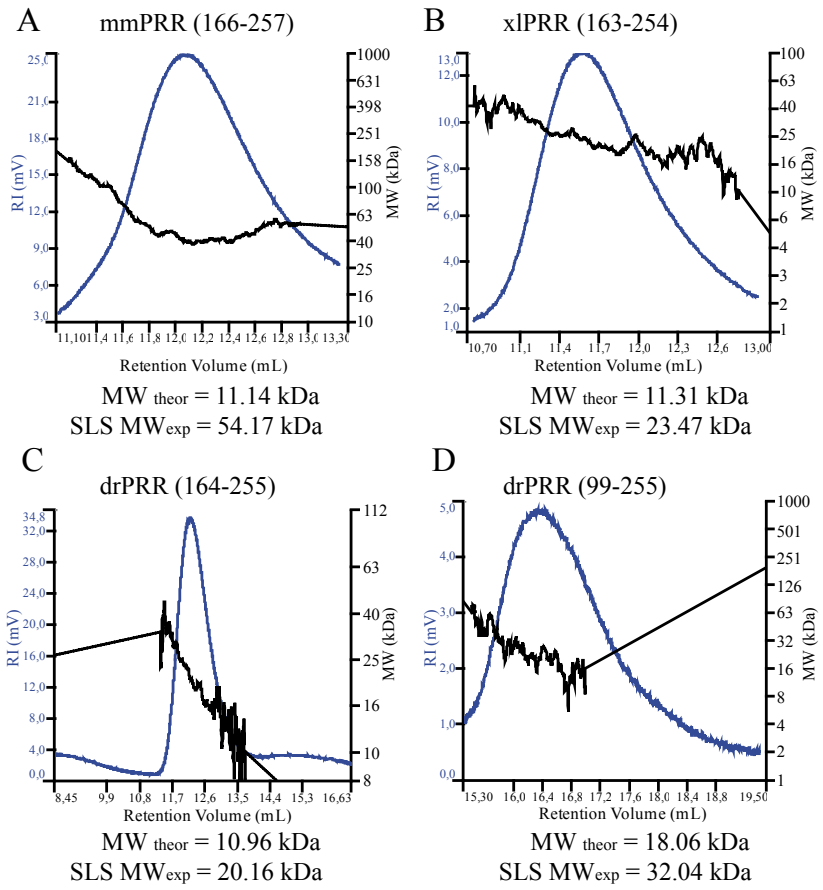

Figure 34. Right angle light scattering (RALS) analysis of PRR constructs.

The refractive index (blue line) and the calculated molecular weight (black line) are plotted. The theoretical and calculated molecular weights are shown below the graph. (A) mmPRR (166-257) (B) xlPRR (163-254) (C) drPRR(164-255) (D) drPRR (99-255)

4.3. Structural studies

4.3.1. Crystallization trials

One of the major aims of this thesis was to determine the structure of hsPRR by X-ray crystallography. However, only a few of the PRR constructs were soluble and could be produced in sufficient amount and quality. Therefore, crystallization trials were only performed with hsPRR (170-303), hsPRR (101-257), hsPRR (166-257), hsPRR (166-257 $_{201AAAAAA207}$) and drPRR (164-255). All proteins were screened for initial hits on 96-well plates using predesigned crystal screens. Approximatly, 20,000 initial conditions were screened for each of the different PRR constructs. Screens were performed at either 4 °C or 20 °C, using different protein stock concentrations. None of these initial screens resulted in the formation of crystals. Manual screens were then performed. Thereby, different precipitants, pH conditions and salt additives were tested. Results of these screens were then

considered for the design of the additional manual screens. Other variables tested include crystal trials where low concentrations of proteases were added. Also, methylating the proteins was tried, as this has been shown previously to improve the likelihood of crystal formation [155]. Unfortunately, all of these attempts were unsuccessful and no protein crystals were obtained.

4.3.2. Nuclear magnetic resonance (NMR) spectroscopy

As all of the crystallization screens tested did not result in the formation of protein crystals, solution-state nuclear magnetic resonance spectroscopy (NMR) was performed, as another method to obtain structural information. For NMR studies of proteins it is necessary to label the sample with the isotopes ^{13}C and ^{15}N, as the naturally occurring isotopes are not NMR active. Therefore hsPRR (166-257) was single and double labelled with ^{13}C and ^{15}N isotopes. For the incorporation of these isotopes into the protein, it is essential to grow the bacteria in minimal medium. As not all constructs can be expressed in minimal media, a small scale expression assay was first tested (Figure 35). The best protein expression of hsPRR (166-257) in minimal media was achieved when protein expression was induced at a cell density of OD_{600nm} = 0.4. A larger scale protein expression and purification was then performed, resulting in a yield of ~3 mg per 1 L of minimal medium with a final purity of ~95 %.

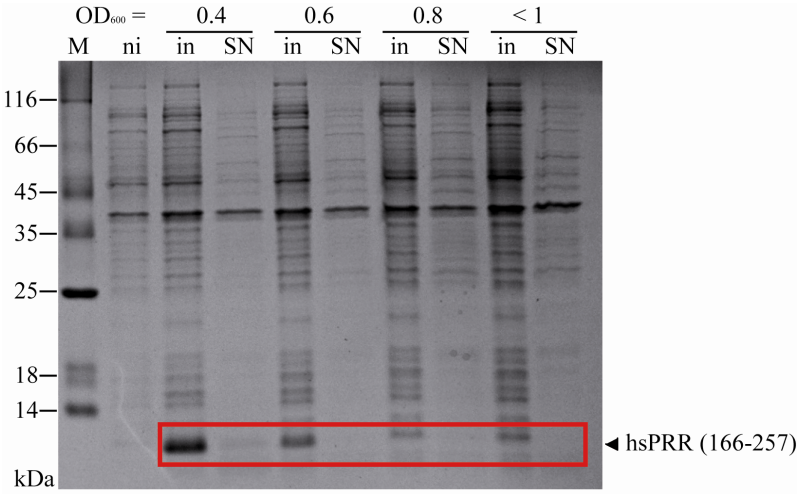

Figure 35. Test expression of hsPRR (166-257) in minimal medium

The optimal induction time was tested. IPTG was added at the indicated optical densities. Lane contents: ni not induced, in induced, SN supernatant, M marker

The single and double labelled hsPRR (166-257) was analysed by NMR at a concentration of 1 mM in 100 mM NaCl and 50 mM phosphate buffer pH 7.5 at 20 °C. First, a one-

dimensional ^{1}H-NMR spectrum was recorded to determine if the unlabelled hsPRR (166-257) is NMR suitable. Figure 36 A shows the one-dimensional spectrum. The protein is folded, indicated by a good overall dispersion of the observed resonances. The resonances in the range of 8.5 to 10 ppm for the amide protons and the resonances in the range of 0.7 to 0 for the methyl groups in the ^{1}H-NMR spectrum indicate well folded protein. Following this, a two-dimensional NMR experiment was performed. Figure 36 B shows a heteronuclear single-quantum correlation spectroscopy (HSQC) spectrum of the single labelled hsPRR (166-257), with correlated frequencies for the ^{1}H–^{15}N. In theory, each resonance in the spectrum represents a bonded N-H pair, with its two coordinates corresponding to the chemical shifts of each of the H and N atoms. Most of the peaks for hsPRR (166-257) are around the 8ppm area, typical for alpha helical proteins [156]. Key to the determination of protein structure by NMR is the assignment of amino acids to the peaks. It was assumed from the one-dimensional experiment that double labelling (^{13}C, ^{15}N) of the samples could result in better spectra. Despite having recorded three-dimensional spectra with double labelled samples an assignment was not possible. One reason for this is the poor dispersion (i.e. overlapping) of the peaks in the area at 8ppm area, which makes assignment difficult. Additionally problematic is the fact that hsPRR (166-257) only has a few aromatic residues that give unique peaks, which are easy to assign.

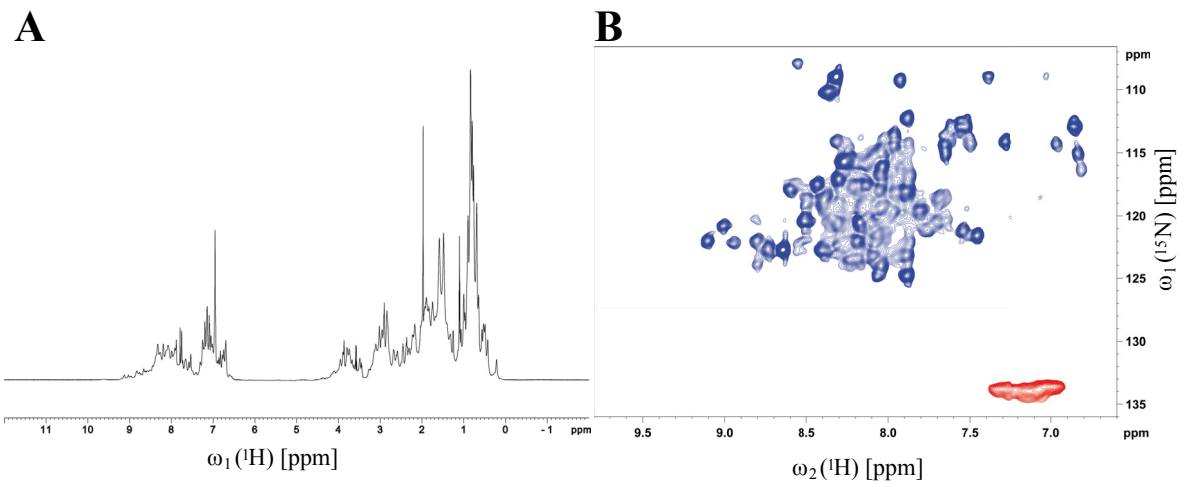

Figure 36. Structural investigation of hsPRR (166-257) with nuclear magnetic resonance (NMR).
A) One dimensional ^{1}H-NMR spectrum of unlabelled hsPRR (166-257) (B) ^{1}H–^{15}N HSQC spectrum of single labelled hsPRR (166-257).

4.4. Function of PRR in T cells

In the first part of this PhD thesis the *in vitro* characteristics of the PRR were examined. For the second part the role of the PRR in an *in vivo* system were analyzed. The role of the PRR for T cell maturation in a mice model was examined.

4.4.1. Conditional PRR knock-out model

To test the hypothesis that PRR plays a role in T cell function, maintenance and development a conditional knock-out (KO) model was used (Figure 37). To generate T cell specific KO mouse, the PRR gene was targeted by homologous recombination using a construct in which exon 2 of the PRR was flanked by loxP sites. Female heterozygous loxP PRR mice were mated with male heterozygous Cre mice. T cell specificity was achieved by using a Cre recombinase under the control of the LCK promoter. LCK is expressed solely in T cells and expression starts early in development at the DN3 stage. Since the PRR gene is localised on the X chromosome, male conditional KO (cKO) mice were obtained in the first offspring generation.

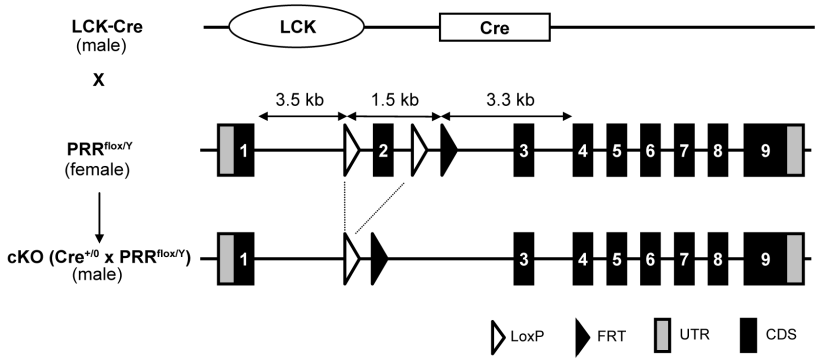

Figure 37.Targeting strategy for the conditional KO of the PRR in T cells.
To generate T cell specific PRR KO mice, female mice bearing a loxP flanked PRR gene were mate with male mice expressing the Cre transgene under the control of the LCK promoter.

To confirm the specific deletion of the PRR gene, genomic DNA was isolated from several tissues and analysed by PCR. If the floxed PRR was excised by the Cre recombinase a shorter PCR fragment for the PRR (326 bp) would be expected. In tissues without the deletion, a full length PRR PCR fragment of 1426 bp is expected. Figure 38 shows the PRR PCR fragments of different tissues from cKO mice. In liver, lung and kidney the PRR is not excised and only the 1426 bp band is apparent. Also in the spleen, only full length DNA for PRR is present. The spleen is a tissue that is composed of several cell types, including B cells but also T cells.

Only in thymocytes (which are almost exclusively T cells) the PRR is deleted, confirmed by the short PRR DNA fragment.

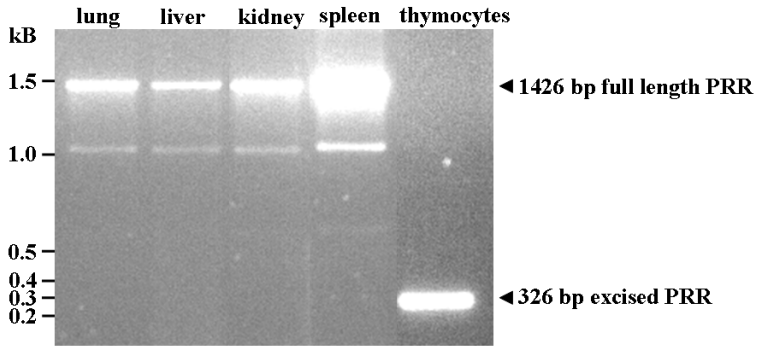

Figure 38. Excision of exon 2 of PRR.

Agarose gel of PCR fragments. Genomic DNA of lung, liver, kidney, spleen and thymocytes was analyzed for the deletion of the PRR. Tissues or cells without the deletion of exon 2 showed a longer PCR fragment of 1426 bp. Excision of the PRR results in a shorter PCR fragment of 326 bp.

Additionally, RNA was isolated from diverse tissues from either cKO or WT mice and analyzed for PRR expression by RT-PCR. Figure 39 shows no difference in PRR expression in the kidney, heart, liver and lung for WT or cKO mice. In the cKO spleen and thymus, PRR expression is slightly decreased compared to WT. This might be explained by the existence of several immune cells, including T cells, in the spleen. However, this decrease is small due to the presence of other cells, such as B cells, which would still express PRR. Additionally, a decrease of PRR expression is observed in the DP+SP pool of thymocytes that are double positive (DP) for $CD4^+$ and $CD8^+$ or single positive (SP) $CD4^+$ and $CD8^+$ cells; the DP cells are the largest population of T cells in the thymus. The decrease of PRR gene expression in the thymus and DP and SP cells alone, indicates that the cKO model is T cell specific.

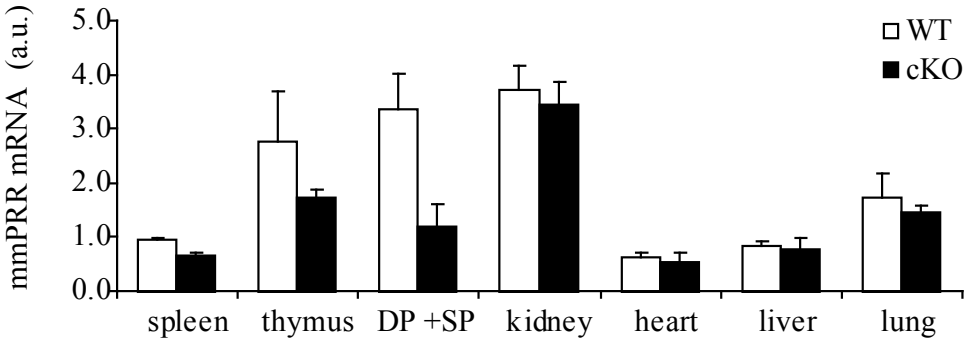

Figure 39: PRR expression in cKO and WT mice.

RT-PCR mRNA analyses in different organs of WT (white) and cKO (black). DP+SP, thymic pool of double positive $CD4^+$ and $CD8^+$ cells and or single positive $CD4^+$ and $CD8^+$ cells.

4.4.2. Characterization of lymphocytes in the cKO model

To determine the effect of conditional PRR deletion on peripheral T cell numbers, spleens from 6-8 week old male WT and cKO mice were collected and analyzed by flow cytometry. Splenocytes were stained for B cell (CD45R) and T cell (CD3) markers. In addition, leucocytes from the blood were isolated and their lymphocyte composition examined. The total number of splenocytes was not altered in cKO mice compared to WT mice (data not shown). However, a change in the composition of the splenic cells was observed (Figure 40 A). The proportion of B cells in the spleen was 38 % ± 3 in the WT, compared to 49 % ± 4 in cKO mice (B). This was also observed in the blood; 30 % ± 4 in WT compared to in 38 % ± 10 in cKO mice (C).

.

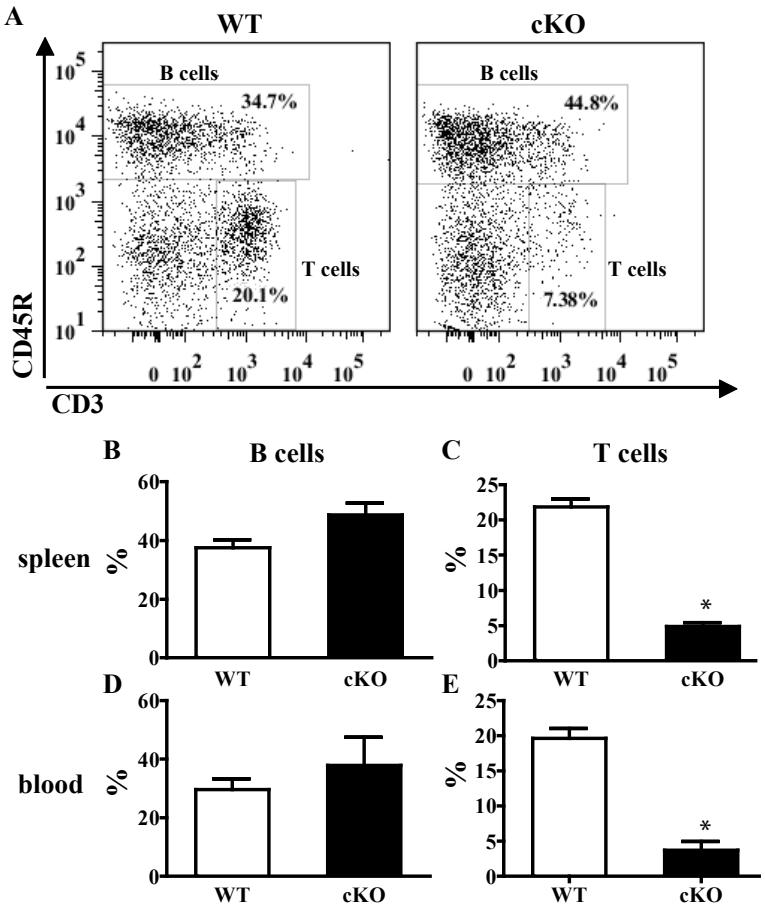

Figure 40. B and T cells in spleen and blood.

Splenoyctes and lymphocytes from the blood were stained for CD3 (T cells) and CD45R (B cells) and analyzed for their B and T cell composition. (A) Depicted is the typical staining of WT and cKO splenocytes and the gating strategy employed for T and B cells. Comparison of the B (B) and T cell (C) composition in WT (white) and cKO (black) mice in the spleen (B and C, respectively) and the blood (D and E, respectively). WT n=6, cKO n=3, * p>0.05.

However, these increases were not significant. A large reduction in the proportion of T cells from 22 % ± 1 in WT to 4.9 % ± 0.6 in cKO splenocytes was observed (D). The same was found in blood lymphocytes, where T cells were reduced from 20 % ± 1 in WT to 4 % ± 1. in cKO (E). These results indicate that deletion of the PRR in T cells results in a decreased T cell number of about 80 % in the spleen and in the blood, whilst B cell numbers are not significantly changed.

T cells can be further divided into several cellular subsets. The two major types are cytotoxic T cells ($CD8^+$ cells) and T helper cells ($CD4^+$ cells), which are characterized by their surface expression of the molecules CD4 and CD8. T cells isolated from blood and the spleen as described above were subsequently analyzed for their composition of $CD4^+$ and $CD8^+$ cells. Figure 41 A shows a typical staining for $CD4^+$ and $CD8^+$ T cells isolated from the spleen. Analysis of the proportion of $CD4^+$ and $CD8^+$ cells showed that the percentage of $CD4^+$ cells was significantly reduced from 20 % ± 2 in WT, to 2.9 % ± 0.03 in cKO mice (B). $CD8^+$ cells were also significantly reduced from 13 % ± 2 in WT, down to 3.1 % ± 0.7 in cKO (C). Similar results were obtained for T cells isolated from blood: $CD4^+$ cells WT 15 % ± 1 vs. cKO 2.3 % ± 0.7 (D), CD8+ cells WT 9.7 % ± 0.8 vs. cKO 4 % ± 2 (E). In summary, it was found that in cKO mice, the percentages of peripheral $CD4^+$ and $CD8^+$ cells decreased by approximately 85 % and 70 %, respectively.

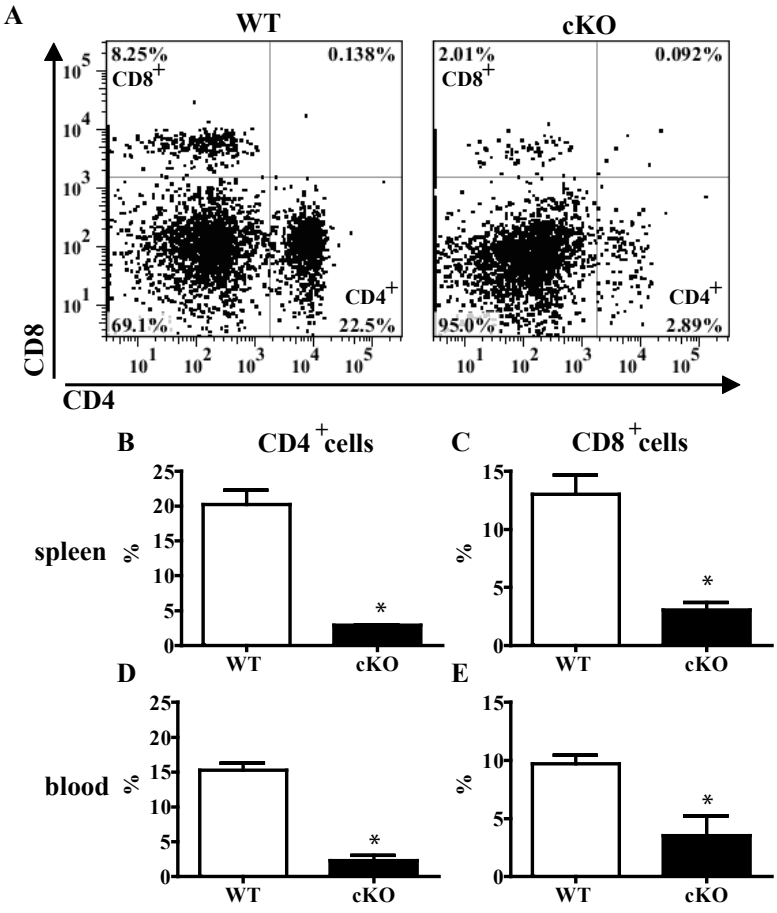

Figure 41. CD4$^+$ and CD8$^+$ cells are reduced in the spleen and blood of PRR cKO mice.

Splenoyctes and lymphocytes from the blood were stained for CD4$^+$ and CD8$^+$ markers and analyzed for their T cell composition. (A) Depicted is the typical staining of WT and cKO splenocytes, with the gating strategy used to identify CD4$^+$ and CD8$^+$ cells. Comparison of the CD4$^+$ and CD8$^+$ cells composition in the spleen (B and C) and in blood (D and E). WT n=7, cKO n=4, * p>0.05.

4.4.3. Characterization of T cell proliferation and apoptosis

An explanation for the decrease in circulating and splenic T cells could be due to the deletion of PRR inhibiting proliferation, or alternatively, increasing T cell death (apoptosis).

To analyze the affect of PRR cKO on T cell proliferation, CD4$^+$ cells were isolated, stained with CFSE and cultured for several days. CFSE is a dye, which stains the extracellular membrane of cells. When cells undergo division, the dye is diluted and this decrease of CFSE positive cells can be measured by flow cytometry. However, it was not possible to purify sufficient amounts of CD4$^+$ cells from the cKO mice for this type of experiment, because of the low amount of CD4$^+$ cells. So the question of whether PRR deletion affects T cell proliferation could not be answered.

To investigate if the loss of T cells was due to an enhanced rate of apoptosis, freshly isolated splenic T cells were stained for the apoptosis marker, AnnexinV. Figure 42 shows the AnnexinV staining for $CD4^+$ and $CD8^+$ splenic T cells. In black, are the WT cells, in red the cKO cells. Overlay of the histograms shows almost identical Annexin V staining for $CD4^+$ and $CD8^+$ cells from WT and cKO mice. The cKO T cells did not show signs of increased numbers of cell death.

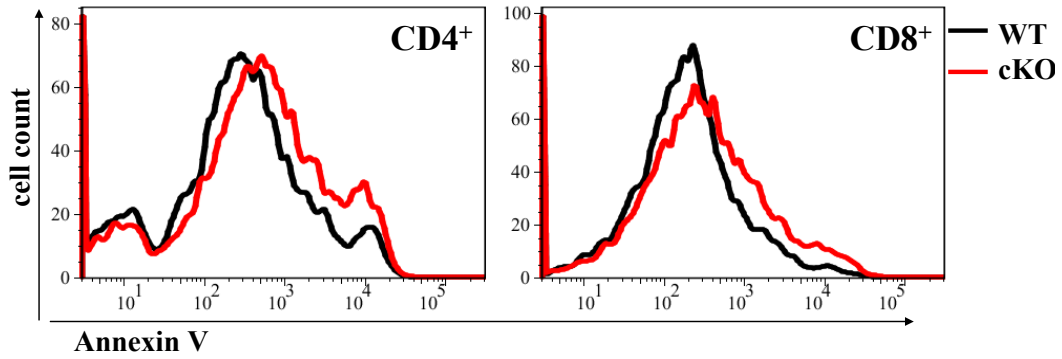

Figure 42. Apotosis staining of splenic T cells.

The cells were gated for $CD4^+$ or $CD8^+$ and analysed for Annexin V staining. WT cells are in black, cKO are in red.

4.4.4. Characterization of thymocyte maturation

Another explanation for the observed decrease in mature T cells could be a defect in T cell development. T cells mature in the thymus of young mice. During maturation of T cells the cells are first negative for the expression of CD4 and CD8 and are therefore called DN (double negative) cells. In the next step, they start to express both CD4 and CD8 and are therefore DP (double positive) cells. After this stage, the T cells develop into single positive cells, expressing either CD4 or CD8. Thymocytes from 4-6 week old male WT or cKO mice were first analyzed for their CD4 and CD8 expression. The proportion and type of thymocytes in WT and cKO mice were notably different (Figure 43 A). DN cells were significantly elevated from 3.5 % ±0.6 in WT, up to 38 % ±9 in cKO mice (B). DP cells were significantly reduced from 79 % ±2 in WT, down to 50 % ±8 in cKO mice (C). This is a relative reduction in DP cells of ~40 % and an increase of DN cells of ~90 %. The proportion of single positive (SP) cells in the cKO were unchanged compared to WT ($CD4^+$ cells: WT 15 % ±1, cKO 14 % ±2 (D); $CD8^+$ cells: WT 2.3 % ±0.4, cKO 5 % ±1.0 (E)). These results indicate that deletion of PRR blocks the transition of T cells from DN to DP cells.

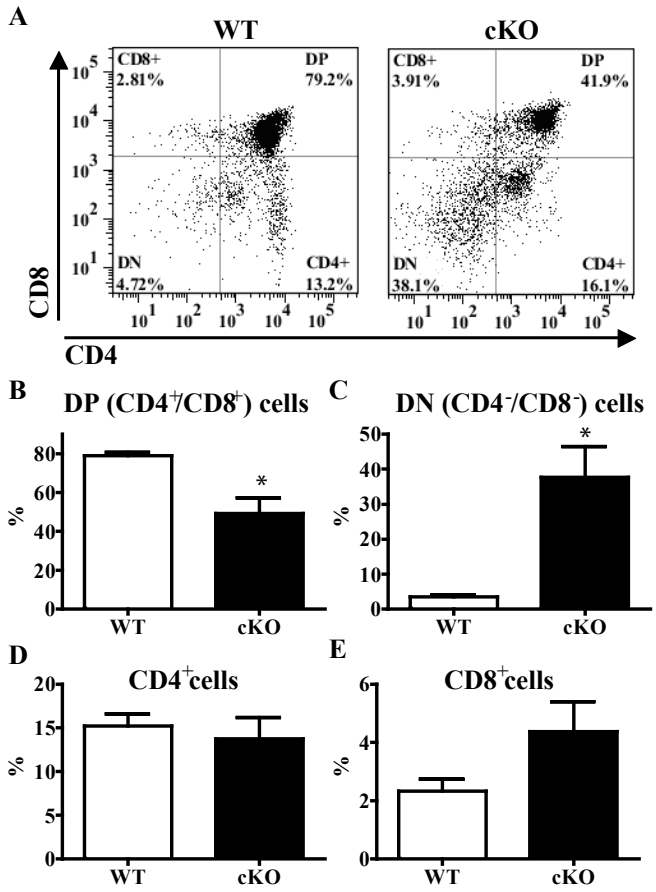

Figure 43. PRR cKO blocks T cell development.

A) Typical CD4 and CD8 staining of WT and cKO thymocytes. Comparison of the composition of T cells in the thymus of WT and cKO mice: DP (B), DN (C), $CD4^+$ (D) and $CD8^+$ (E) cells. WT n=8, cKO n=4, * p>0.05.

DN thymocytes can be further subdivided into DN1-DN4 types. As shown before the deletion of the PRR resulted in a dramatic increase of DN cells (Figure 43). Therefore the composition of DN cell subsets should be analysed. These are classified by the expression of CD25 and CD44 (DN1 = $CD25^-/CD44^+$, DN2 = $CD25^+/CD44^+$, DN3 = $CD25^+/CD44^-$, DN4 = $CD25^-/CD44^-$). To determine which stage PRR deletion blocks T cell development, WT and cKO DN cells were isolated and analyzed for their CD25 and CD44 expression (Figure 44 A). DN3 cells are significantly elevated from WT 72 % ± 3 to 82 % ± 1 in cKO mice (B). This is complemented by a decrease in DN4 cells from 22 % ± 2 in WT, to 14 % ± 1 in cKO (C). As the LCK Cre expression only begins at the DN3 stage, the proportion of DN1 (D) and DN2 (E) cells are unaffected (DN1: WT 5 % ± 2, cKO 3.0 % ± 0.2; DN2: WT 0.4 % ± 0.04, cKO 0.6 % ± 0.3). In conclusion, these results indicate that PRR deficiency impairs the DN3-to-DN4 transition in thymocytes.

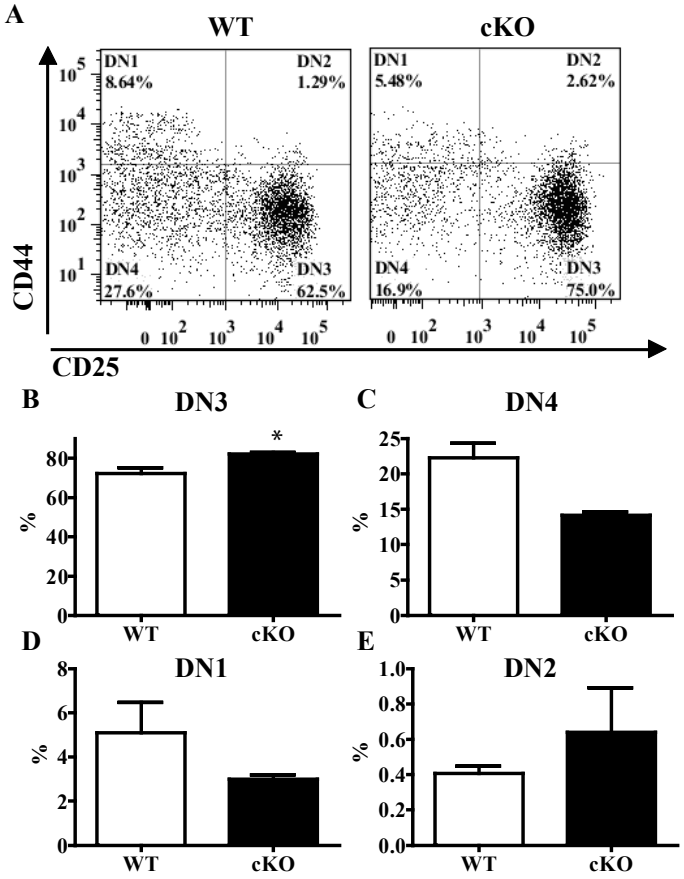

Figure 44. PRR deficiency blocks transition from DN3 to DN4.

A) WT and cKO DN thymocytes were stained for the markers CD25 and CD44. Evaluation of the DN1-4 cell composition comparing WT (white) and cKO (black). (B) DN3; (C) DN4; (D) DN1; (E) DN2. WT n=4 compared to cKO n=3, * p>0.05

Deletion of the PRR in T cells results in a reduction of T cells. This might be due to a developmental block in the DN cells. This data confirm a crucial role for the PRR for T cell maturation.

5. Discussion

The PRR is a single transmembrane receptor that is thought to be important for various cellular processes by influencing the activity of the RAS cascade, the WNT/β-catenin signalling pathway and vATPase activity. It has been shown that PRR binds renin, LRP6, Frizzled and is an accessory protein of vATPase. No structural data is available about the soluble part of the PRR and how PRR interacts with its ligands is not clear. In this thesis, several recombinant constructs of the soluble part of the human PRR could be purified. The hsPRR (101-257) was found to exist in a concentration and pH dependent monomer/oligomer equilibrium, while hsPRR (166-257) was present in a monomer/dimer equilibrium. This biochemical characterization and structural analysis will ultimately aid in understanding the function of PRR and the relation to the RAS, WNT/β-catenin pathway and vATPase and are the basics for further structural and functional investigations. Additionally, using a conditional KO the physiological effect of PRR deletion in T cells was investigated *in vivo*. Specific deletion of PRR resulted in a loss of mature T cells in the circulation and in the peripheral lymphoid tissue. This reduction was found to be due to a defect in T cell maturation. These data help to understand the involvement of the PRR for T cell development.

5.1. Characterization of PRR constructs

5.1.1. Purification of PRR constructs

For structural analysis soluble protein is needed in milligram amounts. Therefore a bacterial expression system to obtain sufficient amount of recombinant protein was used. The purification protocol for the hsPRR (170-303), hsPRR (101-257) and hsPRR (166-257) was established and optimized. These soluble constructs are now the basis for further characterization, structural studies and cellular assays.

The PRR was in most conditions insoluble. One explanation for this could be that the correct folding of PRR depends on the eukaryotic folding machinery. It is known that many proteins require molecular chaperones to fold efficiently [157]. During the folding procedure partially folded states may become transiently populated as kinetically trapped species. Partially folded or misfolded states tend to aggregate in a concentration-dependent manner. This is due to the fact that these forms typically expose hydrophobic amino-acid residues and regions of unstructured polypeptide backbone to the solvent [157]. To overcome this problem it would be of interest to switch the expression system to an eukaryotic system. Different expression

systems in eukaryotic cells for PRR were already published. Several groups expressed full-length and the soluble part of PRR in the baculovirus expression system [158, 159]. Both recombinant proteins bound renin or prorenin and facilitated the conversion of angiotensinogen. A different approach was to over-express the full-length PRR and PRR without the cytoplasmic domain in the fat body and the soluble PRR in the hemolymph of silkworm larvae [160-162]. These proteins bound to renin and prorenin, but all of these trials resulted in low amounts of protein that was never in the milligram range needed for crystallization trials.

A second explanation could be that the PRR needs for its correct folding, additional binding partners [163]. If a binding partner is missing, possible hydrophobic surface patches involved in the binding are exposed and could trigger aggregation. Co-expression of a binding partner often improves the solubility of proteins [153]. Because of the membrane localization of vATPase only subunits of the V_0 domain are likely to interact with the extracellular part of the PRR [68]. Additionally, the PRR could need its transmembrane region for correct folding, but this is in contrast to the published eukaryotic expression systems where expression of the extracellular part of the PRR was possible in low amounts [160-162].

Stably folded, globular domains of proteins are more likely to be solubly expressed [153]. So another possibility is that the PRR has large unordered regions in the extracellular region that reduce its solubility when over-expressed in *E.coli*. The secondary structure prediction (see Appendix) predicts approximately ~40% alpha helices and ~10% beta strand for the full length PRR. Accordingly, ~50% of the protein is predicted to be not structured or to form loop regions. It was hypothesized that introduction of mutations that are supposed to reduce the surface entropy of the protein, which is usually beneficial for crystallization, might also improve the solubility of proteins [152]. But the only approach to obtain soluble protein from *E.coli*, was to modify the constructs by cutting flexible loops or predicted disordered regions.

5.1.2. Binding to renin and prorenin

The binding site for renin or prorenin is thought to be located in the extracellular domain, given that renin and prorenin are found almost exclusively in the circulation [1]. Therefore, soluble PRR is expected to bind renin or prorenin. In the GST pull-down experiments no binding to renin or prorenin was observed for the purified constructs. Also using analytical ultracentrifugation binding-assay with hsPRR (166-257), no binding to renin was observed.

This was not surprising as hsPRR (166-257) covers the same amino acid sequence as hsPRR (101-257).

There are several possibilities to explain this lack of binding to renin and prorenin. Firstly, the GST pull-down experiments could be negatively influenced by the presence of the 26 kDa GST tag. The GST tag is N-terminally linked to PRR and could sterically inhibit binding to the ligands. Additionally, placing the tag to the C-terminus might prevent tag interference. Nevertheless, this possibility only accounts for the GST pulldown-assay. In the analytical ultracentrifugation experiments, no GST was linked to the PRR. This experiment showed also no binding of renin to the truncated PRR, suggesting that the GST tag was not the reason for the lack of renin binding.

Some binding affinities, especially for protein-protein interactions involved in signal transduction processes or for cell surface receptors, are described to be rather low in the micromolar range. This is often described for functions that require the interaction to be transient [164]. An alternative explanation for the lack of binding is therefore that the affinity of renin and prorenin to the truncated PRR constructs is to low and the ligands are lost during the experimental GST pull-down protocol. But this explanation contrasts the already published binding affinities of renin and prorenin to the PRR that are in the low nanomolar range. Batenburg et al and Nabi et al published almost identical Kd values for renin/PRR binding with a Kd of 20 nM, while prorenin bound with a Kd of 7 nM and 8 nM, respectivley to the PRR [40, 165]. Additionally, low binding affinities should be detectable with analytical ultracentrifugation.

Another possible reason for the lack of binding might be that the binding site for renin is disrupted. This would happen if the binding site for renin or prorenin is localized in the N-terminal region (amino acid 1-100) of the extracellular part of PRR. Alternatively, only parts of the N-terminal region are involved in binding and are needed to form the binding interface. But not only might the N-terminal region be missing for binding to renin or prorenin. It is also possible that the extracellular domain together with the transmembrane domain of PRR is needed to display full functional binding. This was first described by Du et al. who showed that the purified full-length PRR displayed a higher binding affinity to renin (Kd 46 nM) then a PRR variant lacking the transmembrane and intracellular domain. The extracellular PRR was found to loose its binding affinity after purification, but this could be recovered by

addition of microsomes [160]. This study suggests that the transmembrane region stabilizes the extracellular domain of PRR. The lack of the transmembrane region in the purified constructs might weaken the affinity of PRR to renin.

Still another explanation is that the PRR in fact does not bind to renin or prorenin. PRR/renin or prorenin interaction was confirmed in cellular assays with radiolabeled renin in human mesangial cells [1]. Additional studies showed binding of renin to rat smooth muscle cells overexpressing the human PRR [40]. However, it is likely that the major PRR function is not on the RAS. It has already been questioned in the interpretation of PRR binding studies whether the affinity of PRR to renin or prorenin is sufficient to bind to renin or prorenin under physiological conditions [65]. Renin and prorenin are usually found in picomolar levels in the circulation and this makes activation of the RAS by binding of renin and prorenin to the PRR *in vivo* implausible, as renin and prorenin could not quantitatively bind to PRR. Higher prorenin levels might occur at sites of prorenin expression, but whether its concentration is high enough to bind to PRR is not known [65]. Additional evidence against an interaction *in vivo* came from Batenburg *et al* showing that direct renin and prorenin induced effects *via* the PRR require renin and prorenin concentrations far above the levels found *in vivo*. They concluded that renin and prorenin interaction with PRR is unlikely to take place in non-renin synthesizing organs [166]. Recently, Cruciat et al showed that the PRR functions in a renin independent way by mediating WNT/β-catenin signalling [17]. Deletion of PRR results in early lethality and since the RAS system is not required for survival at this stage [14], this points to renin and prorenin independent function of PRR [11]. Thus, PRR seems to be more likely involved in acidification and WNT/β-catenin signalling, rather then in the RAS.

5.1.3. Oligomerization of PRR proteins

A surprising finding from this thesis was that hsPRR (101-257) and hsPRR (166-257) had different oligomerization properties. The hsPRR (101-257) was in a monomer/oligomer equilibrium and the hsPRR (166-257) in a monomer/dimer equilibrium. This change in oligomerization of hsPRR (101-257) occurred at almost physiological pH between pH 7.5 and pH 8. Therefore, a histidine might be involved in this process, whose imidazol ring has a pKa of 6 [167]. By truncating hsPRR (101-257) to produce hsPRR (166-257), the oligomer was no longer observed. In the additional 65 amino acids of the hsPRR (101-257), only one histidine is found at position 114 (Figure 45). This histidine is conserved among all species, pointing to

an important role of this residue in the function of PRR. Mutating this histidine, might result in the breakdown of the oligomer.

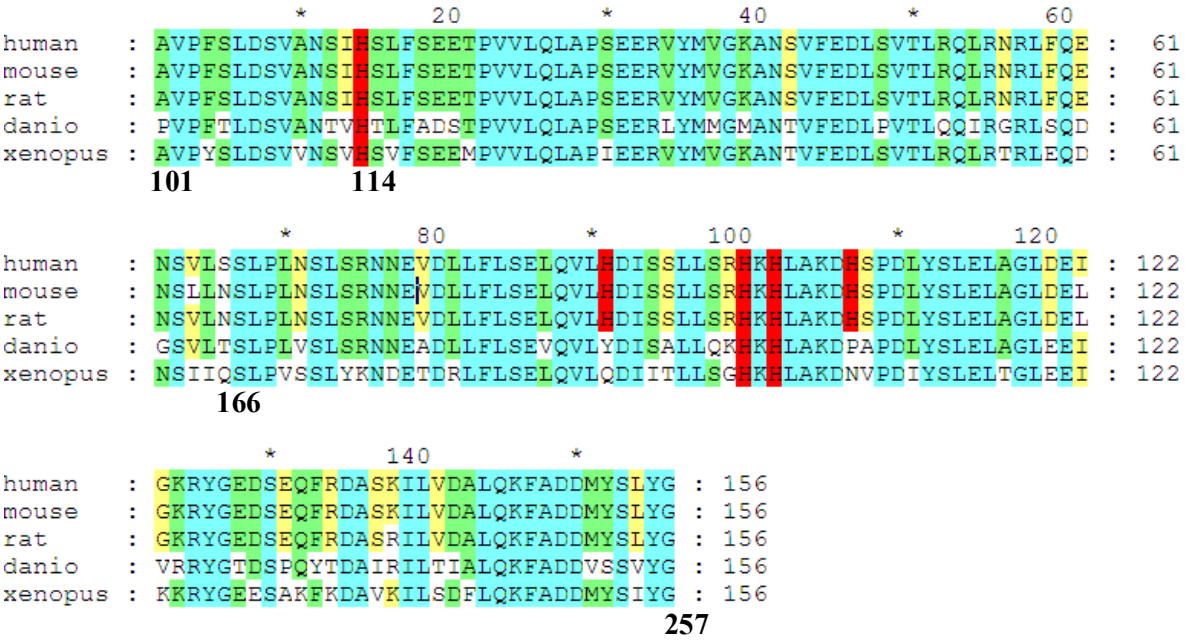

Figure 45: Amino acid alignment of the hsPRR (101-257) with different species (mouse, rat, danio/ zebrafish and xenopus/frog.

100% conserved residues are boxed in light blue, 80% conserved residues are boxed in light green and 60% conserved residues are in light yellow boxes. Histidines are highlighted in red.

It is possible that the full-length PRR has the same pH- and concentration-dependent monomer/oligomer equilibrium. Schefe *et al* showed that the full-length PRR could be co-immunoprecipitated with itself [8]. They concluded that the PRR assemblees as a homodimer, but the formation of larger oligomers would also be compatible with their results. For the full length PRR proteins, oligomerization would be mediated by the extracellular domain of the PRR, but could still influence *via* the transmembrane region and the short intracellular domain an interaction with the intracellular V_1 or the transmembrane V_0 domain of the vATPase. The RALS analysis of hsPRR (101-257) indicates that it assembles as pentamer or hexamer. Interestingly, the vATPase displays as well a hexameric structure. The *A* and *B* subunit of the V_1 domain are arranged as a heterohexamer and also the proteolipid of the V_0 domain is described as a hexameric ring [68]. The soluble part of the PRR would be localized at the extracellular part of the plasmamembrane or in intracellular vesicles. An interaction of the soluble PRR with the intracellular V_1 domain of the vATPase, is therefore not possible, but an interaction with the transmembrane proteolipid ring of the V_0 domain would be feasible.

Therefore a hypothetical link of the PRR oligomer and the vATPase hexamer is possible and might play a role for binding and function.

The pH dependent oligomerization points towards a functional implication of pH for the role of PRR. As already described, the vATPase is a proton pump required for acidification of intracellular compartments or extracellular fluid [66]. How the vATPase senses pH is not fully understood. The shift of hsPRR (101-257) from a monomer to monomer/oligomer equilibrium occurred between pH 7.5 and pH 8 at basic conditions. This somehow contrast with the fact that vATPase is only mediating acidification (pH below 7), but for the full length PRR the pH dependent oligomerization could occur at lower pH. Furthermore, other factors are described to influence vATPase activity in a pH dependent manner. It was already shown that Arf6 and ARNO partially co-localize with vATPase in the apical endosomes in proximal tubules in the kidney [168]. Both proteins were recruited in a pH dependent fashion from the cytosol to endosomes. Arf6 interacts with the *c* subunit, whereas ARNO interacts with the *a2* isoform of vATPase. Inhibition of the vATPase/ARNO/Arf6 interactions inhibited early endocytosis. This indicates that Arf6 and ARNO play an important role in the pH dependent regulation of receptor-mediated endocytosis [169]. The functional difference for the hsPRR (101-257) and hsPRR (166-257) and the pH dependent oligomerization will be investigated in the future.

5.1.4. Structural investigations of the PRR proteins

Structural information will broaden the understanding of the function of the PRR. Crystallization is still a process that is not predictable. Some factors can influence crystallizability of proteins and some decrease the likelihood of forming crystal contacts [170]. In numerous trials, crystallization of the soluble PRR constructs was not successful, but I was able to obtain significant insights into the biochemical behaviour of hsPRR (101-257) and hsPRR (166-257) were obtained, which may provide explanations for this phenomena.

The hsPRR (101-257) is present in solution in a monomer/oligomer equilibrium. Such an equilibrium is not favourable for crystal formation, as two or more species are present in solution [170]. During initial screens, this pH and concentration dependent monomer/oligomer equilibrium was not known. Therefore most of the screens were performed at a pH of 7.5 and below. From the biochemical characterization, it is now clear that the hsPRR (101-257) precipitates at pH 6.5 and below, which is close to the theoretical pI value of 4.9 of the PRR. At this point the hsPRR (101-257) has the lowest solubility in solution and precipitates. As

discussed previously, it was found that the hsPRR (101-257) is present as a monomer at pH 8 and above. Thus, future crystallization trials for hsPRR (101-257) will be optimized at these higher pH, where hsPRR (101-257) is predominantly monomeric, increasing the likelihood of the crystal formation.

During purification of hsPRR (166-257), it appeared that this protein would be ideal for crystallization trials. In contrast to hsPRR (101-257), the protein could be concentrated up to 90 mg/ml without precipitation. Additionally, the purity of this protein was above 95 % and the samples seemed to be homogenous by gel filtration. However, it turned out that hsPRR (166-257) was present in solution as a monomer/dimer equilibrium. Unlike hsPRR (101-257), the equilibrium for the hsPRR (166-257) could not be shifted to a monomeric protein by increasing the pH to 8 and above. Whether this equilibrium might be influenced by changing the buffer conditions (e.g, salt or pH) is still under investigation. This information should be used for the design of following crystal screens.

It appeared that hsPRR (166-257) was not stable over the time at 20 °C and this may affect crystallization. During the sedimentation equilibrium run a loss of the UV signal was observed (Figure 46). The difference in the absorbance signal after 44 h and 68 h at the radial distance of 6 cm is not compensated at the radial distance at 6.1 cm.

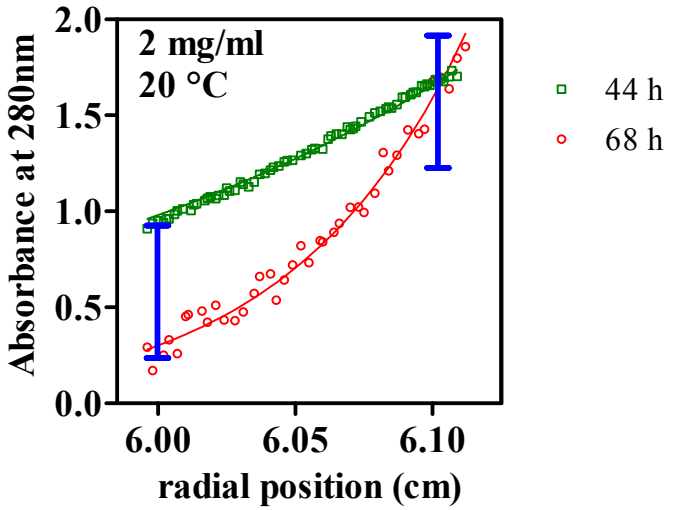

Figure 46. Sedimentation equilibrium analysis of hsPRR (166-257) at 2mg/ml.

Absorbance scans were taken after the sample reached equilibrium after 44 h at 20,000 (green) and after 68h at 35,000 (red) rpm. The capped blue line indicates the difference in OD signal at radial position 6 cm that was not observed at radial position 6.1 cm.

The area under the curve reflects the amount of protein in the sample and this area decreases over the time. This was especially observed at higher concentrations, 2mg/ml and above, whilst this was not seen at concentrations below 1mg/ml. This can be explained by the slow precipitation of the protein at 20°C.

In NMR measurements, the HSQC spectrum for the hsPRR (166-257) revealed that the protein was folded but the dispersion of the resonances was not good and several resonances were overlapping. The monomer/dimer equilibrium might explain why the spectrum was not useful. The sample is in constant exchange and therefore the peaks seem to smear [156]. Since assignments are crucial for structure determination and this was impossible, NMR experiments were not continued. Another possibility would be to test the longer construct, the hsPRR (101-257), in NMR spectroscopy. 18 kDa are still in the size range for NMR structure determination, although the low amount of aromatic residues and the high alpha helical composition of the hsPRR (101-257) might still be problematic. An advantage of this sample would be the possibility to perform measurements at pH 8 where the protein is a monomer. A homogenous sample might ameliorate the quality of the spectra.

5.2. Conditional deletion of PRR in T cells

5.2.1. PRR cKO causes a decrease in T cell numbers due to a block in development

One hypothesis of this thesis was that the deletion of PRR in T cells would result in a phenotype similar to a conditional deletion of β-catenin in T cells. This is based on recent studies showing PRR to be essential for Wnt/ β-catenin signalling [17]. Deletion of β-catenin resulted in an impaired T cell development in the thymus [120]. A comparison of both models would help to understand the role of PRR for Wnt/ β-catenin signalling. In both models a cre recombinase under the control of the Lck promoter was used. The cre expression starts at the DN3 stage during T cell development.

The PRR knockout model showed a reduced number of T cells in the spleen, whereas the number of B cells rose only marginally. Interestingly, a similar reduction of T cells in the spleen for the PRR cKO and for the T cell specific β-catenin KO is described [120]. For the PRR model, both $CD4^+$ and $CD8^+$ cells were affected, which was also shown for the β-catenin deletion model. Two possible explanations for this decrease in T cell numbers might account

for this: a reduction in cell proliferation or a block in development. In the β-catenin KO, Xu et al described that mature KO T cells had a decreased proliferation rate [120]. In the present study, this was not possible to determine as not enough T cells could be isolated from PRR cKO mice for proliferation assays. However, a defect in the maturation in the thymus was shown, at the DN-DP stage. The DN cells usually make only a small minority of about 5 % in WT mice, but in the PRR cKO mice this number of DN cells was increased to ~37 %, corresponding with a decrease in DP cells from 80 % to 50 %. These changes in DN/DP cell proportions are more dramatic in the PRR cKO then those described for the β-catenin phenotype, where the authors only describe an increase in DN cells from 3% in WT mice to 8 % in the cKO [120]. In consequence, the phenotype in mature T cells in the periphery is similar to the one observed in β-catenin KO animals, but the closer analysis of the development in the thymus shows some differences and are even more dramatic in the PRR cKO model. A role for the PRR for Wnt/β-catenin signalling can not be excluded.

5.2.2. Block in the transition from DN3-DN4 might be due to PRR affecting pre-TCR signalling

The mature T cells are decreased in the PRR cKO model and it seems that these T cells have a developmental block in the DN stage in the thymus. The recombinase expression starts at the DN3 stage in the thymus, so therefore one explanation for the decrease in the PRR cKO T cell could be that the T cells die as soon as the PRR is deleted. But this is in contrast to the remaining mature T cells and the DP cells that are still able to develop into T cells.

The phenotype of the T cell specific PRR cKO model is in many ways similar to the β-catenin KO phenotype. By deleting the PRR in T cells a decrease in the percentage of DN4 cells and an increase of DN3 cells was observed. The same was true for the β-catenin deletion in T cells [120]. The authors favour the explanation that the deletion of β-catenin affects pre-TCR signalling, that in turn leads to impaired T cell differentiation. They propose that the β-selection checkpoint at the DN3 cell stage is influenced by WNT/β-catenin signalling and, as a result, the cells cannot proliferate and further develop at this stage. As PRR is shown to be important for WNT signalling [17], it is possible that PRR deletion in T cells affects T cell development in a similar manner.

Another link for the involvement of the pre-TCR was shown previously. The pre-TCR is down-regulated by constitutive internalization and degradaded in lysosomes [171]. This might be

required for the development of T cells and their function. This phenomenon is only described for the αβTCR [171]. Since degradation of the pre-TCR occurs in lysosomes it is likely to be vATPase dependent. Another possibility is that this degradation process and the internalization of the pre-TCR is regulated by WNT/β-catenin signalling. By deletion of the PRR, downregulation might be interrupted and T cell development might be disturbed. This could also explain the block at the DN stage since the pre TCR expression starts in the beginning of the DN3 stadium.

5.2.3. Role of the vATPase in T cell development

It has also been recently shown that PRR is important for vATPase activity [87, 92]. Conditional KO in other cell types, like cardiomyocytes [87] and podocytes [91, 92], have shown a disturbance in vacuolar pH as a result of reduced vATPase activity. Defective autophagy is also described in these PRR cKO models [87, 91, 92]. Currently, no conditional KO for any subunits of the vATPase in hematopoetic cells or T lymphocytes has been performed, and so no direct comparison between PRR cKO can be made. The vATPase is a crucial factor for autophagy, a conserved intracellular protein degradation process, depending on the acidification of intracellular vesicles. Autophagy is also an important process for T cell development and function. In ATG5 deficient mice (a protein involved in autophagy), T cells fully matured, but the number of peripheral $CD4^+$ and $CD8^+$ cells is reduced. These cells show increased cell death and have a proliferation defect after TCR stimulation, indicating that ATG5 is important for survival and proliferation of T cells [131]. This is in contrast to another autophagy associated KO model. Beclin-1 deficient Rag $1^{-/-}$ chimeras have a dramatically reduced number of thymocytes, but the peripheral T cell compartment is unchanged. Proliferation of peripheral T cells is not affected, but they showed a reduced number of autophagosomes. The authors of this study conclude that Beclin-1 is required for maintenance of undifferentiated/early lymphocyte progenitor populations and plays a role in the development of T cells [172]. The described phenotypes for these models are not directly comparable to the PRR cKO phenotype, but indicate a role for autophagy in early T cell development and function. This is turn suggests that PRR *via* its vATPase function might play a role in T cell maturation by affecting autophagy.

5.2.4. PRR deletion decreases but does not completely reduce T cells

Deletion of the PRR in T cells reduces mature T cells down to 5 %, but does not result in a complete lack of T cells. There are several reasons to explain the existence of the remaining T cells.

One explanation for the surviving 5 % of the T cells is that the recombination of the cre-recombinase is not a 100 % efficient and the floxed exon 2 of the PRR is not deleted in all T cells. For thymocytes a complete deletion of the PRR exon 2 (as well as for DN and for DP/SP cells, data not shown) was seen, whereas in the spleen the full-length PRR was still apparent. This could be due to the cellular composition of the spleen. The spleen harbours not only T cell, but also B cells and other immune cells that still express the PRR. Another aspect is the loss in T cells, while they T cells are only present in low amount in the spleen it is difficult to determine the excised PRR. But the data from the thymus show a complete recombination there. The Lck promoter is known to be active only at early stages of T cell development [173] and is expressed only transiently in the thymus [174]. Therefore the recombinase has only limited time to delete the floxed gene of interest. Thus, some T cell might escape recombination in the thymus, mature and are found then in the periphery. The amount of not excised T cells in the thymus might be to low to be detected, but as soon as the mature T cells are in the circulation they proliferate and represent the 5 % of surviving T cells. The T cells in the periphery need further experiments to determine their background.

Another possibility is that the 5 % of surviving T cells are PRR deleted and still are able to develop into mature T cells. If this is the case, it would be interesting to analyze if they are functional and can be activated by TCR stimulus. A different explanation would be that γδ T cells are now found in the circulation. T cells are characterized by their TCR which is in most T cells the αβ TCR. But a small subset expresses a γδ TCR on their surface [121]. This subset should not be affected by the PRR deletion, because they have a different developmental pathway and are not affected by the Lck cre expression. It could be that the main T cell subset, the αβ T cells, are completely decreased because of PRR deletion and the suriving cells are now only γδ T cells. A further suggestion is that an alternative signalling pathway might be involved in the regulation of T cell development. If the PRR interferes with WNT /β-catenin pathway and WNT /β-catenin signalling is disregulated in this model, another pathway might take over the function. Notch signalling is as well known to be involved on T cell development and could play a role [175].

5.3. Outlook and perspectives

Since the PRR was originally described as a component of the RAS and it was shown that binding of renin or prorenin to the PRR resulted in an activation or enhancement of the angiotensinogen cleavage [1], the PRR has been postulated as a potential drug target . The first putative blocker (HRP) of the PRR was described by Ichihara *et al* [59]. Beneficial cardiovascular and renal effects for HRP were described in diverse animal models, like spontaneous hypertensive rats and diabetic models [60, 61]. Here, HRP and PRR blockade had an organ protective effect. This was already controversially discussed since a variety of other models could not confirm these beneficial effects [43, 63, 176]. With the finding that the PRR is involved in WNT signalling and might be a regulator of the function of vATPase [17], the PRR as a drug target has to be seen sceptical. Additionally, deletion of the PRR in cardiomyocytes and podocytes resulted in cellular death and early mortality [87, 91, 92]. cKO of the PRR in T cells resulted in impaired maturation. The PRR is present in all cells and tissues and seems to have fundamental functions for cellular development and function, therefore inhibition of the PRR seems to be critical.

The function of the soluble PRR is still unknown, but it was shown that the PRR is processed by furin [4]. This soluble protein is shedded into the medium of cultured cells and might play an important role in the circulation [6]. The function of the soluble PRR is still unknown, but could be analyzed with an ELISA. The hsPRR (101-257) led to the development of an ELISA to detect soluble PRR in human serum. This ELISA measures reproducibly the soluble PRR in the range of 100 pg/ml and 30 ng/ml (personal communication G. Nguyen, Paris). Currently, various pathologic and healthy patient groups are analyzed for differences in the soluble PRR levels. Thus, with this ELISA it can be analyzed if the soluble PRR is linked to diseases, like cardiovascular disease.

A focus for the ongoing work is to functionally characterize the PRR constructs. All human PRR constructs produced in this work are not binding to renin or prorenin, so they do not seem to be involved in the function of the RAS. Nevertheless, several implications for the PRR are described. It was shown that the PRR influences Wnt/β-catenin signalling [17] and might play a role in vATPase mediated acidification [109, 110]. The next aim would be to find a cellular assay to test the functionality of the PRR proteins for Wnt/β-catenin signalling and acidification. The effect of the PRR proteins in cell culture should be investigated. To analyze the role of the soluble PRR, the purified PRR constructs can be used for Wnt/β-catenin

reporter gene assays. To analyze *in vitro* acidification, it could be determined if the PRR constructs influence acidification in lysosomes and intracellular vesicles.

One possibility to gain more insights into the role of the PRR is a rescue of the cKO phenotype. As the β-catenin deletion showed a similar phenotype as the PRR deletion, a rescue of the PRR cKO with a constitutive active β-catenin would be of interest. β-catenin can be expressed in transgenic animals as a stabilized active mutant. When over-expressed in immature thymocytes, T cells develop, but they lack the αβ TCR and develop in the absence of pre-TCR signaling and TCR selection [177]. This points to the fact that the WNT pathway needs to be in homeostasis. Since reduction and over-expression of components of the pathway leads to a deregulation of the system, a rescue strategy with a constitutive active β-catenin could probably not answer the question if the PRR is involved in the WNT pathway. Another option would be the rescue of the cKO PRR T cell model with the soluble recombinant proteins of PRR. By purifying the hsPRR (101-257) and hsPRR (166-257) in sufficient amount and quality and solving the structure, this could be used as a tool to investigate its function *in vivo*. It would be interesting to examine if the recombinant PRR constructs are able to rescue T cell development in cKO animals. If rescue is possible it could be analyzed if this mechanism is due to activation of Wnt/ β-catenin signalling or if impaired autophagy and acidification are involved. An analysis of the effect of the soluble PRR on T cell culture could help to understand the effect of the PRR on T cell function. Also for other *in vitro* and *in vivo* models this might be a useful tool for the future.

This thesis showed that truncated versions of the human PRR are in a monomer/oligomer equilibrium that could have functional implications. The recombinant PRR proteins could be the basis for future investigations to analyse the structure of PRR and carry out a detailed structure/ function analysis. These constructs could now help to understand the role of the soluble PRR *in vivo*. In addition the deletion of the PRR in T cells resulted in impaired thymocyte development pointing to an important role for the PRR and cell maturation. Further understanding of the role of PRR for cellular function and development is needed.

6. Zusammenfassung

Der (Pro)Renin Rezeptor (PRR) ist ein evolutionär hoch konservierter Transmembranrezeptor, der ursprünglich beschrieben wurde Renin und Prorenin zu binden. Durch Bindung an Renin und Prorenin ist der PRR in der Lage, die Aktivität des Renin-Angiotensin-Systems (RAS) zu beeinflussen und MAP-Kinase-Signaltransduktion zu induzieren. Es wurde bereits gezeigt, dass der verkürzte Transmembranteil des PRR assoziiert ist mit der vakuolären H^+-ATPase (vATPase), welche wichtig für die Azidifizierung zellulärer Organellen ist. Kürzlich wurde eine neue Funktion des PRR für den WNT/β-catenin Signalweg beschrieben. Hier dient der PRR als Verbindungsglied zwischen den WNT Rezeptoren und der vATPase. Die genauen Mechanismen der Funktionen des PRR sind bislang noch nicht verstanden, aber es wird angenommen, dass der PRR in die Regulation verschiedenster zellulärer Mechanismen involviert ist.

Es gibt bis jetzt keine biochemische Charakterisierung oder strukturelle Analyse über diesen verkürzten Teil des PRR. Um die Funktion des PRR besser zu verstehen, wurden in der vorliegenden Arbeit strukturelle Studien mit verschiedenen verkürzten Konstrukten des extrazellulären Teils des PRR durchgeführt. Alle PRR Konstrukte (hsPRR (170-303), hsPRR (101-257) und hsPRR (166-257)) zeigten eine alpha-helikale Faltung und konnten nicht an Renin oder Prorenin binden. Des Weiteren wurde die oligomere Zusammensetzung dieser Konstrukte untersucht. Der hsPRR (101-257) liegt in einem Konzentrations- und pH-abhängigen Monomer-/Oligomerequilibrium vor, während der hsPRR (166-257) als Monomer/Dimerequilibrium vorkommt. Diese Daten bilden die Grundlage für weitere strukturelle und funktionelle Untersuchungen.

Konditionelle KO Mäuse sind eine exzellente Methode, um die physiologische Rolle des PRR *in vivo* zu untersuchen. Eines der wichtigsten Proteine des Wnt/β-catenin Signaltransduktionsweges, β-catenin, ist fundamental für die T-Zell Entwicklung. Aus diesem Grund wurde untersucht, ob die Deletion des PRR in T-Zellen ebenfalls zu einem Verlust von T-Zellen führt. Des Weiteren wurde analysiert, ob es zu einer Entwicklungsstörung im Thymus kommt. Die Ergebnisse zeigen, dass der PRR wichtig für eine vollständige T-Zellentwicklung ist und unterstützen die Hypothese, dass der PRR eine Rolle für Wnt/β-catenin Singaltransduktion in T-Zellen spielt.

7. Appendix

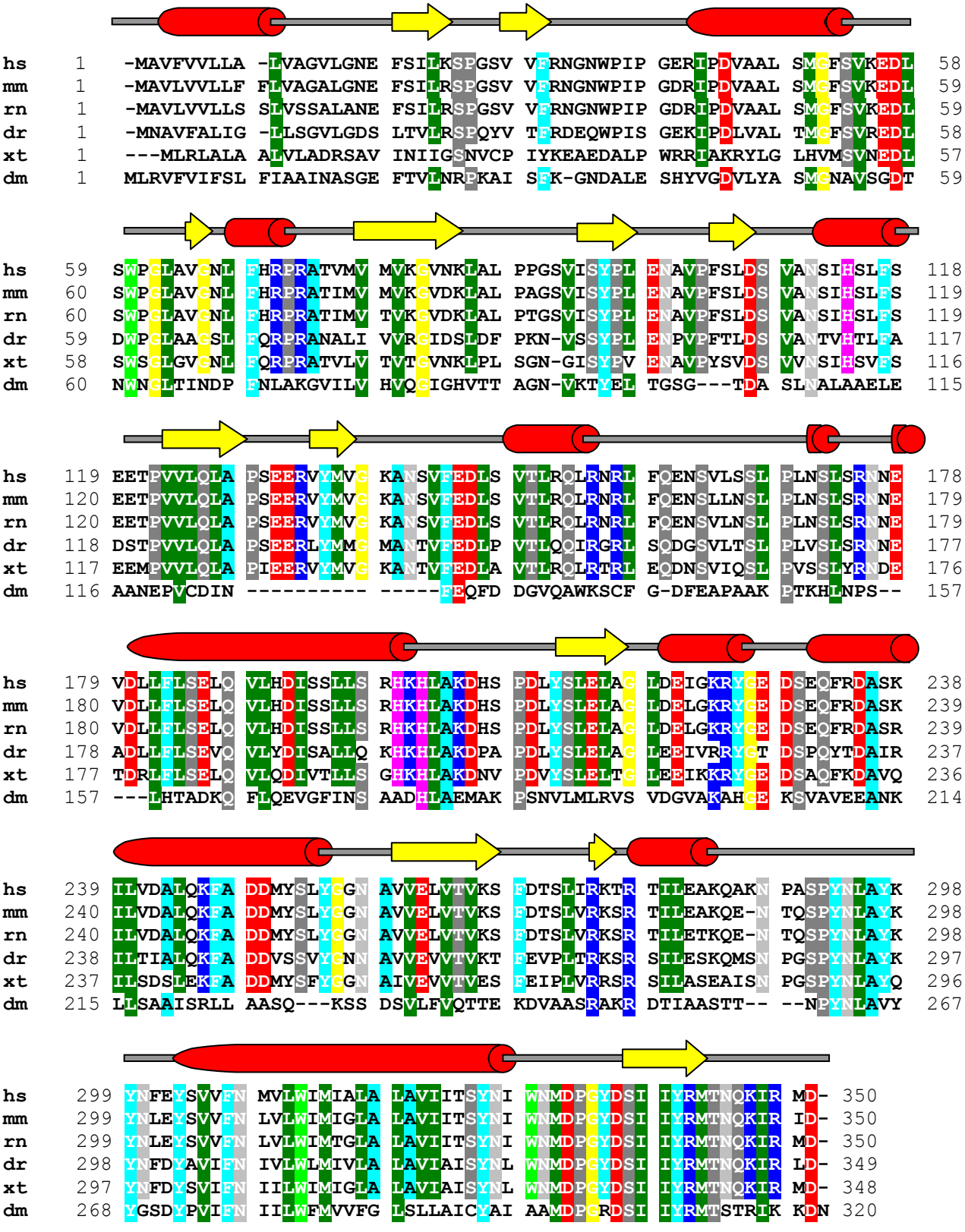
hs 1 -MAVFVVLLA -LVAGVLGNE FSILKSPGSV VFRNGNWPIP GERIPDVAAL SMGFSVKEDL 58
mm 1 -MAVLVVLLF FLVAGALGNE FSILRSPGSV VFRNGNWPIP GDRIPDVAAL SMGFSVKEDL 59
rn 1 -MAVLVVLLS SLVSSALANE FSILRSPGSV VFRNGNWPIP GDRIPDVAAL SMGFSVKEDL 59
dr 1 -MNAVFALIG -LLSGVLGDS LTVLRSPQYV TFRDEQWPIS GEKIPDLVAL TMGFSVREDL 58
xt 1 ---MLRLALA ALVLADRSAV INIIGSNVCP IYKEAEDALP WRRIAKRYLG LHVMSVNEDL 57
dm 1 MLRVFVIFSL FIAAINASGE FTVLNRPKAI SFK-GNDALE SHYVGDVLYA SMGNAVSGDT 59
hs 59 SWPGLAVGNL FHRPRATVMV MVKGVNKLAL PPGSVISYPL ENAVPFSLDS VANSIHSLFS 118
mm 60 SWPGLAVGNL FHRPRATIMV MVKGVDKLAL PAGSVISYPL ENAVPFSLDS VANSIHSLFS 119
rn 60 SWPGLAVGNL FHRPRATIMV TVKGVDKLAL PTGSVISYPL ENAVPFSLDS VANSIHSLFS 119
dr 59 DWPGLAAGSL FQRPRANALI VVRGIDSLDF PKN-VSSYPL ENPVPFTLDS VANTVHTLFA 117
xt 58 SWSGLGVGNL FQRPRATVLV TVTGVNKLPL SGN-GISYPV ENAVPYSVDS VVNSIHSVFS 116
dm 60 NWNGLTINDP FNLAKGVILV HVQGIGHVTT AGN-VKTYEL TGSG---TDA SLNALAAELE 115
hs 119 EETPVVLQLA PSEERVYMVG KANSVFEDLS VTLRQLRNRL FQENSVLSSL PLNSLSRNNE 178
mm 120 EETPVVLQLA PSEERVYMVG KANSVFEDLS VTLRQLRNRL FQENSLLNSL PLNSLSRNNE 179
rn 120 EETPVVLQLA PSEERVYMVG KANSVFEDLS VTLRQLRNRL FQENSVLNSL PLNSLSRNNE 179
dr 118 DSTPVVLQLA PSEERLYMMG MANTVFEDLP VTLQQIRGRL SQDGSVLTSL PLVSLSRNNE 177
xt 117 EEMPVVLQLA PIEERVYMVG KANTVFEDLA VTLRQLRTRL EQDNSVIQSL PVSSLYRNDE 176
dm 116 AANEPVCDIN ---------- -----FEQFD DGVQAWKSCF G-DFEAPAAK PTKHLNPS-- 157
hs 179 VDLLFLSELQ VLHDISSLLS RHKHLAKDHS PDLYSLELAG LDEIGKRYGE DSEQFRDASK 238
mm 180 VDLLFLSELQ VLHDISSLLS RHKHLAKDHS PDLYSLELAG LDELGKRYGE DSEQFRDASK 239
rn 180 VDLLFLSELQ VLHDISSLLS RHKHLAKDHS PDLYSLELAG LDELGKRYGE DSEQFRDASR 239
dr 178 ADLLFLSEVQ VLYDISALLQ KHKHLAKDPA PDLYSLELAG LEEIVRRYGT DSPQYTDAIR 237
xt 177 TDRLFLSELQ VLQDIVTLLS GHKHLAKDNV PDVYSLELTG LEEIKKRYGE DSAQFKDAVQ 236
dm 157 ---LHTADKQ FLQEVGFINS AADHLAEMAK PSNVLMLRVS VDGVAKAHGE KSVAVEEANK 214
hs 239 ILVDALQKFA DDMYSLYGGN AVVELVTVKS FDTSLIRKTR TILEAKQAKN PASPYNLAYK 298
mm 240 ILVDALQKFA DDMYSLYGGN AVVELVTVKS FDTSLVRKSR TILEAKQE-N TQSPYNLAYK 298
rn 240 ILVDALQKFA DDMYSLYGGN AVVELVTVKS FDTSLVRKSR TILETKQE-N TQSPYNLAYK 298
dr 238 ILTIALQKFA DDVSSVYGNN AVVEVVTVKT FEVPLTRKSR SILESKQMSN PGSPYNLAYK 297
xt 237 ILSDSLEKFA DDMYSFYGGN AIVEVVTVES FEIPLVRRSR SILASEAISN PGSPYNLAYQ 296
dm 215 LLSAAISRLL AASQ---KSS DSVLFVQTTE KDVAASRAKR DTIAASTT-- --NPYNLAVY 267
hs 299 YNFEYSVVFN MVLWIMIALA LAVIITSYNI WNMDPGYDSI IYRMTNQKIR MD- 350
mm 299 YNLEYSVVFN LVLWIMIGLA LAVIITSYNI WNMDPGYDSI IYRMTNQKIR ID- 350
rn 299 YNLEYSVVFN LVLWIMTGLA LAVIITSYNI WNMDPGYDSI IYRMTNQKIR MD- 350
dr 298 YNFDYAVIFN IVLWLMIVLA LAVIAISYNL WNMDPGYDSI IYRMTNQKIR LD- 349
xt 297 YNFDYSVIFN IILWIMIGLA LAVIAISYNL WNMDPGYDSI IYRMTNQKIR MD- 348
dm 268 YGSDYPVIFN IILWFMVVFG LSLLAICYAI AAMDPGRDSI IYRMTSTRIK KDN 320

Figure 47. Alignment of PRR

Protein sequences of *Homo sapiens* (hs) (Swiss Prot Acession No. O75787), *Mus musculus* (mm) (Q9CYN9), *rattus norvegicus* (rn) (Q6AXS4), *Danio rerio* (dr) (Q6PBY2), *Xenopus tropicalis* (xt)(Q5M8F1) and *Drosophila melanogaster* (dm) (Q 9VHG4) PRR were aligned using ClustalW [136]. Residues with a conservation of greater than 70% are color-coded (L, V, I, M in green; W in light green; S, P, Q, T in grey; N in light grey; A, Y, F in cyan; R, K in blue; G in yellow; E, D in red; H in magenta). The predicted secondary structure of human PRR (Jpred [137]) is shown on top with α-helices indicated as red barrels and β-strands as yellow arrows.

8. Abbreviations

A	Absorbance
a.u.	arbitrary units
ACE	angiotensin-converting-enzyme
AIM	autoinduction medium
Amp	Ampicillin
ANGI	Angiotensin I
ANGII	Angiotensin II
AOGEN	angiotensinogen
AT1R	angiotensin II type 1 receptor
AUC	analytical ultracentrifugation
bp	Base pair
Cam	Chloramphenicol
Carb	Carbenecillin
CD	circular dichroism
Da	Dalton
DNA	deoxyribonucleic acid
dNTP	Desoxynukleosidtriphosphate
DTT	dithiothreitol
E.coli	*Escherichia coli*
ED	extracellular domain
EDTA	Ethylenediaminetetraacetic acid
FCS	fetal calf serum
g	Acceleration of gravity
GSH	reduced Gluthathione
GST	Gluthathione-S-transferase
HEPES	4-(2-hydroxyethyl)-1-piperazineethanesulfonic acid
HSQC	Heteronuclear single quantum coherence
ID	intracellular domain
IMAC	Immobilised metal affinity chromatography
IPTG	isopropyl-1-β-D-thiogalactopyranoside
Kan	Kanamycin
LB	Luria-Bertani media
M	Molar
MW	molecular weight
NMR	Nuclear magnetic resonance

OD	optical density
PBS	phosphate buffered saline
PCR	Polymerase chain reaction
PRR	(Pro)renin receptor
RALS	right angle light scattering
RAS	renin-angiotensin-system
RNA	Ribonucleic acid
rpm	revolutions per minute
RT	Room temperature
SDS-PAGE	sodium dodecylsulfate polyacrylamide gel electrophoresis
SP	signal peptide
TAE	Tris/Acetic acid/EDTA buffer
TB	teriffic broth
TCR	T cell receptor
TM	transmembrane domain
Tris	Tris(hydroxmethyl)aminomethane
vATPase	vacuolar proton ATPase
WT	Wild type
β-ME	beta-Mercaptoethanol
θ	molar ellipticity
λ	wavelength

Amino acid	3- letter code	1-letter code	Amino acid	3- letter code	1-letter code
Alanine	**Ala**	**A**	Leucine	**Leu**	**L**
Arginine	**Arg**	**R**	Lysine	**Lys**	**K**
Asparagine	**Asn**	**N**	Methionine	**Met**	**M**
Aspartate	**Asp**	**D**	Phenylalanine	**Phe**	**F**
Cysteine	**Cys**	**C**	Proline	**Pro**	**P**
Glutamate	**Glu**	**E**	Serine	**Ser**	**S**
Glutamine	**Gln**	**Q**	Threonine	**Thr**	**T**
Glycine	**Gly**	**G**	Tryptophan	**Trp**	**W**
Histidine	**His**	**H**	Tyrosine	**Tyr**	**Y**
Isoleucine	**Ile**	**I**	Valine	**Val**	**V**

9. Acknowledgement

First of all I would like to thank Prof. Andreas Herrmann who agreed to be my official supervisor at Humboldt-Universität zu Berlin.

I would like to thank Prof. Dominik Müller who gave me the opportunity to work on this exciting and complex, but also challenging topic. During the last years he was at all times interested in my project and was open for new ideas and discussions. He supported me working independently and was always motivating when things were not going that successful. He especially made the cooperation with Prof. Oliver Daumke possible and allowed me to spend a lot of my PhD time in his lab. Many thanks as well to PD Ralf Dechend and Prof. Friedrich C. Luft.

I would like to thank Prof. Oliver Daumke for his friendly and open acceptance for several years in his group. His enthusiasm and optimism was really encouraging for me during the last years. He was always involved in my project and helped me with all small and big problems.

I would like to thank Katja Fälber who introduced me to many methods in the protein world. She always had great ideas and feedback on my project and motivated me a lot. But also all other members of the Daumke lab; David, Song, Janko, Claudio, Verena, Chris, Stephan and Kathrin, I would like to thank. The atmosphere in the lab with all of you was fantastic. For great technical help I would like to thank Sabine and Marion. I really enjoyed being a part of the Daumke lab.

I would like to thank Florian Herse for being supportive throughout my whole PhD time. I really enjoyed a lot being together in the lab or the office with Lydia, Bastian, Lajos, Lukasz and Claudia. Thanks. For introducing me to the FACS world, I would like to thank Verena Fokuhl. Many thanks for fantastic technical help to Gabi, Jule, Ilona, Jana and Frau Gerhardt.

I would like to thank Katrina Binger for bringing so many new great ideas into my research field. Thanks also for being such a “picky”, but also encouraging reviewer.

I would like to thank Genevieve Nguyen for collaboration and making all the interesting meetings possible. The constant and friendly exchange was really motivating for me.

I would like to thank Prof. Udo Heinemann and his group, especially Yvette and Anja, for support with the crystal facility.

Manne took this field to completely new levels for me. Thanks for the especially non-scientific support during the last year, but also for offering your flat for writing and always taking care to have enough distraction.

Besides the research community a lot of people supported me the last years. Thanks a lot.

Finally, I would like to thank my family who always supported me throughout my whole life.

10. Publications

10.1. Peer-reviewed journal articles

Riediger F, Quack I, Qadri F, Hartleben B, Park JK, Potthoff SA, Sohn D, Sihn G, Rousselle A, Fokuhl V, **Maschke U**, Purfürst B, Schneider W, Rump LC, Luft FC, Dechend R, Bader M, Huber TB, Nguyen G, Muller DN. Prorenin Receptor Is Essential for Podocyte Autophagy Survival. J Am Soc Nephrol. 2011 Dec;22(12):2193-202.

Batenburg WW, Lu X, Leijten F, **Maschke U**, Müller DN, Danser AH. Renin- and Prorenin-Induced Effects in Rat Vascular Smooth Muscle Cells Overexpressing the Human (Pro)Renin Receptor: Does (Pro)Renin-(Pro)Renin Receptor Interaction Actually Occur? Hypertension. 2011 Dec;58(6):1111-9.

Maschke U, Muller DN. The (pro)renin receptor and the mystic HRP- is there a role in cardiovascular disease? Front Biosci (Elite Ed). 2010 Jun 1;2:1250-3. Review.

Peters J, Schlüter T, Riegel T, Peters BS, Beineke A, **Maschke U**, Hosten N, Mullins JJ, Rettig R. Lack of cardiac fibrosis in a new model on high prorenin hyperaldosteronism. Am J Physiol Heart Circ Physiol. 2009 Nov;297(5):H1845-52.

Feldt S, **Maschke U**, Dechend R, Luft FC, Muller DN. The putative (pro)renin receptor blocker HRP fails to prevent (pro)renin signaling. J Am Soc Nephrol. 2008 Apr;19(4):743-8.

Feldt S, Batenburg WW, Mazak I, **Maschke U**, Wellner M, Kvakan H, Dechend R, Fiebeler A, Burckle C, Contrepas A, Jan Danser AH, Bader M, Nguyen G, Luft FC, Muller DN. Prorenin and renin-induced extracellular signal-regulated kinase 1/2 activation in monocytes is not blocked by aliskiren or the handle-region peptide. Hypertension. 2008 Mar;51(3):682-8.

10.2. Active Congress participation

10.2.1. Talks

02.2012 Gordon Research Seminar, Angiotensin, invited speaker

04.2011 Cardiovascular and Metabolic Disease Retreat, Neuruppin, Germany

10.2.2. Poster

09.2010 Council Meeting for High Blood Pressure Research, Washington, USA

09.2010 11. MDC/FMP PhD Student Retreat in Rheinsberg, Germany

04.2010 Cardiovascular and Metabolic Disease Retreat, Neuruppin, Germany

09.2009 10. MDC/FMP PhD Student Retreat in Sommerfeld, Germany

Berlin, 13.12.2011 Ulrike Maschke

11.Curriculum vitae

Der Lebenslauf wurde aus Datenschutzgründen entfernt.

12. Eigenständigkeitserklärung

Hiermit erkläre ich, Ulrike Maschke, geboren am 05.07.1981 in Oranienburg, dass ich die vorliegende Arbeit selbstständig erarbeitet und verfasst, sowie keine anderen als die angegebenen Quellen und Hilfsmittel verwendet habe.

Berlin, 13.12.2011 Ulrike Maschke

13. References

1. Nguyen G, Delarue F, Burckle C, Bouzhir L, Giller T, Sraer JD. Pivotal role of the renin/prorenin receptor in angiotensin II production and cellular responses to renin. *J Clin Invest.* 2002;109(11):1417-1427.

2. Nguyen G, Burckle CA, Sraer JD. Renin/prorenin-receptor biochemistry and functional significance. *Curr Hypertens Rep.* 2004;6(2):129-132.

3. Thomas G. FURIN AT THE CUTTING EDGE: FROM PROTEIN TRAFFIC TO EMBRYOGENESIS AND DISEASE. *Nat Rev Mol Cell Biol.* 2002(3(10)):753–766.

4. Cousin C, Bracquart D, Contrepas A, Corvol P, Muller L, Nguyen G. Soluble form of the (pro)renin receptor generated by intracellular cleavage by furin is secreted in plasma. *Hypertension.* 2009;53(6):1077-1082.

5. Mahmud H, Sillje HH, Cannon MV, van Gilst WH, de Boer RA. Regulation of the (pro)renin-renin receptor in cardiac remodeling. *J Cell Mol Med.* 2011.

6. Yoshikawa A, Aizaki Y, Kusano K, Kishi F, Susumu T, Iida S, Ishiura S, Nishimura S, Shichiri M, Senbonmatsu T. The (pro)renin receptor is cleaved by ADAM19 in the Golgi leading to its secretion into extracellular space. *Hypertens Res.* 2011;34(5):599-605.

7. Ludwig J, Kerscher S, Brandt U, Pfeiffer K, Getlawi F, Apps DK, Schagger H. Identification and characterization of a novel 9.2-kDa membrane sector-associated protein of vacuolar proton-ATPase from chromaffin granules. *J Biol Chem.* 1998;273(18):10939-10947.

8. Schefe JH, Menk M, Reinemund J, Effertz K, Hobbs RM, Pandolfi PP, Ruiz P, Unger T, Funke-Kaiser H. A novel signal transduction cascade involving direct physical interaction of the renin/prorenin receptor with the transcription factor promyelocytic zinc finger protein. *Circ Res.* 2006;99(12):1355-1366.

9. Zhang Y, Gao X, Michael Garavito R. Structural analysis of the intracellular domain of (pro)renin receptor fused to maltose-binding protein. *Biochem Biophys Res Commun.* 2011;407(4):674-679.

10. Liang P, Jones CA, Bisgrove BW, Song L, Glenn ST, Yost HJ, Gross KW. Genomic characterization and expression analysis of the first nonmammalian renin genes from zebrafish and pufferfish. *Physiol Genomics.* 2004;16(3):314-322.

11. Burckle C, Bader M. Prorenin and its ancient receptor. *Hypertension.* 2006;48(4):549-551.

12. Ramser J, Abidi FE, Burckle CA, Lenski C, Toriello H, Wen G, Lubs HA, Engert S, Stevenson RE, Meindl A, Schwartz CE, Nguyen G. A unique exonic splice enhancer mutation in a family with X-linked mental retardation and epilepsy points to a novel role of the renin receptor. *Hum Mol Genet.* 2005;14(8):1019-1027.

13. Amsterdam A, Nissen RM, Sun Z, Swindell EC, Farrington S, Hopkins N. Identification of 315 genes essential for early zebrafish development. *Proc Natl Acad Sci U S A.* 2004;101(35):12792-12797.

14. Sihn G, Rousselle A, Vilianovitch L, Burckle C, Bader M. Physiology of the (pro)renin receptor: Wnt of change? *Kidney Int.* 2010;78(3):246-256.

15. Nguyen G, Muller DN. The biology of the (pro)renin receptor. *J Am Soc Nephrol.* 2009;21(1):18-23.

16. Cruciat CM, Ohkawara B, Acebron SP, Karaulanov E, Reinhard C, Ingelfinger D, Boutros M, Niehrs C. Requirement of prorenin receptor and vacuolar H+-ATPase-mediated acidification for Wnt signaling. *Science.*327(5964):459-463.

17. Cruciat CM, Ohkawara B, Acebron SP, Karaulanov E, Reinhard C, Ingelfinger D, Boutros M, Niehrs C. Requirement of prorenin receptor and vacuolar H+-ATPase-mediated acidification for Wnt signaling. *Science.* 2010;327(5964):459-463.

18. Dinh DT, Frauman AG, Johnston CI, Fabiani ME. Angiotensin receptors: distribution, signalling and function. *Clin Sci (Lond).* 2001;100(5):481-492.

19. Danser AH. The increase in renin during renin inhibition: does it result in harmful effects by the (pro)renin receptor? *Hypertens Res.* 2009;33(1):4-10.

20. Danser AH. Local renin-angiotensin systems: the unanswered questions. *Int J Biochem Cell Biol.* 2003;35(6):759-768.

21. Danser AH, Saris JJ, Schuijt MP, van Kats JP. Is there a local renin-angiotensin system in the heart? *Cardiovasc Res.* 1999;44(2):252-265.

22. Sielecki AR, Hayakawa K, Fujinaga M, Murphy ME, Fraser M, Muir AK, Carilli CT, Lewicki JA, Baxter JD, James MN. Structure of recombinant human renin, a target for cardiovascular-active drugs, at 2.5 A resolution. *Science.* 1989;243(4896):1346-1351.

23. Zhou A, Carrell RW, Murphy MP, Wei Z, Yan Y, Stanley PL, Stein PE, Broughton Pipkin F, Read RJ. A redox switch in angiotensinogen modulates angiotensin release. *Nature.* 2011;468(7320):108-111.

24. Derkx FH, Deinum J, Lipovski M, Verhaar M, Fischli W, Schalekamp MA. Nonproteolytic "activation" of prorenin by active site-directed renin inhibitors as demonstrated by renin-specific monoclonal antibody. *J Biol Chem.* 1992;267(32):22837-22842.

25. Reudelhuber TL, Ramla D, Chiu L, Mercure C, Seidah NG. Proteolytic processing of human prorenin in renal and non-renal tissues. *Kidney Int.* 1994;46(6):1522-1524.

26. Neves FA, Duncan KG, Baxter JD. Cathepsin B is a prorenin processing enzyme. *Hypertension.* 1996;27(3 Pt 2):514-517.

27. Sealey JE, Moon C, Laragh JH, Alderman M. Plasma prorenin: cryoactivation and relationship to renin substrate in normal subjects. *Am J Med.* 1976;61(5):731-738.

28. Lumbers ER. Activation of renin in human amniotic fluid by low pH. *Enzymologia.* 1971;40(6):329-336.

29. Danser AH, Deinum J. Renin, prorenin and the putative (pro)renin receptor. *Hypertension.* 2005;46(5):1069-1076.

30. Kurtz A. Renin release: sites, mechanisms, and control. *Annu Rev Physiol.* 2010;73:377-399.

31. Luetscher JA, Kraemer FB, Wilson DM, Schwartz HC, Bryer-Ash M. Increased plasma inactive renin in diabetes mellitus. A marker of microvascular complications. *N Engl J Med.* 1985;312(22):1412-1417.

32. Deinum J, Ronn B, Mathiesen E, Derkx FH, Hop WC, Schalekamp MA. Increase in serum prorenin precedes onset of microalbuminuria in patients with insulin-dependent diabetes mellitus. *Diabetologia.* 1999;42(8):1006-1010.

33. RD T. Microalbuminuria: definition, detection, and clinical significance. *J Clin Hypertens (Greenwich).* 2004(6(11 Suppl 3)):2-7.

34. Takahashi S, Ohsawa T, Miura R, Miyake Y. Purification of high molecular weight (HMW) renin from porcine kidney and direct evidence that the HMW renin is a complex of renin with renin binding protein (RnBP). *J Biochem.* 1983;93(1):265-274.

35. Schmitz C, Gotthardt M, Hinderlich S, Leheste JR, Gross V, Vorum H, Christensen EI, Luft FC, Takahashi S, Willnow TE. Normal blood pressure and plasma renin activity in mice lacking the renin-binding protein, a cellular renin inhibitor. *J Biol Chem.* 2000;275(20):15357-15362.

36. Saris JJ, Derkx FH, Lamers JM, Saxena PR, Schalekamp MA, Danser AH. Cardiomyocytes bind and activate native human prorenin : role of soluble mannose 6-phosphate receptors. *Hypertension.* 2001;37(2 Part 2):710-715.

37. Saris JJ, Derkx FH, De Bruin RJ, Dekkers DH, Lamers JM, Saxena PR, Schalekamp MA, Jan Danser AH. High-affinity prorenin binding to cardiac man-6-P/IGF-II

receptors precedes proteolytic activation to renin. *Am J Physiol Heart Circ Physiol.* 2001;280(4):H1706-1715.

38. Saris JJ, van den Eijnden MM, Lamers JM, Saxena PR, Schalekamp MA, Danser AH. Prorenin-induced myocyte proliferation: no role for intracellular angiotensin II. *Hypertension.* 2002;39(2 Pt 2):573-577.

39. Nguyen G, Delarue F, Berrou J, Rondeau E, Sraer JD. Specific receptor binding of renin on human mesangial cells in culture increases plasminogen activator inhibitor-1 antigen. *Kidney Int.* 1996;50(6):1897-1903.

40. Batenburg WW, Krop M, Garrelds IM, de Vries R, de Bruin RJ, Burckle CA, Muller DN, Bader M, Nguyen G, Danser AH. Prorenin is the endogenous agonist of the (pro)renin receptor. Binding kinetics of renin and prorenin in rat vascular smooth muscle cells overexpressing the human (pro)renin receptor. *J Hypertens.* 2007;25(12):2441-2453.

41. Feldt S, Batenburg WW, Mazak I, Maschke U, Wellner M, Kvakan H, Dechend R, Fiebeler A, Burckle C, Contrepas A, Jan Danser AH, Bader M, Nguyen G, Luft FC, Muller DN. Prorenin and renin-induced extracellular signal-regulated kinase 1/2 activation in monocytes is not blocked by aliskiren or the handle-region peptide. *Hypertension.* 2008;51(3):682-688.

42. Huang Y, Wongamorntham S, Kasting J, McQuillan D, Owens RT, Yu L, Noble NA, Border W. Renin increases mesangial cell transforming growth factor-beta1 and matrix proteins through receptor-mediated, angiotensin II-independent mechanisms. *Kidney Int.* 2006;69(1):105-113.

43. Feldt S, Maschke U, Dechend R, Luft FC, Muller DN. The putative (pro)renin receptor blocker HRP fails to prevent (pro)renin signaling. *J Am Soc Nephrol.* 2008;19(4):743-748.

44. Zhang J, Noble NA, Border WA, Owens RT, Huang Y. Receptor-dependent prorenin activation and induction of PAI-1 expression in vascular smooth muscle cells. *Am J Physiol Endocrinol Metab.* 2008;295(4):E810-819.

45. Sakoda M, Ichihara A, Kaneshiro Y, Takemitsu T, Nakazato Y, Nabi AH, Nakagawa T, Suzuki F, Inagami T, Itoh H. (Pro)renin receptor-mediated activation of mitogen-activated protein kinases in human vascular smooth muscle cells. *Hypertens Res.* 2007;30(11):1139-1146.

46. Uraoka M, Ikeda K, Nakagawa Y, Koide M, Akakabe Y, Nakano-Kurimoto R, Takahashi T, Matoba S, Yamada H, Okigaki M, Matsubara H. Prorenin induces ERK activation in endothelial cells to enhance neovascularization independently of the renin-angiotensin system. *Biochem Biophys Res Commun.* 2009;390(4):1202-1207.

47. Huang Y, Noble NA, Zhang J, Xu C, Border WA. Renin-stimulated TGF-beta1 expression is regulated by a mitogen-activated protein kinase in mesangial cells. *Kidney Int.* 2007;72(1):45-52.

48. Huang J, Matavelli LC, Siragy HM. Renal (pro)renin receptor contributes to development of diabetic kidney disease through transforming growth factor-beta1-connective tissue growth factor signalling cascade. *Clin Exp Pharmacol Physiol.* 2011;38(4):215-221.

49. Kaneshiro Y, Ichihara A, Takemitsu T, Sakoda M, Suzuki F, Nakagawa T, Hayashi M, Inagami T. Increased expression of cyclooxygenase-2 in the renal cortex of human prorenin receptor gene-transgenic rats. *Kidney Int.* 2006;70(4):641-646.

50. Huang J, Siragy HM. Glucose promotes the production of interleukine-1beta and cyclooxygenase-2 in mesangial cells via enhanced (Pro)renin receptor expression. *Endocrinology.* 2009;150(12):5557-5565.

51. Matavelli LC, Huang J, Siragy HM. (Pro)renin receptor contributes to diabetic nephropathy by enhancing renal inflammation. *Clin Exp Pharmacol Physiol.* 2009;37(3):277-282.

52. Saris JJ, t Hoen PA, Garrelds IM, Dekkers DH, den Dunnen JT, Lamers JM, Jan Danser AH. Prorenin induces intracellular signaling in cardiomyocytes independently of angiotensin II. *Hypertension.* 2006;48(4):564-571.

53. Schefe JH, Unger T, Funke-Kaiser H. PLZF and the (pro)renin receptor. *J Mol Med (Berl).* 2008;86(6):623-627.

54. Schefe JH, Neumann C, Goebel M, Danser J, Kirsch S, Gust R, Kintscher U, Unger T, Funke-Kaiser H. Prorenin engages the (pro)renin receptor like renin and both ligand activities are unopposed by aliskiren. *J Hypertens.* 2008;26(9):1787-1794.

55. Hirose T, Hashimoto M, Totsune K, Metoki H, Asayama K, Kikuya M, Sugimoto K, Katsuya T, Ohkubo T, Hashimoto J, Rakugi H, Takahashi K, Imai Y. Association of (pro)renin receptor gene polymorphism with blood pressure in Japanese men: the Ohasama study. *Am J Hypertens.* 2009;22(3):294-299.

56. Ott C, Schneider MP, Delles C, Schlaich MP, Hilgers KF, Schmieder RE. Association of (pro)renin receptor gene polymorphism with blood pressure in Caucasian men. *Pharmacogenet Genomics.* 2011;21(6):347-349.

57. Burckle CA, Jan Danser AH, Muller DN, Garrelds IM, Gasc JM, Popova E, Plehm R, Peters J, Bader M, Nguyen G. Elevated blood pressure and heart rate in human renin receptor transgenic rats. *Hypertension.* 2006;47(3):552-556.

58. Kaneshiro Y, Ichihara A, Sakoda M, Takemitsu T, Nabi AH, Uddin MN, Nakagawa T, Nishiyama A, Suzuki F, Inagami T, Itoh H. Slowly progressive, angiotensin II-independent glomerulosclerosis in human (pro)renin receptor-transgenic rats. *J Am Soc Nephrol.* 2007;18(6):1789-1795.

59. Ichihara A, Hayashi M, Kaneshiro Y, Suzuki F, Nakagawa T, Tada Y, Koura Y, Nishiyama A, Okada H, Uddin MN, Nabi AH, Ishida Y, Inagami T, Saruta T. Inhibition of diabetic nephropathy by a decoy peptide corresponding to the "handle" region for nonproteolytic activation of prorenin. *J Clin Invest.* 2004;114(8):1128-1135.

60. Takahashi H, Ichihara A, Kaneshiro Y, Inomata K, Sakoda M, Takemitsu T, Nishiyama A, Itoh H. Regression of nephropathy developed in diabetes by (Pro)renin receptor blockade. *J Am Soc Nephrol.* 2007;18(7):2054-2061.

61. Ichihara A, Suzuki F, Nakagawa T, Kaneshiro Y, Takemitsu T, Sakoda M, Nabi AH, Nishiyama A, Sugaya T, Hayashi M, Inagami T. Prorenin receptor blockade inhibits development of glomerulosclerosis in diabetic angiotensin II type 1a receptor-deficient mice. *J Am Soc Nephrol.* 2006;17(7):1950-1961.

62. Satofuka S, Ichihara A, Nagai N, Yamashiro K, Koto T, Shinoda H, Noda K, Ozawa Y, Inoue M, Tsubota K, Suzuki F, Oike Y, Ishida S. Suppression of ocular inflammation in endotoxin-induced uveitis by inhibiting nonproteolytic activation of prorenin. *Invest Ophthalmol Vis Sci.* 2006;47(6):2686-2692.

63. Susic D, Zhou X, Frohlich ED, Lippton H, Knight M. Cardiovascular effects of prorenin blockade in genetically spontaneously hypertensive rats on normal and high-salt diet. *Am J Physiol Heart Circ Physiol.* 2008;295(3):H1117-H1121.

64. Krebs C, Weber M, Steinmetz O, Meyer-Schwesinger C, Stahl R, Danser AH, Garrelds I, van Goor H, Nguyen G, Muller D, Wenzel U. Effect of (pro)renin receptor inhibition by a decoy peptide on renal damage in the clipped kidney of Goldblatt rats. *Kidney Int.* 2008;74(6):823-824.

65. Campbell DJ. Critical review of prorenin and (pro)renin receptor research. *Hypertension.* 2008;51(5):1259-1264.

66. Nishi T, Forgac M. The vacuolar (H+)-ATPases--nature's most versatile proton pumps. *Nat Rev Mol Cell Biol.* 2002;3(2):94-103.

67. Cross RL, Muller V. The evolution of A-, F-, and V-type ATP synthases and ATPases: reversals in function and changes in the H+/ATP coupling ratio. *FEBS Lett.* 2004;576(1-2):1-4.

68. Forgac M. Vacuolar ATPases: rotary proton pumps in physiology and pathophysiology. *Nat Rev Mol Cell Biol.* 2007;8(11):917-929.

69. Graham LA, Flannery AR, Stevens TH. Structure and assembly of the yeast V-ATPase. *J Bioenerg Biomembr.* 2003;35(4):301-312.

70. Malkus P, Graham LA, Stevens TH, Schekman R. Role of Vma21p in assembly and transport of the yeast vacuolar ATPase. *Mol Biol Cell.* 2004;15(11):5075-5091.

71. Davis-Kaplan SR, Compton MA, Flannery AR, Ward DM, Kaplan J, Stevens TH, Graham LA. PKR1 encodes an assembly factor for the yeast V-type ATPase. *J Biol Chem.* 2006;281(42):32025-32035.

72. Kawasaki-Nishi S, Bowers K, Nishi T, Forgac M, Stevens TH. The amino-terminal domain of the vacuolar proton-translocating ATPase a subunit controls targeting and in vivo dissociation, and the carboxyl-terminal domain affects coupling of proton transport and ATP hydrolysis. *J Biol Chem.* 2001;276(50):47411-47420.

73. Morel N, Dedieu JC, Philippe JM. Specific sorting of the a1 isoform of the V-H+ATPase a subunit to nerve terminals where it associates with both synaptic vesicles and the presynaptic plasma membrane. *J Cell Sci.* 2003;116(Pt 23):4751-4762.

74. Hurtado-Lorenzo A, Skinner M, El Annan J, Futai M, Sun-Wada GH, Bourgoin S, Casanova J, Wildeman A, Bechoua S, Ausiello DA, Brown D, Marshansky V. V-ATPase interacts with ARNO and Arf6 in early endosomes and regulates the protein degradative pathway. *Nat Cell Biol.* 2006;8(2):124-136.

75. Toyomura T, Murata Y, Yamamoto A, Oka T, Sun-Wada GH, Wada Y, Futai M. From lysosomes to the plasma membrane: localization of vacuolar-type H+ -ATPase with the a3 isoform during osteoclast differentiation. *J Biol Chem.* 2003;278(24):22023-22030.

76. Pietrement C, Sun-Wada GH, Silva ND, McKee M, Marshansky V, Brown D, Futai M, Breton S. Distinct expression patterns of different subunit isoforms of the V-ATPase in the rat epididymis. *Biol Reprod.* 2006;74(1):185-194.

77. Hirata T, Iwamoto-Kihara A, Sun-Wada GH, Okajima T, Wada Y, Futai M. Subunit rotation of vacuolar-type proton pumping ATPase: relative rotation of the G and C subunits. *J Biol Chem.* 2003;278(26):23714-23719.

78. Kawasaki-Nishi S, Nishi T, Forgac M. Arg-735 of the 100-kDa subunit a of the yeast V-ATPase is essential for proton translocation. *Proc Natl Acad Sci U S A.* 2001;98(22):12397-12402.

79. Kawasaki-Nishi S, Nishi T, Forgac M. Interacting helical surfaces of the transmembrane segments of subunits a and c' of the yeast V-ATPase defined by disulfide-mediated cross-linking. *J Biol Chem.* 2003;278(43):41908-41913.

80. Wang Y, Inoue T, Forgac M. TM2 but not TM4 of subunit c" interacts with TM7 of subunit a of the yeast V-ATPase as defined by disulfide-mediated cross-linking. *J Biol Chem.* 2004;279(43):44628-44638.

81. Huss M, Ingenhorst G, Konig S, Gassel M, Drose S, Zeeck A, Altendorf K, Wieczorek H. Concanamycin A, the specific inhibitor of V-ATPases, binds to the V(o) subunit c. *J Biol Chem.* 2002;277(43):40544-40548.

82. Bowman BJ, Bowman EJ. Mutations in subunit C of the vacuolar ATPase confer resistance to bafilomycin and identify a conserved antibiotic binding site. *J Biol Chem.* 2002;277(6):3965-3972.

83. Kane PM. The where, when, and how of organelle acidification by the yeast vacuolar H+-ATPase. *Microbiol Mol Biol Rev.* 2006;70(1):177-191.

84. Seol JH, Shevchenko A, Deshaies RJ. Skp1 forms multiple protein complexes, including RAVE, a regulator of V-ATPase assembly. *Nat Cell Biol.* 2001;3(4):384-391.

85. Shao E, Nishi T, Kawasaki-Nishi S, Forgac M. Mutational analysis of the non-homologous region of subunit A of the yeast V-ATPase. *J Biol Chem.* 2003;278(15):12985-12991.

86. Lafourcade C, Sobo K, Kieffer-Jaquinod S, Garin J, van der Goot FG. Regulation of the V-ATPase along the endocytic pathway occurs through reversible subunit association and membrane localization. *PLoS One.* 2008;3(7):e2758.

87. Kinouchi K, Ichihara A, Sano M, Sun-Wada GH, Wada Y, Kurauchi-Mito A, Bokuda K, Narita T, Oshima Y, Sakoda M, Tamai Y, Sato H, Fukuda K, Itoh H. The (pro)renin receptor/ATP6AP2 is essential for vacuolar H+-ATPase assembly in murine cardiomyocytes. *Circ Res.* 2011;107(1):30-34.

88. Sautin YY, Lu M, Gaugler A, Zhang L, Gluck SL. Phosphatidylinositol 3-kinase-mediated effects of glucose on vacuolar H+-ATPase assembly, translocation, and acidification of intracellular compartments in renal epithelial cells. *Mol Cell Biol.* 2005;25(2):575-589.

89. Feng Y, Forgac M. Inhibition of vacuolar H(+)-ATPase by disulfide bond formation between cysteine 254 and cysteine 532 in subunit A. *J Biol Chem.* 1994;269(18):13224-13230.

90. Advani A, Kelly DJ, Cox AJ, White KE, Advani SL, Thai K, Connelly KA, Yuen D, Trogadis J, Herzenberg AM, Kuliszewski MA, Leong-Poi H, Gilbert RE. The (Pro)renin receptor: site-specific and functional linkage to the vacuolar H+-ATPase in the kidney. *Hypertension.* 2009;54(2):261-269.

91. Riediger F QI, Qadri F, Hartleben B, Park JK, Potthoff SA, Sohn D, Sihn G, Rousselle A, Fokuhl V, Maschke U, Purfürst B, Schneider W, Rump LC, Luft FC, Dechend R, Bader M, Huber TB, Nguyen G, Muller DN. Prorenin Receptor Is Essential for Podocyte Autophagy and Survival. *J Am Soc Nephrol.* 2011;[Epub ahead of print].

92. Oshima Y KK, Ichihara A, Sakoda M, Kurauchi-Mito A, Bokuda K, Narita T, Kurosawa H, Sun-Wada GH, Wada Y, Yamada T, Takemoto M, Saleem MA, Quaggin SE, Itoh H. Prorenin Receptor Is Essential for Normal Podocyte Structure and Function. *J Am Soc Nephrol.* . 2011;[Epub ahead of print].

93. Sun-Wada GH, Toyomura T, Murata Y, Yamamoto A, Futai M, Wada Y. The a3 isoform of V-ATPase regulates insulin secretion from pancreatic beta-cells. *J Cell Sci.* 2006;119(Pt 21):4531-4540.

94. Hinton A, Bond S, Forgac M. V-ATPase functions in normal and disease processes. *Pflugers Arch.* 2009;457(3):589-598.

95. Shan Z, Shi P, Cuadra AE, Dong Y, Lamont GJ, Li Q, Seth DM, Navar LG, Katovich MJ, Sumners C, Raizada MK. Involvement of the brain (pro)renin receptor in cardiovascular homeostasis. *Circ Res.*107(7):934-938.

96. Adams DS, Robinson KR, Fukumoto T, Yuan S, Albertson RC, Yelick P, Kuo L, McSweeney M, Levin M. Early, H+-V-ATPase-dependent proton flux is necessary for consistent left-right patterning of non-mammalian vertebrates. *Development.* 2006;133(9):1657-1671.

97. Wagner CA, Finberg KE, Breton S, Marshansky V, Brown D, Geibel JP. Renal vacuolar H+-ATPase. *Physiol Rev.* 2004;84(4):1263-1314.

98. Yang Q, Li G, Singh SK, Alexander EA, Schwartz JH. Vacuolar H+ -ATPase B1 subunit mutations that cause inherited distal renal tubular acidosis affect proton pump

assembly and trafficking in inner medullary collecting duct cells. *J Am Soc Nephrol.* 2006;17(7):1858-1866.

99. Li YP, Chen W, Liang Y, Li E, Stashenko P. Atp6i-deficient mice exhibit severe osteopetrosis due to loss of osteoclast-mediated extracellular acidification. *Nat Genet.* 1999;23(4):447-451.

100. Pastor-Soler N, Beaulieu V, Litvin TN, Da Silva N, Chen Y, Brown D, Buck J, Levin LR, Breton S. Bicarbonate-regulated adenylyl cyclase (sAC) is a sensor that regulates pH-dependent V-ATPase recycling. *J Biol Chem.* 2003;278(49):49523-49529.

101. Nanda A, Brumell JH, Nordstrom T, Kjeldsen L, Sengelov H, Borregaard N, Rotstein OD, Grinstein S. Activation of proton pumping in human neutrophils occurs by exocytosis of vesicles bearing vacuolar-type H+-ATPases. *J Biol Chem.* 1996;271(27):15963-15970.

102. Sennoune SR, Bakunts K, Martinez GM, Chua-Tuan JL, Kebir Y, Attaya MN, Martinez-Zaguilan R. Vacuolar H+-ATPase in human breast cancer cells with distinct metastatic potential: distribution and functional activity. *Am J Physiol Cell Physiol.* 2004;286(6):C1443-1452.

103. Gruenke JA, Armstrong RT, Newcomb WW, Brown JC, White JM. New insights into the spring-loaded conformational change of influenza virus hemagglutinin. *J Virol.* 2002;76(9):4456-4466.

104. Gruenberg J, van der Goot FG. Mechanisms of pathogen entry through the endosomal compartments. *Nat Rev Mol Cell Biol.* 2006;7(7):495-504.

105. Geyer M, Yu H, Mandic R, Linnemann T, Zheng YH, Fackler OT, Peterlin BM. Subunit H of the V-ATPase binds to the medium chain of adaptor protein complex 2 and connects Nef to the endocytic machinery. *J Biol Chem.* 2002;277(32):28521-28529.

106. van Amerongen R, Nusse R. Towards an integrated view of Wnt signaling in development. *Development.* 2009;136(19):3205-3214.

107. Luo J, Chen J, Deng ZL, Luo X, Song WX, Sharff KA, Tang N, Haydon RC, Luu HH, He TC. Wnt signaling and human diseases: what are the therapeutic implications? *Lab Invest.* 2007;87(2):97-103.

108. Cadigan KM, Peifer M. Wnt signaling from development to disease: insights from model systems. *Cold Spring Harb Perspect Biol.* 2009;1(2):a002881.

109. Buechling T, Bartscherer K, Ohkawara B, Chaudhary V, Spirohn K, Niehrs C, Boutros M. Wnt/Frizzled signaling requires dPRR, the Drosophila homolog of the prorenin receptor. *Curr Biol.* 2010;20(14):1263-1268.

110. Hermle T, Saltukoglu D, Grunewald J, Walz G, Simons M. Regulation of Frizzled-dependent planar polarity signaling by a V-ATPase subunit. *Curr Biol.* 2010;20(14):1269-1276.

111. Clevers H. Wnt/beta-catenin signaling in development and disease. *Cell.* 2006;127(3):469-480.

112. Grigoryan T, Wend P, Klaus A, Birchmeier W. Deciphering the function of canonical Wnt signals in development and disease: conditional loss- and gain-of-function mutations of beta-catenin in mice. *Genes Dev.* 2008;22(17):2308-2341.

113. Harada N, Tamai Y, Ishikawa T, Sauer B, Takaku K, Oshima M, Taketo MM. Intestinal polyposis in mice with a dominant stable mutation of the beta-catenin gene. *EMBO J.* 1999;18(21):5931-5942.

114. Huelsken J, Vogel R, Erdmann B, Cotsarelis G, Birchmeier W. beta-Catenin controls hair follicle morphogenesis and stem cell differentiation in the skin. *Cell.* 2001;105(4):533-545.

115. Scheller M, Huelsken J, Rosenbauer F, Taketo MM, Birchmeier W, Tenen DG, Leutz A. Hematopoietic stem cell and multilineage defects generated by constitutive beta-catenin activation. *Nat Immunol.* 2006;7(10):1037-1047.

116. Kirstetter P, Anderson K, Porse BT, Jacobsen SE, Nerlov C. Activation of the canonical Wnt pathway leads to loss of hematopoietic stem cell repopulation and multilineage differentiation block. *Nat Immunol.* 2006;7(10):1048-1056.

117. Aoki K, Taketo MM. Adenomatous polyposis coli (APC): a multi-functional tumor suppressor gene. *J Cell Sci.* 2007;120(Pt 19):3327-3335.

118. van Gijn ME, Daemen MJ, Smits JF, Blankesteijn WM. The wnt-frizzled cascade in cardiovascular disease. *Cardiovasc Res.* 2002;55(1):16-24.

119. Janeway CA Jr TP, Walport M, et al. *Immunobiology: The Immune System in Health and Disease.* New York: Garland Science; 2001.

120. Xu Y, Banerjee D, Huelsken J, Birchmeier W, Sen JM. Deletion of beta-catenin impairs T cell development. *Nat Immunol.* 2003;4(12):1177-1182.

121. Born WK, Yin Z, Hahn YS, Sun D, O'Brien RL. Analysis of gamma delta T cell functions in the mouse. *J Immunol.* 2010;184(8):4055-4061.

122. Acuto O, Michel F. CD28-mediated co-stimulation: a quantitative support for TCR signalling. *Nat Rev Immunol.* 2003;3(12):939-951.

123. Pepper M, Jenkins MK. Origins of CD4(+) effector and central memory T cells. *Nat Immunol.* 2011;12(6):467-471.

124. Hammerich L, Heymann F, Tacke F. Role of IL-17 and Th17 cells in liver diseases. *Clin Dev Immunol.* 2011;2011:345803.

125. Korn T, Bettelli E, Oukka M, Kuchroo VK. IL-17 and Th17 Cells. *Annu Rev Immunol.* 2009;27:485-517.

126. Tang Q, Bluestone JA. The Foxp3+ regulatory T cell: a jack of all trades, master of regulation. *Nat Immunol.* 2008;9(3):239-244.

127. Germain RN. T-cell development and the CD4-CD8 lineage decision. *Nat Rev Immunol.* 2002;2(5):309-322.

128. Rothenberg EV, Moore JE, Yui MA. Launching the T-cell-lineage developmental programme. *Nat Rev Immunol.* 2008;8(1):9-21.

129. Yang Q, Jeremiah Bell J, Bhandoola A. T-cell lineage determination. *Immunol Rev.* 2010;238(1):12-22.

130. Zuniga-Pflucker JC. T-cell development made simple. *Nat Rev Immunol.* 2004;4(1):67-72.

131. Pua HH, Dzhagalov I, Chuck M, Mizushima N, He YW. A critical role for the autophagy gene Atg5 in T cell survival and proliferation. *J Exp Med.* 2007;204(1):25-31.

132. Lu X, Yu H, Liu SH, Brodsky FM, Peterlin BM. Interactions between HIV1 Nef and vacuolar ATPase facilitate the internalization of CD4. *Immunity.* 1998;8(5):647-656.

133. Kataoka T, Takaku K, Magae J, Shinohara N, Takayama H, Kondo S, Nagai K. Acidification is essential for maintaining the structure and function of lytic granules of CTL. Effect of concanamycin A, an inhibitor of vacuolar type H(+)-ATPase, on CTL-mediated cytotoxicity. *J Immunol.* 1994;153(9):3938-3947.

134. Muller DN, Kvakan H, Luft FC. Immune-related effects in hypertension and target-organ damage. *Curr Opin Nephrol Hypertens.* 2011;20(2):113-117.

135. Schuck P. Size-distribution analysis of macromolecules by sedimentation velocity ultracentrifugation and lamm equation modeling. *Biophys J.* 2000;78(3):1606-1619.

136. Thompson JD, Higgins DG, Gibson TJ. CLUSTAL W: improving the sensitivity of progressive multiple sequence alignment through sequence weighting, position-specific gap penalties and weight matrix choice. *Nucleic Acids Res.* 1994;22(22):4673-4680.

137. Cole C, Barber JD, Barton GJ. The Jpred 3 secondary structure prediction server. *Nucleic Acids Res.* 2008;36(Web Server issue):W197-201.

138. Sambrook JFF, Fritsch, E., Maniatis, T. Molecular Cloning: A Laboratory Manual. *Cold Spring Harbour Laboratory Press.* 1989.

139. Chung CT, Niemela SL, Miller RH. One-step preparation of competent Escherichia coli: transformation and storage of bacterial cells in the same solution. *Proc Natl Acad Sci U S A.* 1989;86(7):2172-2175.

140. Laemmli U. Cleavage of structural proteins during the assembly of the head of bacteriophage T4. *Nature.* 1970;227(5259):680-685.

141. Gasteiger EH, Gattiker, A., Duvaud,S., Wilkins, M.R., Appel R.R. A Proteomics Protocols Handbook. *Humana Press.* 2005.

142. Bradford MM. A rapid and sensitive method for the quantitation of microgram quantities of protein utilizing the principle of protein-dye binding. *Anal Biochem.* 1976;72:248-254.

143. Studier FW. Protein production by auto-induction in high density shaking cultures. *Protein Expr Purif.* 2005;41(1):207-234.

144. Slotboom DJ, Duurkens RH, Olieman K, Erkens GB. Static light scattering to characterize membrane proteins in detergent solution. *Methods.* 2008;46(2):73-82.

145. Greenfield NJ. Analysis of the kinetics of folding of proteins and peptides using circular dichroism. *Nat Protoc.* 2006;1(6):2891-2899.

146. Greenfield NJ. Using circular dichroism spectra to estimate protein secondary structure. *Nat Protoc.* 2006;1(6):2876-2890.

147. Greenfield NJ. Determination of the folding of proteins as a function of denaturants, osmolytes or ligands using circular dichroism. *Nat Protoc.* 2006;1(6):2733-2741.

148. Greenfield NJ. Using circular dichroism collected as a function of temperature to determine the thermodynamics of protein unfolding and binding interactions. *Nat Protoc.* 2006;1(6):2527-2535.

149. Kelly SM JT, Price NC. How to study proteins by circular dichroism. *Biochim Biophys Acta.* 2005;1751(2):119-139.

150. Schuck P, Perugini MA, Gonzales NR, Howlett GJ, Schubert D. Size-distribution analysis of proteins by analytical ultracentrifugation: strategies and application to model systems. *Biophys J.* 2002;82(2):1096-1111.

151. Lebowitz J, Lewis MS, Schuck P. Modern analytical ultracentrifugation in protein science: a tutorial review. *Protein Sci.* 2002;11(9):2067-2079.

152. Goldschmidt L, Cooper DR, Derewenda ZS, Eisenberg D. Toward rational protein crystallization: A Web server for the design of crystallizable protein variants. *Protein Sci.* 2007;16(8):1569-1576.

153. Graslund S, Nordlund P, Weigelt J, Hallberg BM, Bray J, Gileadi O, Knapp S, Oppermann U, Arrowsmith C, Hui R, Ming J, dhe-Paganon S, Park HW, Savchenko A, Yee A, Edwards A, Vincentelli R, Cambillau C, Kim R, Kim SH, Rao Z, Shi Y, Terwilliger TC, Kim CY, Hung LW, Waldo GS, Peleg Y, Albeck S, Unger T, Dym O, Prilusky J, Sussman JL, Stevens RC, Lesley SA, Wilson IA, Joachimiak A, Collart F, Dementieva I, Donnelly MI, Eschenfeldt WH, Kim Y, Stols L, Wu R, Zhou M, Burley SK, Emtage JS, Sauder JM, Thompson D, Bain K, Luz J, Gheyi T, Zhang F, Atwell S, Almo SC, Bonanno JB, Fiser A, Swaminathan S, Studier FW, Chance MR, Sali A, Acton TB, Xiao R, Zhao L, Ma LC, Hunt JF, Tong L, Cunningham K, Inouye M, Anderson S, Janjua H, Shastry R, Ho CK, Wang D, Wang H, Jiang M, Montelione GT, Stuart DI, Owens RJ, Daenke S, Schutz A, Heinemann U, Yokoyama S, Bussow K, Gunsalus KC. Protein production and purification. *Nat Methods.* 2008;5(2):135-146.

154. Tienhsiung Kua PL, Chenhsiung Chanb, Tsusheng Wangb, Szuming Laib, Pingchiang Lyub, Naiwan Hsiaoc,. Predicting melting temperature directly from protein sequences. *Computational Biology and Chemistry.* 2009;33(6):445-450

155. Thomas S. Walter CM, Rene Assenberg, Kin-Fai Au, Jingshan Re, Anil Verma, Joanne E. Nettleship, Raymond J. Owens, David I. Stuart, and Jonathan M. Grimes. Lysine Methylation as a Routine Rescue Strategy for Protein Crystallization. *Structure.* 2006;Volume 14(Issue 11):1617-1622.

156. Cavanagh J. *Protein NMR spectroscopy: principles and practic.* Vol second edition: Academic Press; 2007.

157. Hartl FU BA, Hayer-Hartl M. Molecular chaperones in protein folding and proteostasis. *Nature.* 2011;475(7356):324-332.

158. Kato T, Kageshima A, Suzuki F, Park EY. Expression and purification of human (pro)renin receptor in insect cells using baculovirus expression system. *Protein Expr Purif.* 2008;58(2):242-248.

159. Kato T, Suzuki F, Park EY. Purification of functional baculovirus particles from silkworm larval hemolymph and their use as nanoparticles for the detection of human prorenin receptor (PRR) binding. *BMC Biotechnol.* 2011;11(1):60.

160. Du D, Kato T, Suzuki F, Park EY. Binding affinity of full-length and extracellular domains of recombinant human (pro)renin receptor to human renin when expressed in the fat body and hemolymph of silkworm larvae. *J Biosci Bioeng.* 2009;108(4):304-309.

161. Du D, Kato T, Suzuki F, Park EY. Expression of protein complex comprising the human prorenin and (pro)renin receptor in silkworm larvae using Bombyx mori nucleopolyhedrovirus (BmNPV) bacmids for improving biological function. *Mol Biotechnol.* 2009;43(2):154-161.

162. Du D, Kato T, Nabi AH, Suzuki F, Park EY. Expression of functional human (pro)renin receptor in silkworm (Bombyx mori) larvae using BmMNPV bacmid. *Biotechnol Appl Biochem.* 2008;49(Pt 3):195-202.

163. Romier C, Ben Jelloul M, Albeck S, Buchwald G, Busso D, Celie PH, Christodoulou E, De Marco V, van Gerwen S, Knipscheer P, Lebbink JH, Notenboom V, Poterszman A, Rochel N, Cohen SX, Unger T, Sussman JL, Moras D, Sixma TK, Perrakis A. Co-expression of protein complexes in prokaryotic and eukaryotic hosts: experimental procedures, database tracking and case studies. *Acta Crystallogr D Biol Crystallogr.* 2006;62(Pt 10):1232-1242.

164. Kastritis PL MI, Hwang H, Weng Z, Bates PA, Bonvin AM, Janin J. A structure-based benchmark for protein-protein binding affinity. *Protein Sci.* . 2011;20(3):482-491.

165. Nabi AH, Kageshima A, Uddin MN, Nakagawa T, Park EY, Suzuki F. Binding properties of rat prorenin and renin to the recombinant rat renin/prorenin receptor prepared by a baculovirus expression system. *Int J Mol Med.* 2006;18(3):483-488.

166. Batenburg WW LX, Leijten F, Maschke U, Müller DN, Danser AH. Renin- and prorenin-induced effects in rat vascular smooth muscle cells overexpressing the human (pro)renin receptor: does (pro)renin-(pro)renin receptor interaction actually occur? *Hypertension.* 2011;58(6):1111-1119.

167. Berg JM TJ, Stryer L. *Biochemistry*. 5th edition ed. New York: W H Freeman; 2002.

168. Maranda B BD, Bourgoin S, Casanova JE, Vinay P, Ausiello DA, Marshansky V. Intra-endosomal pH-sensitive recruitment of the Arf-nucleotide exchange factor ARNO and Arf6 from cytoplasm to proximal tubule endosomes. *J Biol Chem.* 2001;276(21):18540-18550.

169. Hurtado-Lorenzo A SM, El Annan J, Futai M, Sun-Wada GH, Bourgoin S, Casanova J, Wildeman A, Bechoua S, Ausiello DA, Brown D, Marshansky V. V-ATPase

interacts with ARNO and Arf6 in early endosomes and regulates the protein degradative pathway. *Nat Cell Biol.* 2006;8(2):124-136.

170. Rhodes G. *Crystallography Made Crystal Clear; A Guide for Users of Macromolecular Models* 3. Edition ed: Elsevier Inc; 2006.

171. Panigada M, Porcellini S, Barbier E, Hoeflinger S, Cazenave PA, Gu H, Band H, von Boehmer H, Grassi F. Constitutive endocytosis and degradation of the pre-T cell receptor. *J Exp Med.* 2002;195(12):1585-1597.

172. Arsov I, Adebayo A, Kucerova-Levisohn M, Haye J, MacNeil M, Papavasiliou FN, Yue Z, Ortiz BD. A role for autophagic protein beclin 1 early in lymphocyte development. *J Immunol.* 2011;186(4):2201-2209.

173. Sartor O, Gregory FS, Templeton NS, Pawar S, Perlmutter RM, Rosen N. Selective expression of alternative lck mRNAs in human malignant cell lines. *Mol Cell Biol.* 1989;9(7):2983-2988.

174. Gu H, Marth JD, Orban PC, Mossmann H, Rajewsky K. Deletion of a DNA polymerase beta gene segment in T cells using cell type-specific gene targeting. *Science.* 1994;265(5168):103-106.

175. Radtke F, Wilson A, Mancini SJ, MacDonald HR. Notch regulation of lymphocyte development and function. *Nat Immunol.* 2004;5(3):247-253.

176. Muller DN, Klanke B, Feldt S, Cordasic N, Hartner A, Schmieder RE, Luft FC, Hilgers KF. (Pro)renin receptor peptide inhibitor "handle-region" peptide does not affect hypertensive nephrosclerosis in Goldblatt rats. *Hypertension.* 2008;51(3):676-681.

177. Gounari F, Aifantis I, Khazaie K, Hoeflinger S, Harada N, Taketo MM, von Boehmer H. Somatic activation of beta-catenin bypasses pre-TCR signaling and TCR selection in thymocyte development. *Nat Immunol.* 2001;2(9):863-869.